

①

AD A118499

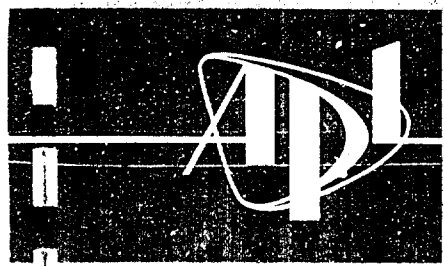
FEASIBILITY OF ACOUSTICALLY DETERMINING THE THICKNESS OF SEA ICE

DTIC FILE COPY

DTIC
ELECTED
AUG 24 1982

APPROVED FOR PUBLIC RELEASE
DISTRIBUTION UNLIMITED

APL-UW 7317
April 1974



82 03 23 162

CONTRACT DAAG17-73-C-0028

12

U
N
I
T
E
D
S
T
A
T
E
S
O
F
A
M
E
R
I
C
A

FEASIBILITY OF ACOUSTICALLY DETERMINING THE THICKNESS OF SEA ICE

by Robert E. Bunney

DTIC
SELECTED
AUG 24 1982
S D
H

APL-UW 7317
April 1974

DISTRIBUTION STATEMENT A
Approved for public release;
Distribution Unlimited

CONTRACT DAAG17-73-C-0028

FOREWORD

The investigation described herein was performed by Dr. R. E. Bunney, Division of Marine Resources, University of Washington, under Contract No. DAAG 17-73-C-0028 for the U.S. Army Cold Regions Research and Engineering Laboratory, sponsored by the Advanced Research Project Agency under ARPA Order 2096.

This contract was technically monitored by Dr. Y. Nakano, U.S. Army Cold Regions Research and Engineering Laboratory, under the instruction of Commander J.R. Seesholtz, Program Manager, ARPA.



Accession For	
NTIS GRA&I	<input checked="" type="checkbox"/>
DTIC TAB	<input type="checkbox"/>
Unannounced	<input type="checkbox"/>
Justification	
By _____	
Distribution/	
Availability Codes	
Avail and/or	
Dist	Special
<i>A</i>	

TABLE OF CONTENTS

SUMMARY	1
INTRODUCTION	2
EXPERIMENTAL TECHNIQUE AND RESULTS	4
Results of Experimental Measurements	4
Approximation of the Elastic Moduli and Transverse Velocity Profiles	12
Discussion of the Results of the Profile Measurements	21
PREDICTIONS OF ACOUSTIC ATTENUATION IN SEA ICE	22
Long Wavelength Isotropic Solution	22
Short Wavelength Solution	26
Total Attenuation Approximation	27
Depth Dependence of the Attenuation	29
ACOUSTIC REFLECTIVITY AT THE ICE-WATER INTERFACE	31
CONCLUSIONS AND RECOMMENDATIONS	43
APPENDIX A - THEORIES	46
APPENDIX B - COMPUTER PROGRAMS	67
REFERENCES	80

SUMMARY

The principal objective of this investigation was to experimentally determine the feasibility of using acoustic pulse echo techniques to measure the thickness of sea ice. Field tests performed on both winter and annual sea ice showed that a pulse echo technique is entirely feasible if 1) adequate coupling between the sound source and the ice surface is obtained, and 2) either the source levels are kept sufficiently high or the frequency is kept low enough that the wavelength of the sound is large compared to the size of the sound-scattering centers in the ice. Our measurements of the compressional and shear wave velocities parallel to the axis of the ice indicate that such thickness measurements can be accurate to within 1.5%.

The tests indicated that the acoustic impedance mismatch at the ice-water interface is sufficient to allow the use of either the compressional or the shear wave. Before the shear wave could be used, however, an efficient method would have to be found for establishing a reliable bond between the ice and the acoustic source. We did not obtain sufficient data to verify reports in the literature that seasonal variations in both the compressional and shear wave velocities approach 20%.

Using the results of this experiment, we empirically predicted the depth dependence of the elastic constants in the ice and the velocity of the vertically polarized shear wave. The average values of these predictions are consistent with those reported in the literature.

The attenuation of both the shear and the compressional wave was then calculated using a combination of viscoelastic and scattering theory. The theory was parametrically fit to measured values, and the results compared favorably with those of other experiments.

Finally, preliminary studies were performed to determine to what extent acoustic surface waves are propagated in sea ice, and to estimate the feasibility of utilizing these modes for thickness measurements. Based on the results of this study and theoretical considerations, it appears that the symmetric Lamb wave could be useful for making ice thickness predictions.

INTRODUCTION

Activities in ice covered regions require a knowledge of ice thickness to assure safety of equipment and personnel. This knowledge is especially important during exercises that call for the operation of heavy equipment, for example, the employment of aircraft on ice runways for logistical support.

During the last 75 years, many studies of ice have been performed to understand its physical, mechanical and chemical properties. A thorough discussion of this work has been published by Weeks and Assur.¹ Even though some of these studies indicate that ice is a relatively good conductor of acoustic disturbances, an efficient method of acoustically determining ice thickness from the top surface still does not exist. Instead, indirect ice thickness measurements are presently based on other physical characteristics of ice and water, such as dielectric permittivity, dielectric loss tangent in ice and in seawater, or elastic oscillations of the total ice cover.

Simple calculations using the idealized assumption of isotropic, homogeneous ice indicate that, because of the low acoustic impedance mismatch at the ice-water interface, an acoustic compressional wave incident on the boundary will be almost entirely transmitted into the water medium. Conversely, because the water will not support shear waves, the shear stress is assumed to vanish at the boundary indicating that the wave will be totally reflected at normal incidence. Thus, neglecting real and apparent attenuation, it would appear from this simple argument that the best method of determining ice thickness acoustically from the top surface would be to generate a shear wave in the ice and, knowing the wave speed, calculate the thickness from the reflection of the wave from the ice-water interface.

This ideal model is, of course, a gross oversimplification of the physics of the problem. It is known that sea ice is not a simple medium, but rather a highly complex inhomogeneous, anisotropic, polycrystalline viscoelastic material for which the acoustic propagation characteristics may be dependent on the growth and life history. The principal areas of concern to be resolved before ice thickness can be reliably measured acoustically are the velocity and attenuation of the various acoustic modes in the medium and the acoustic impedance mismatch of the ice-water interface.

The acoustic velocity data reported for both fresh and saline ice have been acquired by one of three techniques:

- A. Seismics,²⁻⁷ where the bulk sound velocities are determined indirectly from measurements of the longitudinal plate waves. Although this technique is satisfactory for "order of magnitude" estimations, it does contain several deficiencies which include:
 1. The propagation velocities of the plate wave are highly dispersive with the thickness of the medium as was theoretically predicted by Lamb,⁸ Osborn and Hart,⁹ and Bunney and Goodman¹⁰ and experimentally verified by Bunney et al.¹¹ Therefore,

unless the experimenter is very careful to assure that the wavelength is long compared to the ice thickness, large variations in the measured velocity can occur.

2. The medium is anisotropic, and therefore exhibits no true "bulk velocity." Thus, measurements of long-range acoustic propagation in the ice layer yield information on only one component of the velocity vector, and even this is based on the assumption that the medium is homogeneous which, of course, it is not.
 3. Because of the distances involved with this technique, the data received at the sensor have been both temporally and spatially averaged. The information received therefore gives little detail regarding the microstructure of the medium.
- B. Resonance methods,^{12,13} where the velocities in the medium are related to the normal modes of vibration of the sample. With this technique it must be assumed that the test section being measured is homogeneous because inconsistencies in the material will generate dispersive effects thereby altering the measured nodes and antinodes of the resonant column. For natural sea ice, this is an invalid assumption.
- C. Direct determination of the velocity by measuring the time of flight of an acoustic pulse traversing ice samples of known thickness. Research using this technique has been related to velocity measurements in single ice crystals,^{14,15} measurements of lake ice and/or commercially available isotropic ice,¹⁶⁻¹⁸ or quasi in situ velocity measurements in sea ice.¹⁹⁻²¹ Of the latter, only Bunney and Hanse have reported the internal velocity structure of the medium and related it to values of previously measured bulk wave properties.

The attenuation of a sound wave propagating in a material that is not perfectly elastic, homogeneous and isotropic can be considered to be the result of two mechanisms: (1) dissipation processes originating from internal friction, anelastic behavior of the material, thermal dissipation, viscous slippage at crystal boundaries, etc., and (2) scattering originating from the interaction of the acoustic wave with scattering centers in the medium. The relative contribution of each of these mechanisms to the total attenuation depends on the frequency of the sound wave. At low frequencies, the wavelength of the sound is very large compared to the scattering centers; the scattering cross section, i.e., the relative amount of energy scattered out of the incident wave, is therefore extremely small and the attenuation is due almost entirely to dissipation. As the frequency increases, the attenuation due to scattering becomes more important until, when the wavelength becomes approximately on the order of the size of the scattering center, scattering predominates. The attenuation of the compressional wave has been experimentally measured by Pounder and Langleben,²² and the attenuation of both the transverse and compressional waves in annual sea ice has been mathematically approximated by Hanse and Bunney.^{23,24}

Although similarities exist between sea and freshwater ice, the differences in structure and composition are sufficient to preclude mutual substitution of experimental data. For a detailed comparison of freshwater ice and sea ice, the reader is referred to the excellent text on the subject by Pounder.¹⁹ It should also be pointed out that Hunkins⁴ has demonstrated that the physical properties of sea ice exhibit large seasonal variations. Perennial ice, that which has existed for more than one season, changes through the process of free flooding during the summer months and differs greatly from annual ice, that which is less than 1 year old.

EXPERIMENTAL TECHNIQUE AND RESULTS

The experiments reported here were performed in the Chukchi Sea near Pt. Barrow, Alaska, during March 1973. A comparative study of the acoustic properties of annual and perennial ice during this season was planned, but only annual ice samples were available because of unavoidable logistic difficulties. A comprehensive investigation of the acoustic properties of first year sea ice was therefore performed. The data presented are from that portion of the study that utilized direct measurement techniques to determine the depth dependence of the acoustic parameters.

RESULTS OF EXPERIMENTAL MEASUREMENTS

Numerous ice samples were acquired by extracting vertical cores from the ice canopy with a 10-cm diameter SIPRE coring tool. The average depth of the ice was approximately 145 cm and, with the exception of one core where the skeleton structure of the ice-water interface was lost, the lengths of the recovered samples were within 2 cm of the measured ice depth. The temperature profile was obtained by inserting a thermometer in small holes drilled along the extent of the core at 6-7 cm increments. The first temperature taken was near the bottom of the core because of the large temperature difference between that location and the ambient. The composite* results of the temperature tests for all cores are given in Figure 1. It is obvious that the technique employed, although used in similar experiments,^{16,17} is not adequate to predict the temperature profile. Even after 2 or 3 minutes the bottom of the core cools by 4-5°. Because 15-20 minutes were required to obtain an entire contour by this method, errors of 10°C or more are likely. As will be explained later, the best estimate of the core's temperature profile during the experiment is given by

$$T = (0.137z - 21.7)^{\circ}\text{C} \quad , \quad (1)$$

where z is the depth from the surface in centimeters and the average ambient air temperature was -21.7°C . This gradient is shown as the broken line on Figure 1.

*The data points presented in Figures 1 and 3-6 were obtained by plotting the raw data as a function of depth from the surface, interpolating between points and then averaging over all samples at 5-cm increments.

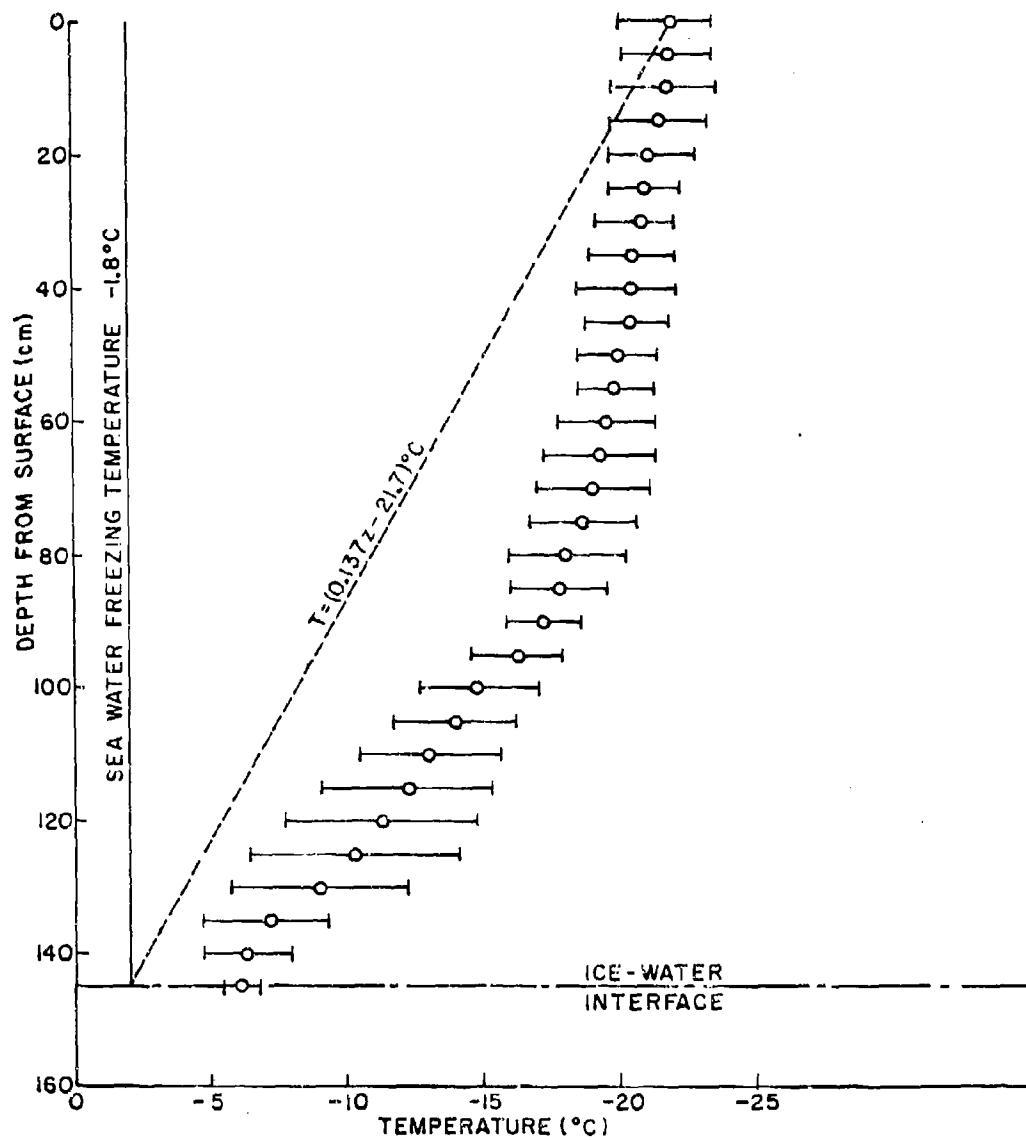


Figure 1. Measured temperature profile vs depth from surface of ice (lines extending from data points represent data spread).

After the temperature measurements, the cores were cut into lengths of 6 or 7 cm and each segment was referenced relative to its position in the sample. The compressional wave velocities parallel and perpendicular to the sample axis were then obtained for each section using the instrumentation diagramed in Figure 2. In this system, a pulse timing generator furnishes pulse length and rate information to a pulsed power oscillator and a trigger signal to the oscilloscope. The oscillator in turn provides a cw pulse of the desired frequency, rate and length to a BaTiO₃ transducer coupled to the sample. The transmitted acoustic signal is received by a second transducer coupled to the opposite side of the test section, amplified, and transmitted to the oscilloscope. The time of flight of the acoustic pulse in the sample is determined by measuring with a calibrated time delay the oscilloscope sweep time from the origin to the first received signal, and then correcting for electronic time losses (7 μ sec for this system). Knowing the specimen length, the velocities can then be calculated. This method is accurate to approximately 1-1/2%, where the largest error is related to the length measurement.

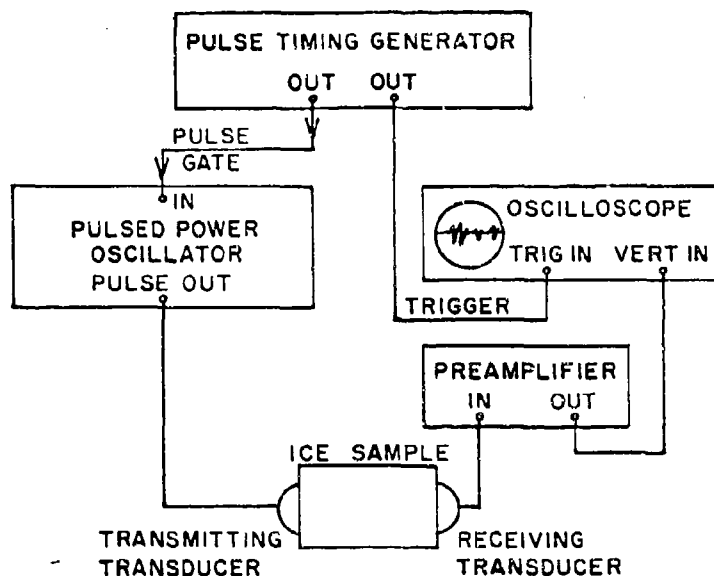


Figure 2. Block diagram of instrumentation for acoustic velocity measurements.

Figures 3 and 4 show the results of the velocity measurements. The velocity profiles exhibited in the graphs increase rapidly for the first 50-55 cm, and then decrease to minima at ~70 cm depth. It is unlikely that these minima are characteristic of all annual sea ice because the ice had obviously undergone severe "rafting" earlier in the growth season. Visual inspection of the cores revealed a "frazil" layer in the region of 70 cm indicating that the area had been "rafted" at least once. Below the 70-cm minima the profiles increase again to maxima at roughly 100 cm and then decrease toward the seawater sound velocity at the ice-water

interface. The average velocities measured for the vertical and horizontal directions were 3840 m/sec and 3635 m/sec, respectively. The velocities compare favorably with results obtained by the bulk velocity measurements reported by other investigators as shown in Table I, page 9.

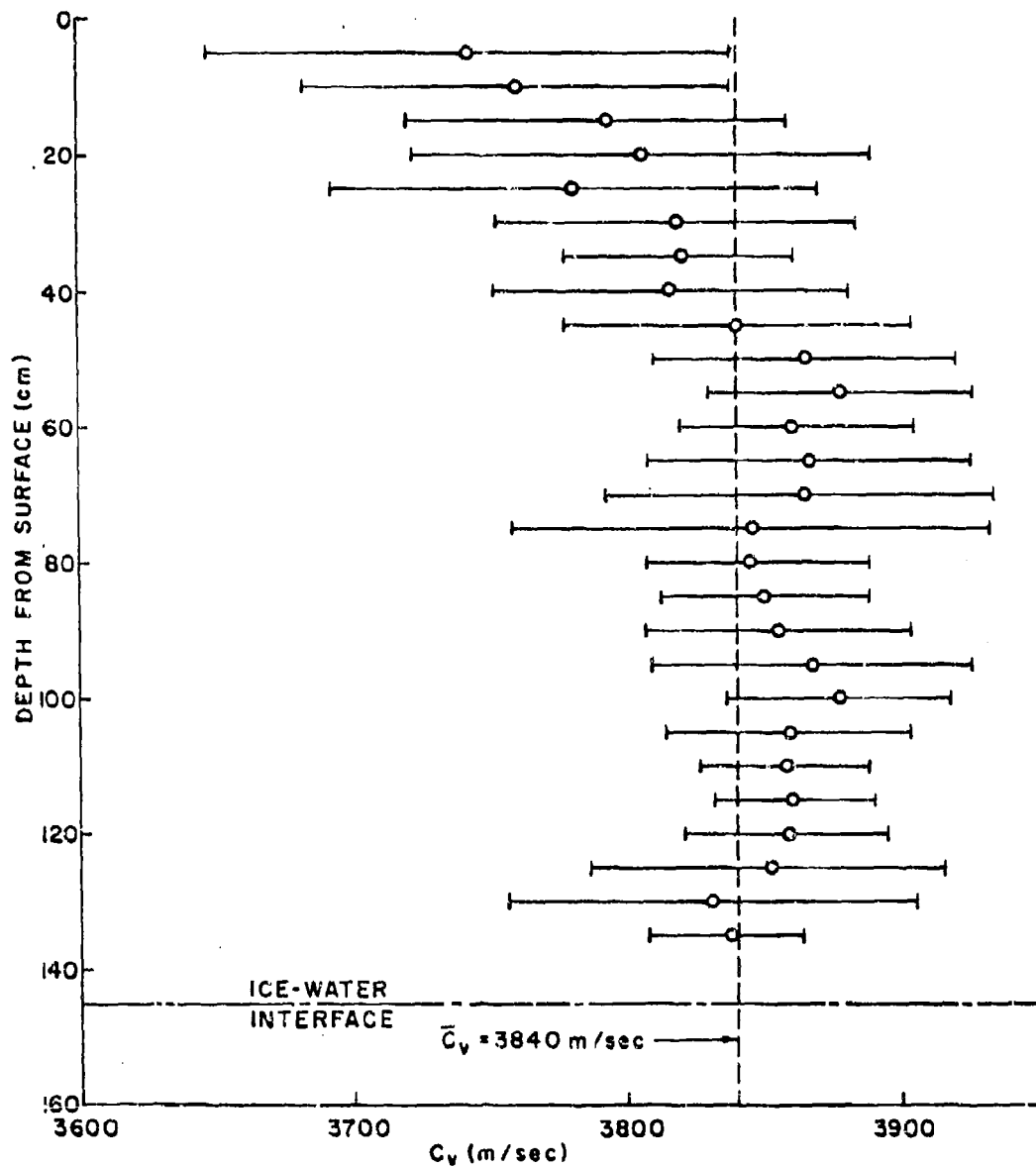


Figure 3. Longitudinal velocity parallel to sample axis as a function of depth from the ice surface (lines extending from data points represent data spread).

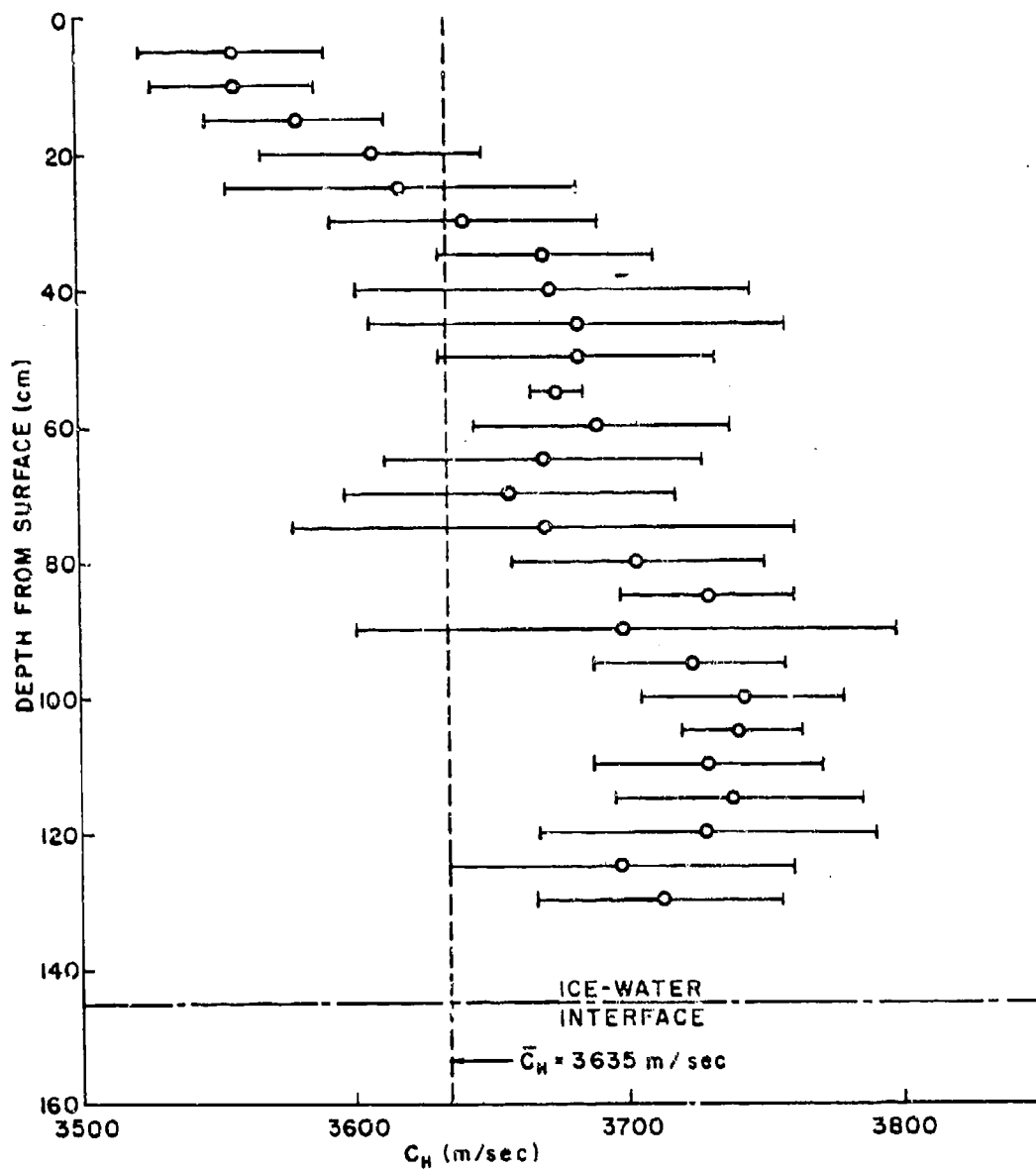


Figure 4. Longitudinal velocity perpendicular to sample axis as a function of depth from the ice surface (lines extending from data points represent data spread).

Ref. No.	Principal Author	Vertical Long. Velocity (m/sec)	Horiz. Long. Velocity (m/sec)	Density (g/cc)	Young's Modulus (dyn/cm ²)	Poisson's Ratio	Trans. ^a Velocity (m/sec)	Shear Modulus (dyn/cm ²)	Lame' Constant (dyn/cm ²)
2	Ewing		3410	0.917 ^b	9.17x10 ¹⁰	0.365		3.36x10 ¹⁰	9.1x10 ¹⁰
2	Ewing						1846		
3 ^c	Oliver		3143	0.90	5.63x10 ¹⁰	0.343		2.1x10 ¹⁰	4.8x10 ¹⁰
4	Hunkins		5344	0.89	8.6x10 ¹⁰	0.382	1856	3.1x10 ¹⁰	10x10 ¹⁰
5	Clarke	3817		0.907					
6	Crary				8.5x10 ¹⁰	0.345	1841	3.1x10 ¹⁰	7.0x10 ¹⁰
15 ^d	Bogorodskii	3800	3300				1770		
16	Roethlisberger	3960	3720				1840		
17 ^c	Pounder		3550	0.941	7.98x10 ¹⁰	0.39			
	This Experiment ^c	3840	3635	0.943	8.81x10 ^{10e}	0.342 ^e	1874 ^e	3.32x10 ^{10e}	7.27x10 ^{10e}

a. Vertically polarized

b. Assumed values

c. Averaged over data presented

d. Measured at 0°C

e. Calculated values

Table I. Comparison of reported data for acoustic velocities and elastic moduli.

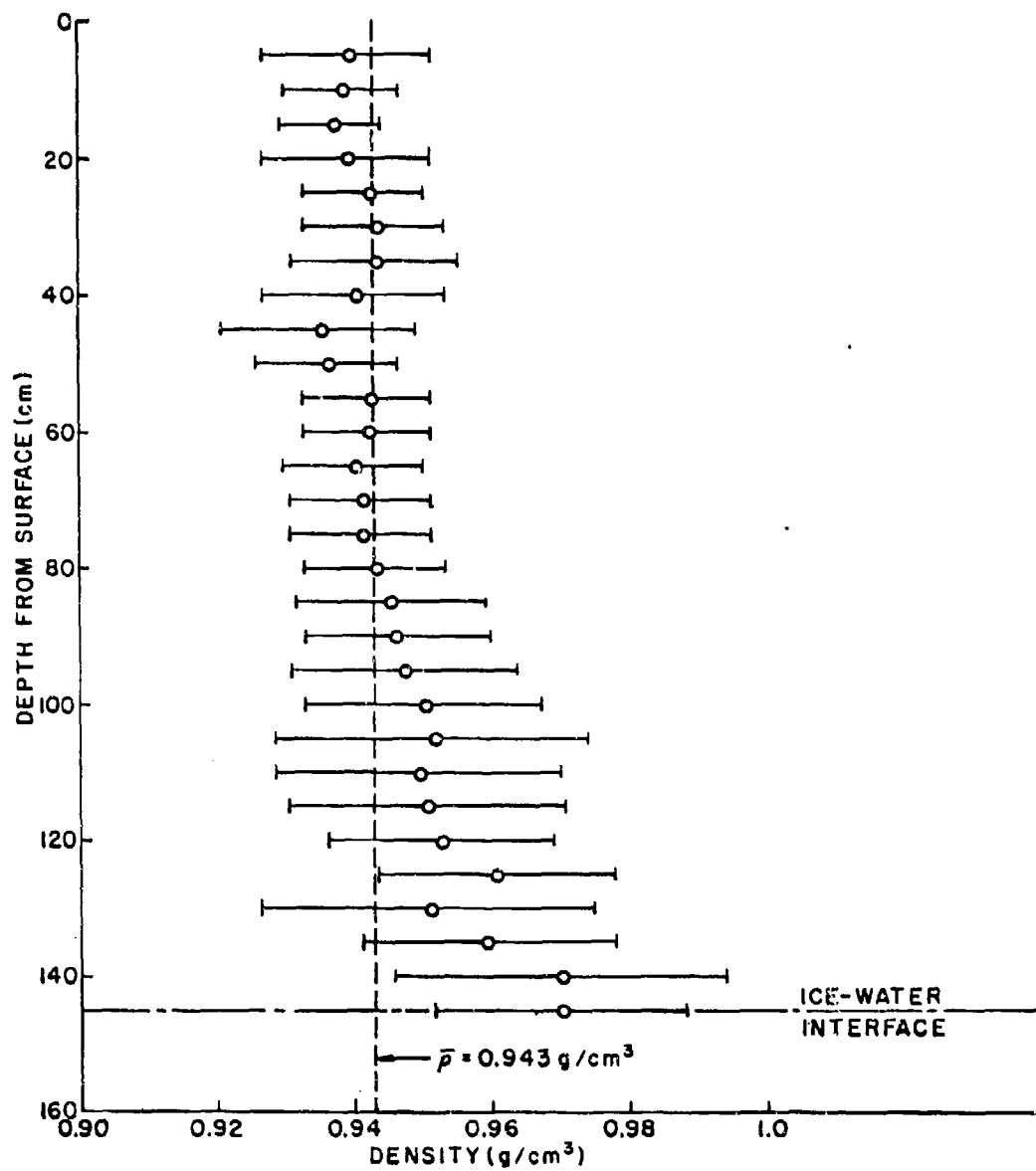


Figure 5. Density as a function of depth from the ice surface (lines extending from data points represent data spread).

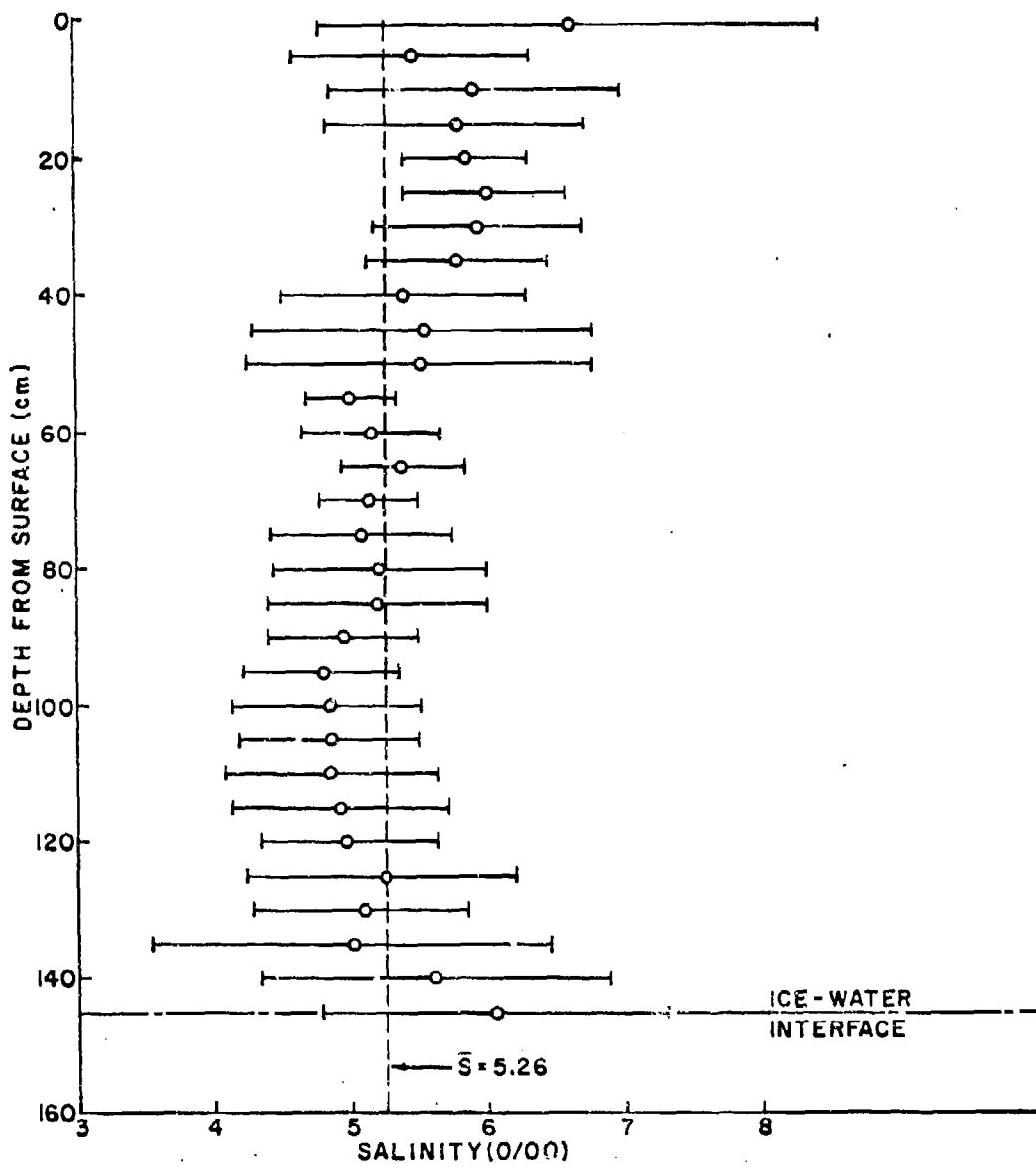


Figure 6. Salinity as a function of depth from the ice surface (lines extending from data points represent data spread).

The experimental results of the sample density measurements are shown in Figure 5 and demonstrate that for depths greater than approximately 100 cm the density increases markedly, indicating a higher liquid saturation. From the "idealized" temperature gradient shown in Figure 1, the in situ medium is predicted to have a temperature of -8.0°C at depths greater than 100 cm. Pounder¹⁹ and Assur²⁰ show that as the temperature of ideal seawater is lowered through the freezing point a two-part system consisting of solid H_2O and uniform brine is formed. Continuing to lower the temperature results in the solidification of sodium sulfate at about -8°C forming a three-part system of solid H_2O , solid $\text{Na}_2\text{SO}_4 \cdot 10\text{H}_2\text{O}$ and brine. This situation exists to approximately -22°C where sodium chloride ($\text{NaCl} \cdot 2\text{H}_2\text{O}$) solidifies. Thus, the increase in density below depths of 100 cm is due to the decreasing amount of solid salt present.

After the temperature and density measurements, the segments were melted and the salinity was measured. The average salinity profile is shown in Figure 6. Although not as large as expected, particularly near the bottom, the depth contour is characteristic, showing increased salinity near the top, which is caused by a thermal gradient across the elongated brine cells, and near the bottom because of gravity.

APPROXIMATION OF THE ELASTIC MODULI AND TRANSVERSE VELOCITY PROFILES

It was demonstrated earlier that the acoustic parameters measured exhibit dependence with depth into the medium. Utilizing the results of the reported experiment, an approximation to the structure and a prediction of the average values of the transverse velocity and elastic moduli can be made. To accomplish this it is assumed that the measurement frequency is sufficient to ignore the viscous terms in the propagation equation, or equivalently, that the viscous terms do not greatly affect the velocity. An elastic medium is thus assumed, for which, according to elasticity theory, the longitudinal and transverse wave velocities are given by

$$C_L = \sqrt{\frac{E}{\rho} \cdot \frac{(1-\sigma)}{(1+\sigma)(1-2\sigma)}} = \sqrt{\frac{\lambda+2\mu}{\rho}} \quad (2)$$

$$C_T = \sqrt{\frac{E}{\rho} \cdot \frac{1}{2(1+\sigma)}} = \sqrt{\frac{\mu}{\rho}}$$

where

- C_L is the velocity of the longitudinal wave
- C_T is the velocity of the transverse wave
- E is Young's modulus
- μ is the shear modulus
- λ is the Lamé constant

ρ is the density of the medium

σ is Poisson's ratio.

There are two empirical equations in the literature that associate Young's modulus (E) with the chemical properties of the medium. Pounder and Stalinski¹⁷ related this parameter to the salinity (S) by

$$E = (9.75 - 0.242 S) \times 10^{10} \text{ dyn/cm}^2 ; \quad (3)$$

however, their work was performed at constant temperature. Langleben¹⁸ related Young's modulus to the brine content (ν) by

$$E = (10.0 - 35.1 \nu) \times 10^{10} \text{ dyn/cm}^2 . \quad (4)$$

The brine content in this equation can be determined from the salinity and temperature by the relations²⁵

$$\begin{aligned} \nu &= S \left(\frac{52.56}{|\theta|} - 2.28 \right) & -2.06^\circ \leq \theta \leq -0.5^\circ \\ \nu &= S \left(\frac{45.917}{|\theta|} + 0.930 \right) & -8.2^\circ \leq \theta \leq -2.06^\circ \\ \nu &= S \left(\frac{43.795}{|\theta|} + 1.189 \right) & -22.9^\circ \leq \theta \leq -8.2^\circ \end{aligned} \quad (5)$$

where

S is the salinity in parts per thousand

ν is the brine content in parts per thousand

θ is the temperature in degrees Celsius.

Because the temperature dependence is included in Eq. 5 it is expected to give a more accurate estimate of Young's modulus than Eq. 4.

As was discussed earlier, the method used to measure the temperature profile during the experiment could lead to large errors because of the temperature difference between the sample and ambient, and the time required to perform the tests. To reconstruct the in situ conditions, we have referred to Untersteiner's²⁶ approximation of the thermal conductivity in sea ice,

$$\kappa_i = \kappa_{i,f} + \frac{\beta S(z)}{T-273} , \quad (6)$$

where

S(z) = salinity at depth z

$\beta = 0.28 \text{ cal cm}^2/\text{g sec}$

$\kappa_{if} = 0.00486 \text{ cal/cm sec } ^\circ\text{K}$

T = temperature in degrees Kelvin.

Examination shows that for absolute temperature values greater than a few degrees and salinities on the order of a few parts per thousand, the second term of this equation can be neglected, yielding a constant thermal conductivity. These conditions are applicable to the problem being discussed, and allow the assumption of a linear temperature gradient between the average ambient during the experiment (-21.7°C) and the seawater freezing temperature (-1.8°C).

Thus, using the relationship

$$T = (0.137z - 21.7)^{\circ}\text{C}$$

and the experimental values of the longitudinal velocity, density and salinity, the depth dependence of the brine content can be approximated along with Young's modulus, Poisson's ratio, the transverse velocity, the shear modulus and the Lamé constant. The results of these calculations are shown in Figures 7 through 12.*

*Each of the results presented can be reduced to an empirical relationship with depth. However, the temptation to do so has been resisted because the data may be unique to the medium for the 1973 season. The dependency with depth shown in the figures has been derived from the raw data acquired and thus will show structure which may not be reproducible in future experiments.

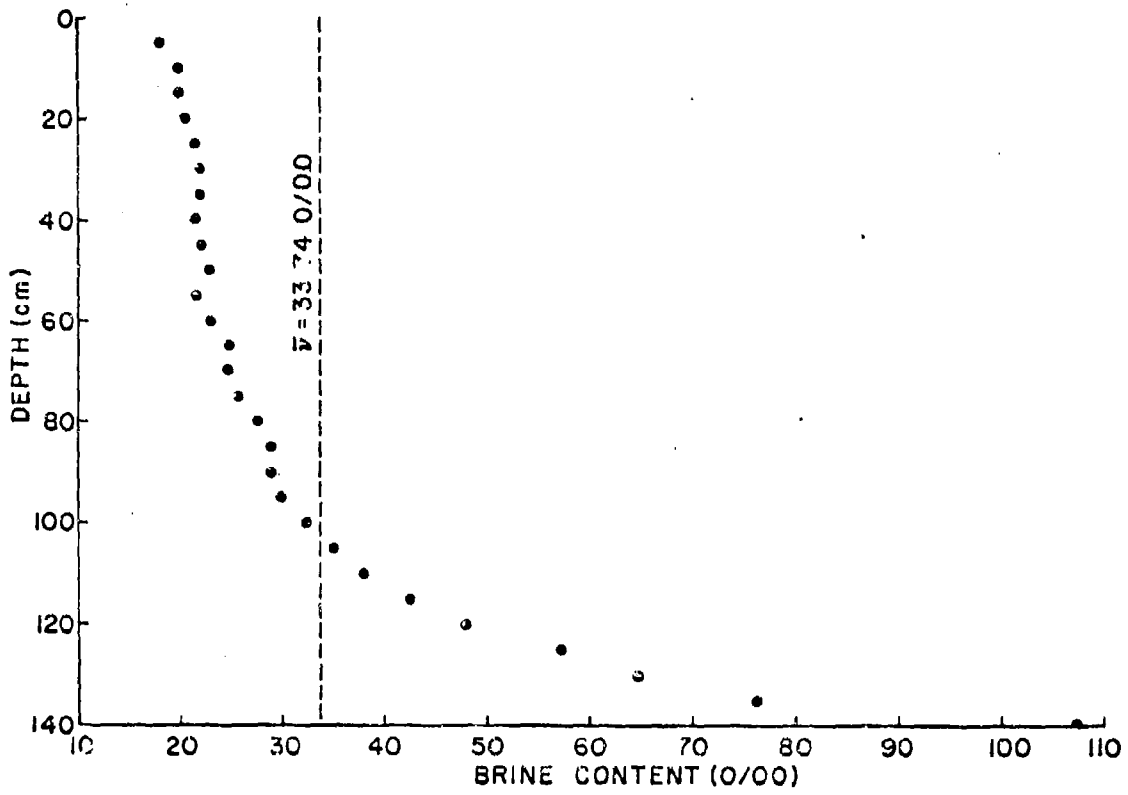


Figure 7. Calculated values of brine content vs depth from surface.

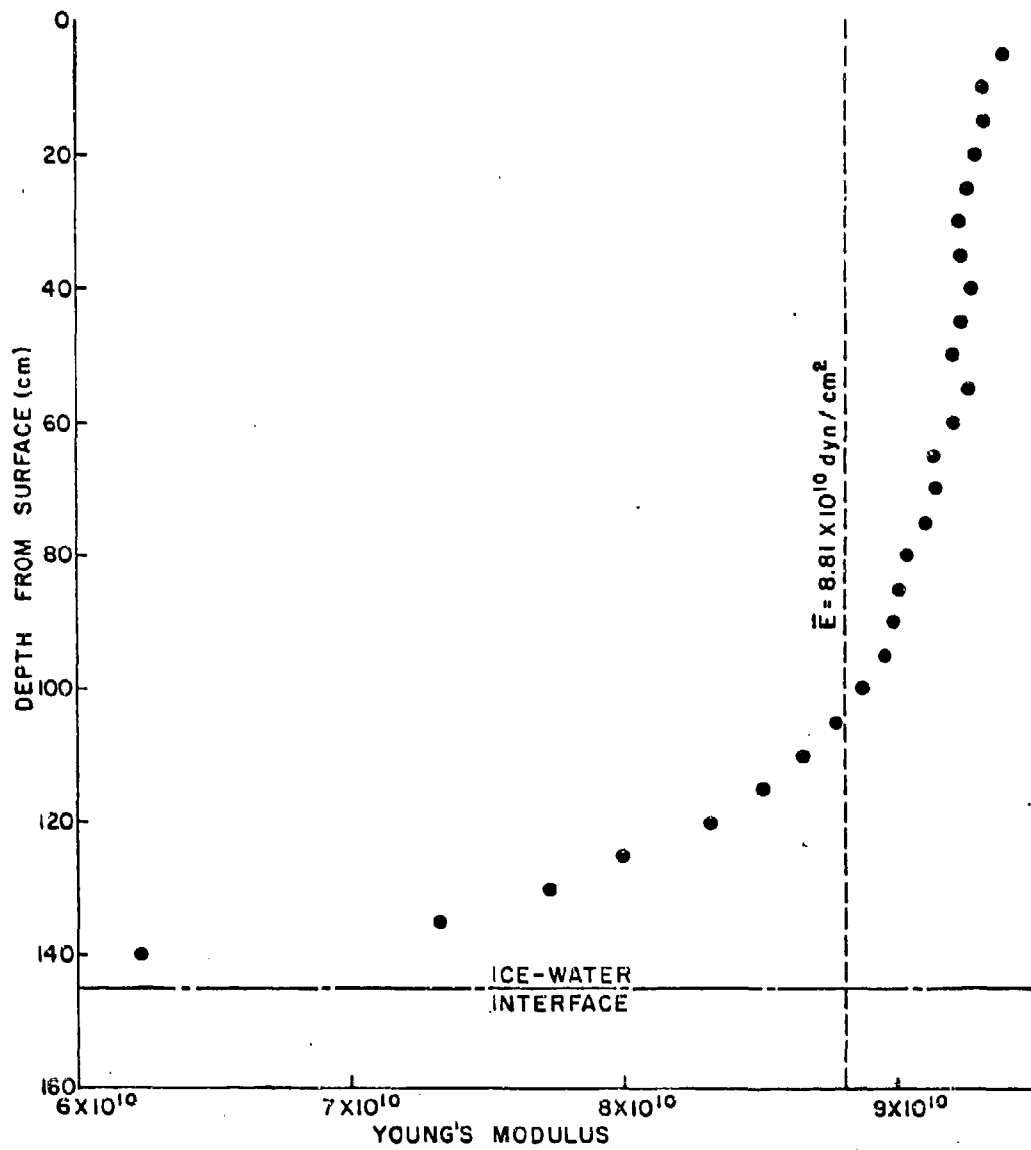


Figure 8. Predicted values of Young's modulus vs depth from surface.

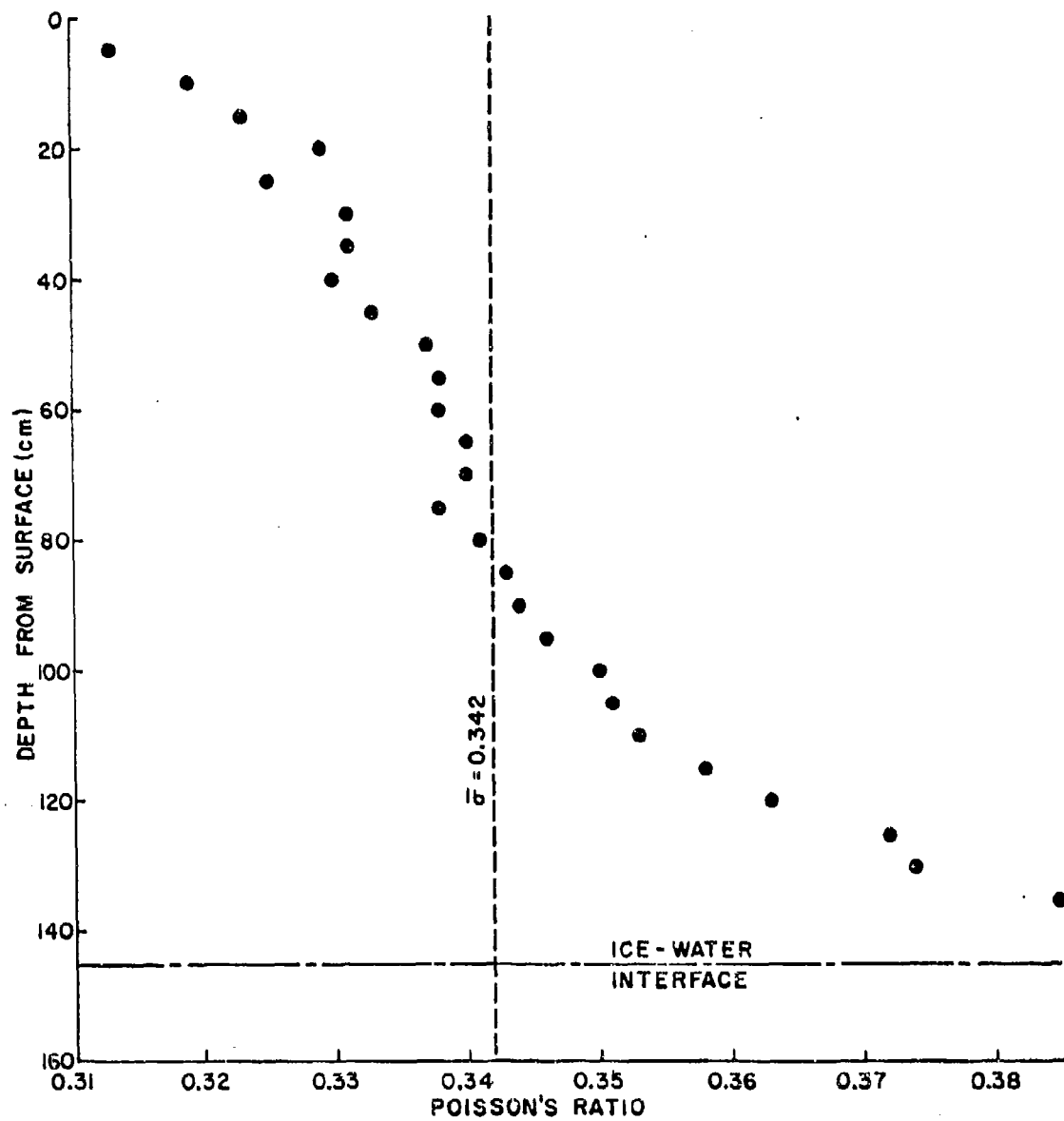


Figure 9. Predicted values of Poisson's ratio vs depth from surface.

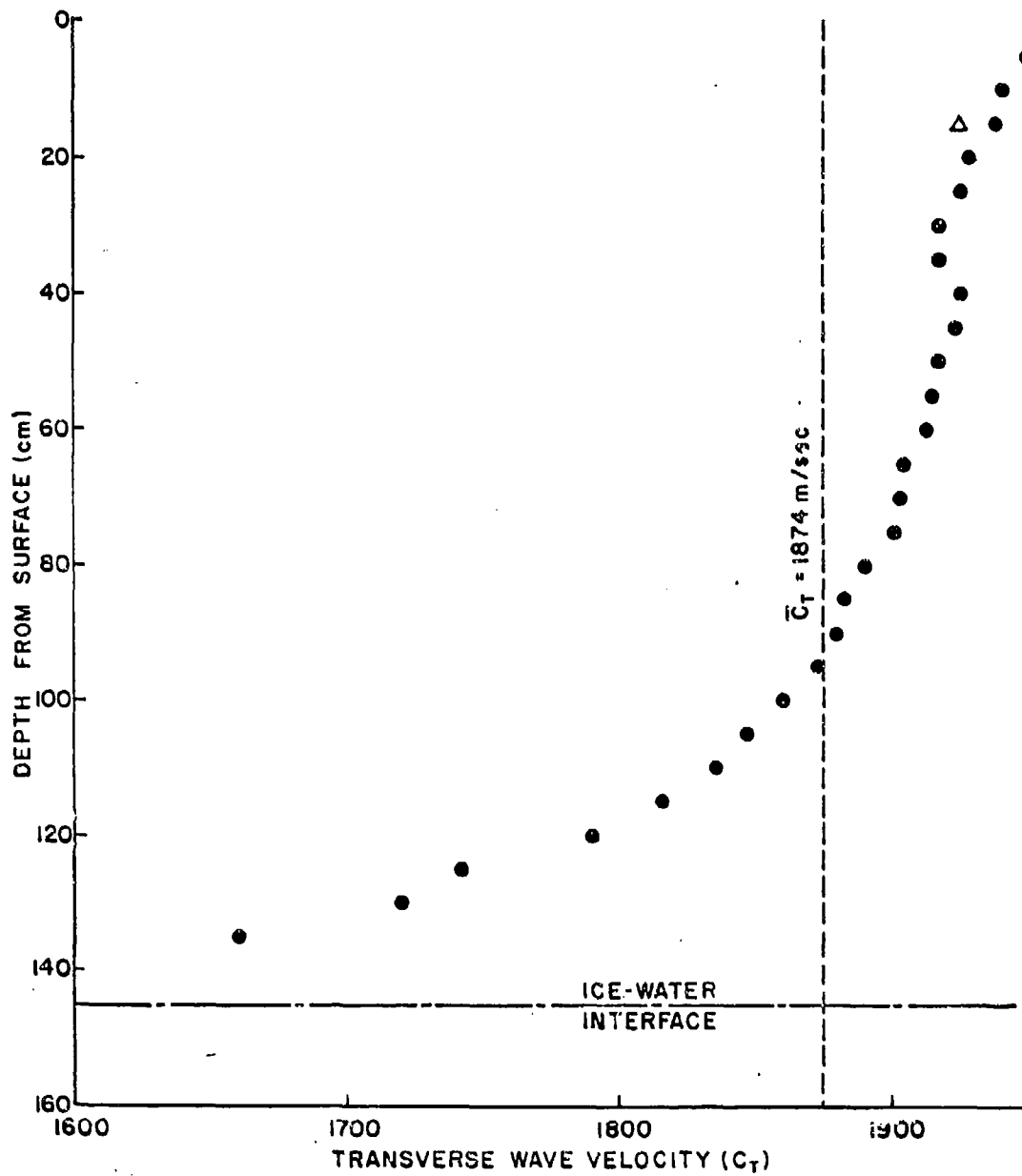


Figure 10. Predicted values of the transverse velocity vs depth from surface (Δ denotes a measured data point).

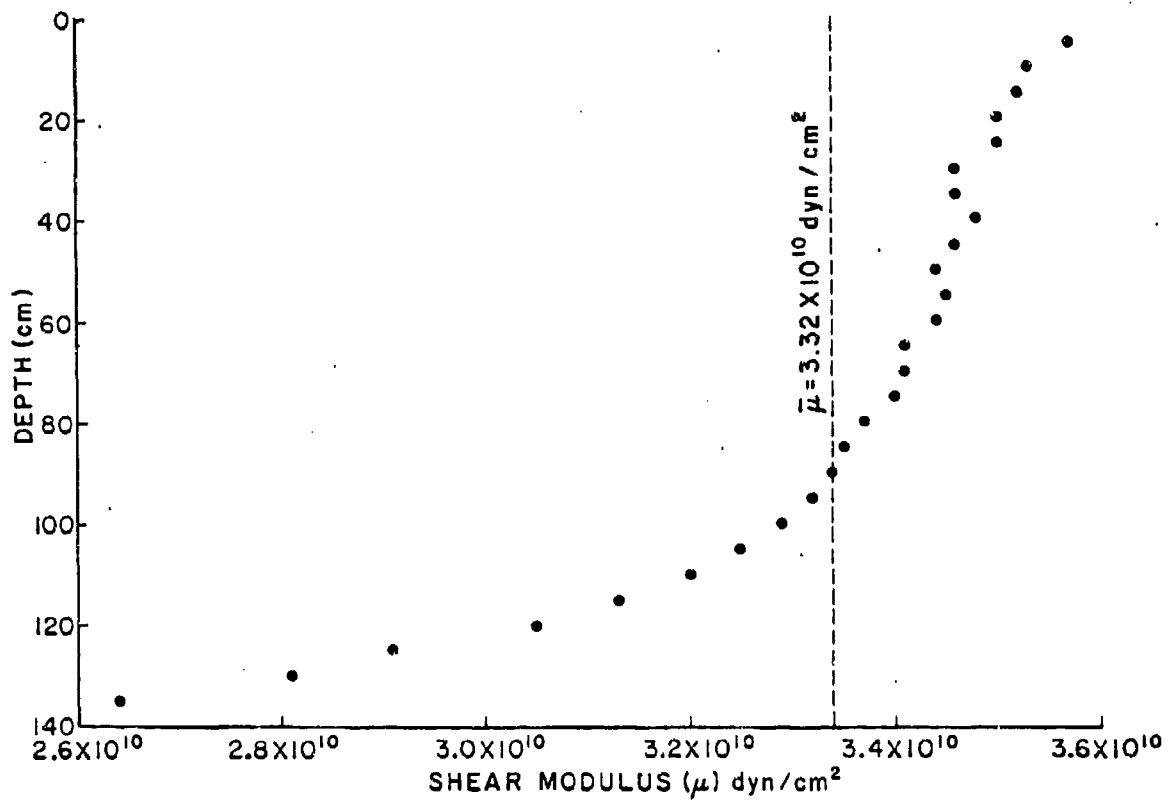


Figure 11. Predicted values of the shear modulus vs depth from surface.

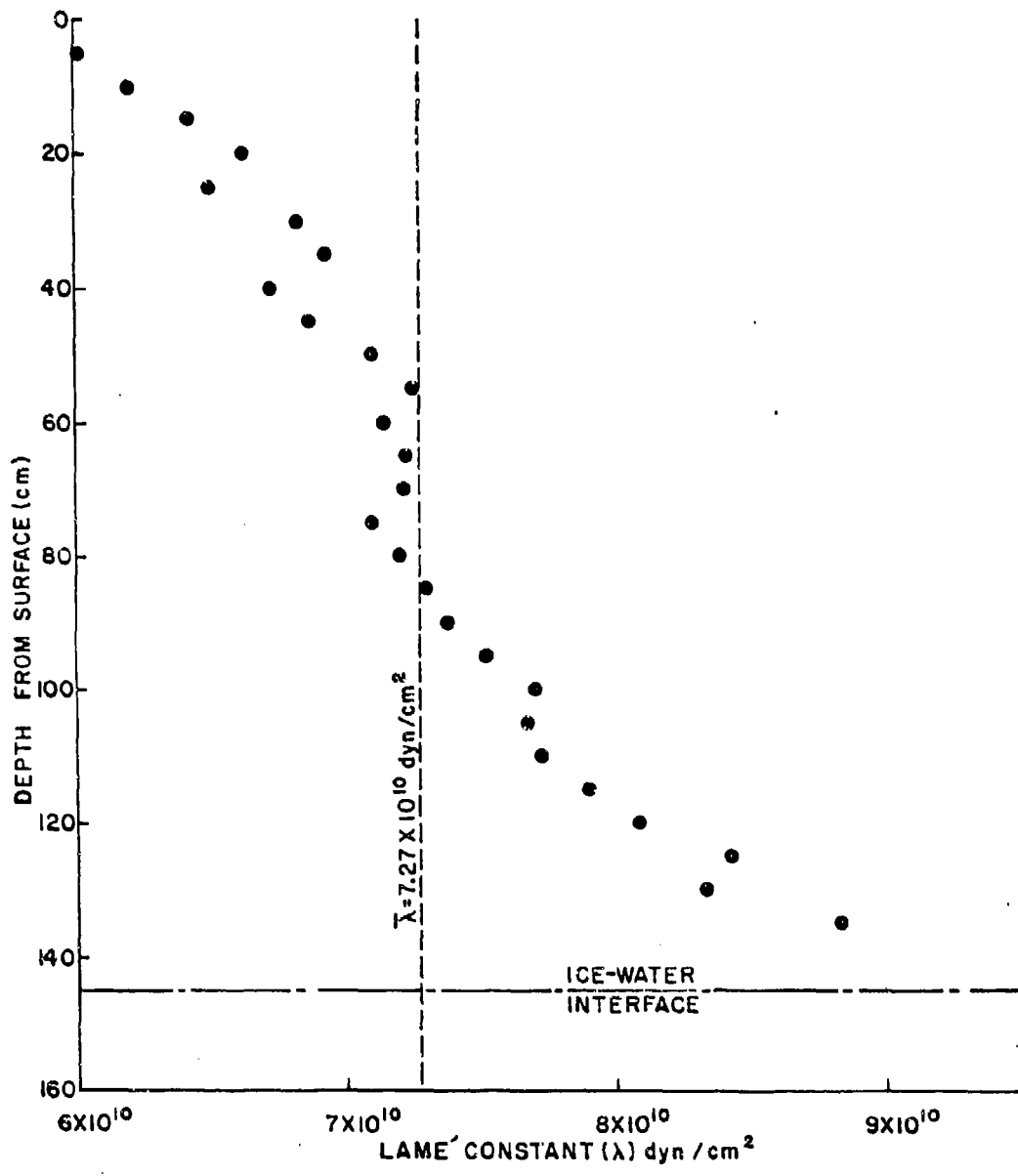


Figure 12. Predicted values of Lamé's constant vs depth from surface.

DISCUSSION OF THE RESULTS OF THE PROFILE MEASUREMENTS

In order to evaluate the credibility of the order of magnitude estimates, the results of our predictions and those reported by others are compared in Table I. Wide variations do occur for some of the values, but in general the predicted values and the average of the experimental data compare very well with those reported in the literature.

Shear wave velocity profile experiments have yet to be successfully performed in sea ice because of the difficulty in establishing a reliable bond between the ice and shear wave generating transducers. This difficulty is largely because the brine "leaches" and produces a highly saline, liquid surface layer. Washing the bonding surface with fresh water has been partially successful in laboratory and *in situ* tests. For example, the experiment shown in Figure 13 was attempted during the field tests reported here. Channels in the ice canopy were cut to a depth of ~45 cm and located a known distance apart. The sides of the channel were washed with fresh water to eliminate the saline boundary layer. The shear-sensitive transducers were quickly coupled to the ice on diametrically opposite sides of the test section at a depth of 15 cm. The electronics used were the same as shown in Figure 2. The time of flight and distance were measured, after which the sample size was incrementally decreased and the process repeated.

The average value of this measurement was 1923 m/sec and is shown as a triangle in Figure 10. Further laboratory measurements of shear wave velocity on sea ice samples show an average of 1870 m/sec, compared to a predicted average profile velocity of 1874 m/sec. Because sea ice is anisotropic, it should be pointed out that these values are for the vertically polarized shear wave. The horizontally polarized wave was measured in a separate experiment and will be discussed later in this report.

Figure 7 reinforces the earlier discussion on density by showing that the brine content increases rapidly for depths greater than 100 cm. However, unlike the "ideal" seawater case where the sodium sulfate solidifies discontinuously at approximately -8.0°C this calculation shows that at least some of the salts solidify uniformly with decreasing temperature.

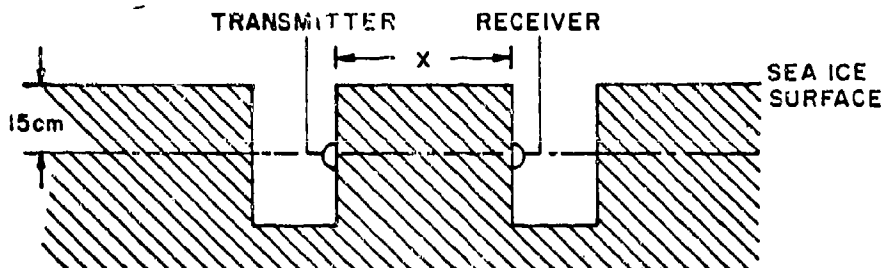


Figure 13. Cross section of *in situ* shear wave experiment.

Although Young's modulus (Figure 8) decreases precipitously below -8°C , indicating a rapid decrease in the material elasticity, the form of the shear modulus (Figure 11) is physically more interesting. Because this parameter must vanish at the ice-water interface, and because in the calculation it appears to be uniformly approaching that asymptote, it is not anticipated that a significant acoustic impedance mismatch for the shear wave will occur at the boundary. If the calculation were definitive, the interface would not be a good acoustic reflector for the transverse mode. However, since strong echoes of this mode have been observed in situ, it is obvious that greater consideration must be given to the theory for the transition region.

PREDICTIONS OF ACOUSTIC ATTENUATION IN SEA ICE

Before the feasibility of measuring sea ice thickness acoustically can be determined, the attenuation of sound in the medium as a function of frequency must be either measured or estimated. As discussed earlier, the attenuation of a sound wave propagating in a material that is not perfectly elastic, homogeneous and isotropic is largely dependent on two mechanisms: (1) dissipation processes originating from internal friction, anelastic behavior of the material, thermal dissipation, viscous slippage at crystal boundaries, etc., and (2) scattering originating from the interaction of the acoustic wave with scattering centers in the medium.

LONG WAVELENGTH ISOTROPIC SOLUTION

For wavelengths that are long compared to the size of the scattering center, the calculation of acoustic velocity and attenuation can be derived ignoring the contributions due to scattering. Even though not all of the internal mechanisms contributing to the dissipation processes are known, the general theory can be developed by grouping all attenuation into a common source. This is accomplished mathematically²⁷ by replacing the shear modulus (M) and the Lamé constant (Λ) in the elastic stress-strain relationship with the first order differential operators

$$\begin{aligned} M &= \mu + \mu' \frac{\partial}{\partial t} \\ \Lambda &= \lambda + \lambda' \frac{\partial}{\partial t} \end{aligned} \quad (7)$$

where the unprimed terms denote the elastic and the primed terms denote the viscous (or attenuative) contributions.

Consider an acoustic shear wave* moving in the positive (downward) z-direction. The displacement potential is given by

$$\psi = Ae^{i(\omega t - \alpha z)} \quad , \quad (8)$$

where

ω is the circular frequency
 t is the time
 α is the complex wavenumber.

This displacement potential obeys the wave equation

$$\rho \frac{\partial^2 \psi}{\partial t^2} = M \nabla^2 \psi \quad , \quad (9)$$

where ρ is the density of the medium and ∇^2 is the Laplacian operator. Substituting Eqs. 7 and 8 into Eq. 9 and carrying out the operations gives the relation

$$\rho \omega^2 = \alpha^2 (\mu + i\omega\mu') \quad , \quad (10)$$

where μ' is the dissipative coefficient. For an attenuative medium, the complex wavenumber can be written as

$$\alpha = k - i\tau \quad , \quad (11)$$

where

k is the running vector, ω/c
 c is the wave velocity
 τ is the generalized attenuation.

Making this substitution into Eq. 11 and separating the real and imaginary components yield the simultaneous equations

$$\begin{aligned} \rho \omega^2 &= \mu(k^2 - \tau^2) + 2\mu'\omega k\tau \\ 0 &= \omega\mu'(k^2 - \tau^2) - 2\mu k\tau \end{aligned} \quad (12)$$

Setting

$$R = \frac{\mu'}{\mu} \quad ,$$

*The derivation for the compressional wave propagation is similar to that presented here, the difference being the introduction of the $(\Lambda + 2M)$ operator in the wave equation, Eq. 9, rather than the shear modulus (M) operator. The displacement potential must, of course, be associated with the compressional rather than the transverse wave.

these equations have the solutions

$$\tau = \frac{k}{R\omega} \left\{ \sqrt{1 + R^2\omega^2} - 1 \right\} \quad (13)$$

$$k^2 = \frac{1}{2} \frac{\rho\omega^2}{\mu} \left\{ \frac{\sqrt{1 + R^2\omega^2} + 1}{1 + R^2\omega^2} \right\}$$

where both μ and R may be frequency dependent. The procedure from this point is to introduce a mathematical model of the medium composed of elastic and viscous constants that are frequency independent, and then fit the results to experimental data.

Maxwell²⁸ suggested that viscoelastic materials could be represented by an elastic element (spring) in series with a viscous element (dashpot) as shown in Figure 14. Voigt²⁹ placed these elements in parallel as in Figure 15. Detailed mathematical analyses of these as well as more complex models are covered in standard texts³⁰⁻³² and will not be discussed here. However, it can be shown that for the Maxwell model

$$\tau = \frac{k\eta_m\omega}{E_m} \left\{ \sqrt{1 + \left(\frac{E_m}{\eta_m\omega}\right)^2} - 1 \right\} \quad (14)$$

$$k^2 = \frac{\rho\omega^2}{2\mu} \left\{ \frac{\sqrt{1 + \left(\frac{E_m}{\eta_m\omega}\right)^2} + 1}{1 + \left(\frac{E_m}{\eta_m\omega}\right)^2} \right\}$$

where

$$\mu = \frac{E_m\omega^2}{\left(\frac{E_m}{\eta_m}\right)^2 + \omega^2} \quad (15)$$

and

$$R\omega = \frac{E_m}{\eta_m\omega} \quad (16)$$

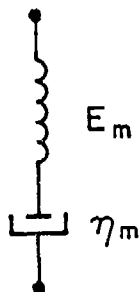


Figure 14. Maxwell's mechanical representation of viscoelastic solids.

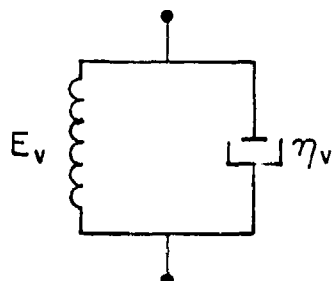


Figure 15. Voigt's mechanical representation of viscoelastic solids.

For the Voigt model

$$\tau = \frac{kE_v}{\eta_v \omega} \left\{ \sqrt{1 + \left(\frac{\eta_v}{E_v} \omega\right)^2} - 1 \right\} \quad (17)$$

$$k^2 = \frac{1}{2} \frac{\rho \omega^2}{E_v} \left\{ \frac{\sqrt{1 + \left(\frac{\eta_v}{E_v} \omega\right)^2} + 1}{1 + \left(\frac{\eta_v}{E_v} \omega\right)^2} \right\},$$

where

$$\begin{aligned} \mu &= E_v \\ R\omega &= (E_v/\eta_v)\omega \end{aligned} \quad (18)$$

Very few solids behave like either the Maxwell or the Voigt model. However, since more complicated models become extremely involved mathematically, and because models specifying a greater number of parameters

require more experimental evidence to substantiate their validity, using a single Maxwell or Voigt element is a convenient method of obtaining a first order approximation of a viscoelastic solid's mechanical properties. This is especially true if there are only limited data on the material, as is the case for sea ice.

SHORT WAVELENGTH SOLUTION

When sea ice freezes, the brine in the water concentrates in small pockets. The result is frozen water with imbedded scattering centers filled with a highly saline brine. Although these inclusions can have various geometries, the author has observed that the vast majority in annual sea ice are spheroidal. This may not hold for other types of sea ice, e.g., multi-year ice, but the acoustic and microscopic analysis necessary for evaluation of other types of sea ice has not been done. For the purposes of this calculation, it will be assumed that all of the scattering centers are brine-filled spheres.

To evaluate the attenuation due to scattering, distribution functions in the medium must be either known or assumed. Because the necessary data are presently unavailable, and to minimize the complexity of the calculation, the following assumptions have been made:

- (a) No interaction exists between the scattering centers, and the wave, once scattered, will not be re-scattered back into the sound beam. Since second order scattering should have only a small effect, particularly in the Rayleigh scattering region, this assumption should not greatly affect the calculation accuracy.
- (b) There are N scattering centers per unit volume and the centers are uniformly distributed throughout the medium. From observations in the laboratory, this assumption appears to be reasonably valid.
- (c) All of the scattering centers are the same size, with a radius a_0 . In fact, the brine pocket sizes vary widely; however, if radius a_0 is selected as the average bubble size, then it can be argued that only the larger bubbles in the distribution will significantly affect the scattering.

Using these assumptions, the attenuation due to scattering can be written

$$\alpha_{\text{scattering}} = \frac{N}{2} \gamma(a_0) \quad (19)$$

where $\gamma(a_0)$ is the scattering cross section of a single scatterer of radius a_0 (see Appendix A for the cross section calculation). Because of (c), above, this equation predicts the minimum attenuation to be expected from this mechanism.

Laboratory measurements of scattering centers in annual sea ice give radii on the order of 0.065 cm and concentrations on the order of 25 holes per cubic centimeter. Using the results of the cross section calculation in Appendix A and the relation

$$ka = \frac{2\pi\nu}{c} a \quad (20)$$

where ν is the frequency in hertz, c is the velocity in centimeters/second, and a is the radius in centimeters, the attenuation due to scattering for values of $ka < 1$ and $ka > 15$ can be approximated by

$$\alpha_{\text{shear}} = \frac{\nu^4}{4.403 \times 10^{-5} + 6.097 \times 10^{-4} \nu^{2.2}} \text{ dB/m} \quad (21)$$

and

$$\alpha_{\text{comp}} = \frac{\nu^4}{2.294 \times 10^{-3} + 3.253 \times 10^{-3} \nu^4} \text{ dB/m} \quad (22)$$

where ν is in megahertz. For values of $1 < ka < 15$, the approximations of Eqs. 21 and 22 are still more or less valid for order of magnitude calculations, but will invariably yield predictions that are significantly low.

TOTAL ATTENUATION APPROXIMATION

As was discussed earlier, the attenuation in sea ice is composed of two parts,

$$\alpha = \alpha_{\text{dissipation}} + \alpha_{\text{scattering}} \quad (23)$$

Before the total attenuation can be estimated, the attenuation due to dissipation must be considered. The experiment shown in Figure 13 gives the results necessary for an approximation to the solution of the two-element models. During this experiment, the total attenuation and velocity were measured in situ 15 cm below the surface in annual sea ice. At 100 kHz, the results of these measurements gave a longitudinal wave velocity of 3790 m/sec, a vertically polarized shear wave velocity of 1923 m/sec, an average density of 0.937 g/cm³, and a generalized attenuation of 0.18 dB/cm. Using these values, and assuming the elastic and viscous constants to be frequency independent, both the Voigt and the Maxwell models were solved as a function of frequency. The results are shown in Figure 16, along with the scattering attenuation for the shear wave. From this representation, it can be concluded that for frequencies above approximately 5 kHz the Maxwell model fails because in nature there is no observed frequency region over which the attenuation remains constant. Thus, assuming the Voigt solution, the total attenuation can be approximated by

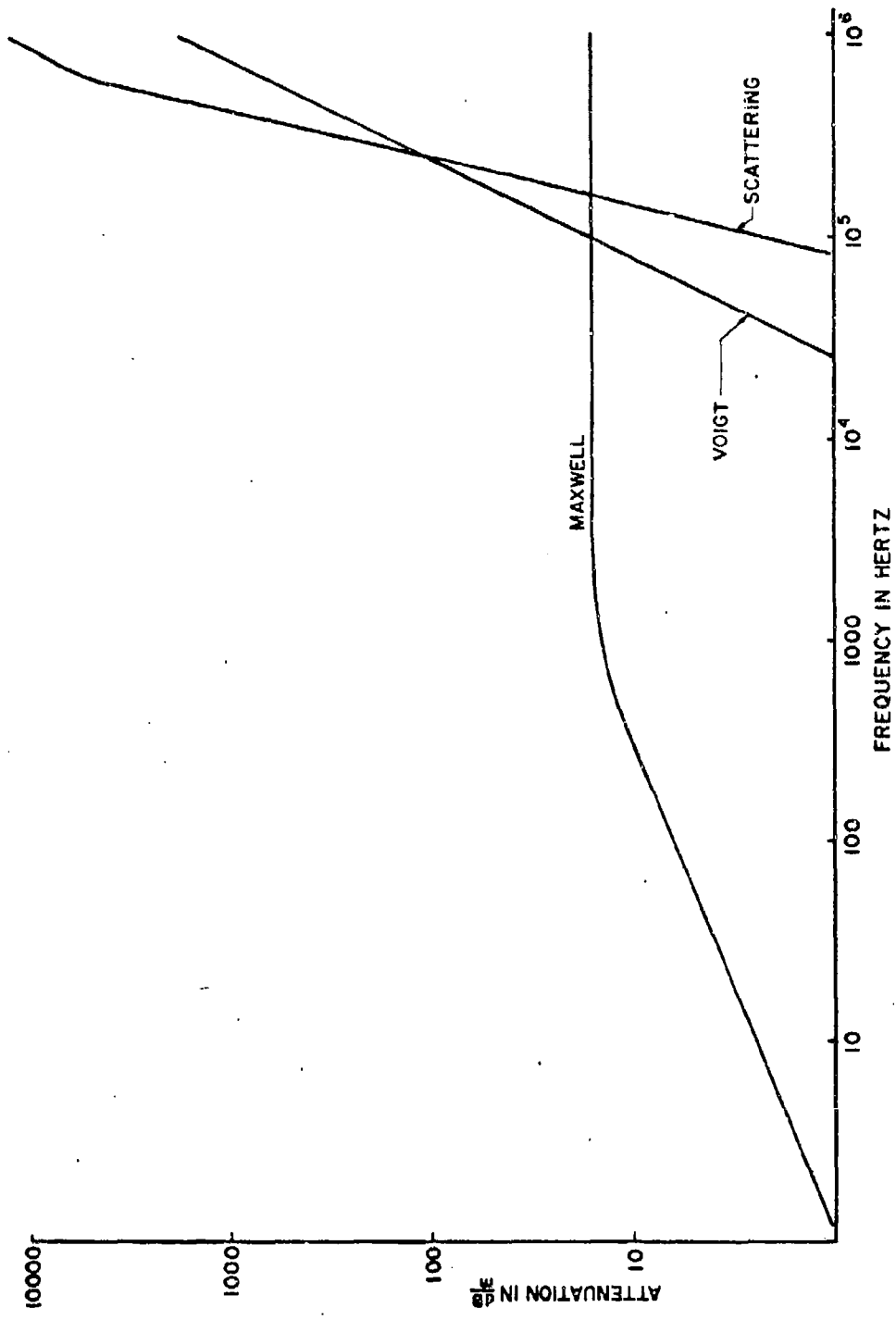


Figure 16. Attenuation contributions of the Maxwell Model, the Voigt Model and scattering.

$$\alpha_{\text{comp}} = \frac{v^4}{2.294 \times 10^{-3} + 3.253 \times 10^{-3} v^4} + \frac{k_c}{1.444v} \left\{ \sqrt{1+276.4v^2} - 1 \right\} \quad (24)$$

$$\alpha_{\text{shear}} = \frac{v^4}{4.403 \times 10^{-5} + 6.097 \times 10^{-4} v^{2.2}} + \frac{k_s}{0.895v} \left\{ \sqrt{1+106.1v^2} - 1 \right\},$$

where

$$k_c^2 = 658.4v^2 \left\{ \frac{\sqrt{1+276.4v^2} + 1}{1+276.4v} \right\} \quad (25)$$

$$k_s^2 = 903.1v^2 \left\{ \frac{\sqrt{1+106.1v^2} + 1}{1+106.1v^2} \right\}$$

and v is in megahertz.

The solution to Eq. 24 is shown in Figure 17 along with some experimental data of Langleben and Pounder²² on compressional wave attenuation taken *in situ* in Tanquary Fiord, Ellesmere Island, during 1967. Although it appears that the theory predicts values of attenuation several decibels too high in the 1-5 kHz region, the form of the frequency dependence is consistent in that the form of the observed relaxation is predicted. Further, the fact that the theory is quite sensitive to the radius of the scattering centers could account for this difference between the prediction and the observed data. Differences in brine pocket sizes and hence deviations in the attenuation could be expected in any event, since Langleben measured the attenuation on 2-year sea ice in a fiord, while the curves were empirically fit to data obtained on annual ice in the Arctic Ocean.

DEPTH DEPENDENCE OF THE ATTENUATION

The recent experimental measurements by the author²¹ have demonstrated that for annual sea ice the velocity of longitudinal waves exhibits dependence on the depth into the medium because of variations in density, salinity, and temperature. From these data a shear wave velocity profile was calculated which predicted a continuous decrease with depth.

Unfortunately, sufficient data do not exist to similarly predict the depth dependence for attenuation. For this determination, the form of both the elastic and viscous coefficients must be known. However, if a near-elastic medium is assumed, it can be shown that for a Voigt solid

$$\tau = \frac{\rho n \omega^2}{2C^3} \quad (26)$$

Therefore, provided the depth dependence of the viscosity (η) does not decrease faster than C^3 , the attenuation will increase with depth.

ACOUSTIC REFLECTIVITY AT THE ICE-WATER INTERFACE

In considering the feasibility of using acoustic techniques to measure ice thickness, a major factor will be the amount of energy reflected from the ice-water interface. For an acoustic wave incident on a boundary between two ideal media, the relative energy distribution calculation is straightforward and is presented in detail in Appendix A. The resulting equations were solved using average values for the density and the compressional and transverse velocity of sea ice as determined in a previous section of this report. The solution for the compressional and transverse waves is shown in Figures 18 and 19, respectively.

Neglecting attenuation effects, this simple model indicates that at normal or near normal incidence the most efficient method of acoustically determining ice thickness would be through the implementation of the transverse mode because of unit reflectivity at the interface. There are at least two difficulties with this approach:

- (a) The true velocity profile of the transverse wave is unknown. It has, however, been predicted to be highly dependent upon the amount of liquid brine present in the medium--the amount varies as a function of temperature. Further, a very sharp transition of the medium occurs in the lower few centimeters of the ice, i.e., the skeleton structure. Therefore, without a great deal more information, which is presently unavailable, it is impossible to ascertain the acoustic impedance mismatch at the interface and thus predict the reflected energy in any given acoustic mode.
- (b) An efficient method of introducing the transverse wave into the medium has yet to be devised. The standard technique of coupling shear wave generating transducers onto the surface fails for the case of sea ice, principally because the saline layer generated by the brine leaching processes precludes a good bond between the transducer and the medium.

Several methods were attempted to introduce sufficient acoustic energy into annual sea ice to observe reflections from the interface. The only successful technique, wherein an acoustic pulse is generated using a low-level explosive charge, is shown in Figure 20. A slit is cut in the ice a known distance from the explosive source to eliminate the direct path to the sensor, a 10-kHz omnidirectional hydrophone implanted in the side of the slit. The explosion excites all of the acoustic modes, and these, in general, propagate at different velocities. The signal received at the sensor should therefore contain contributions from each mode that are separated temporally according to their different velocities. Figures 21 and 22 show typical returns from this experiment. Because the direct

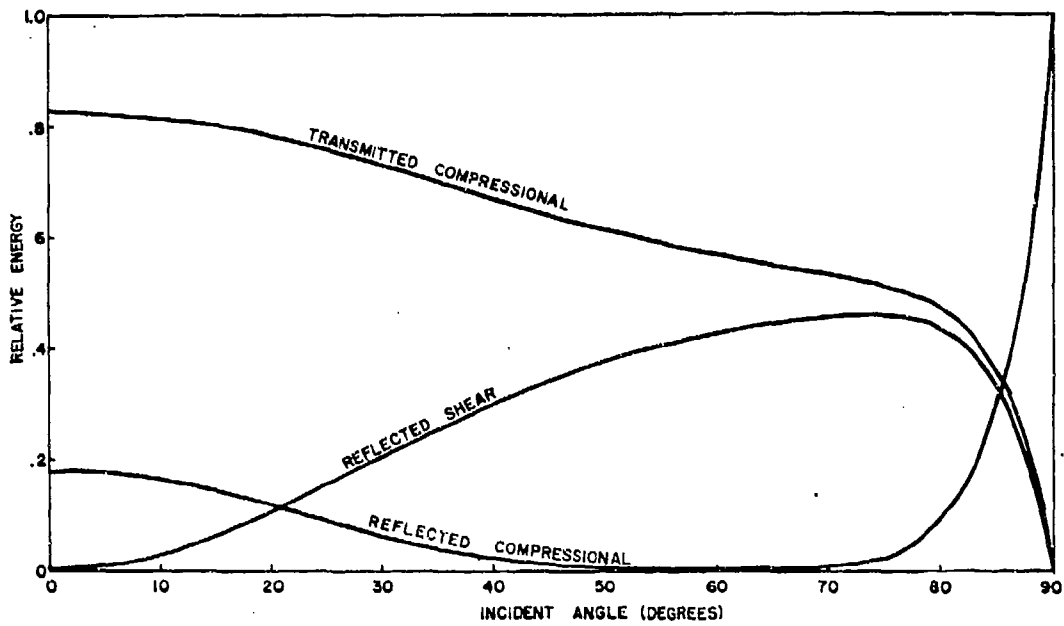


Figure 18. Relative energy distribution, compressional wave incident on ice-water boundary ($C_L = 3840$ m/sec; $\rho = 0.94$ g/cc).

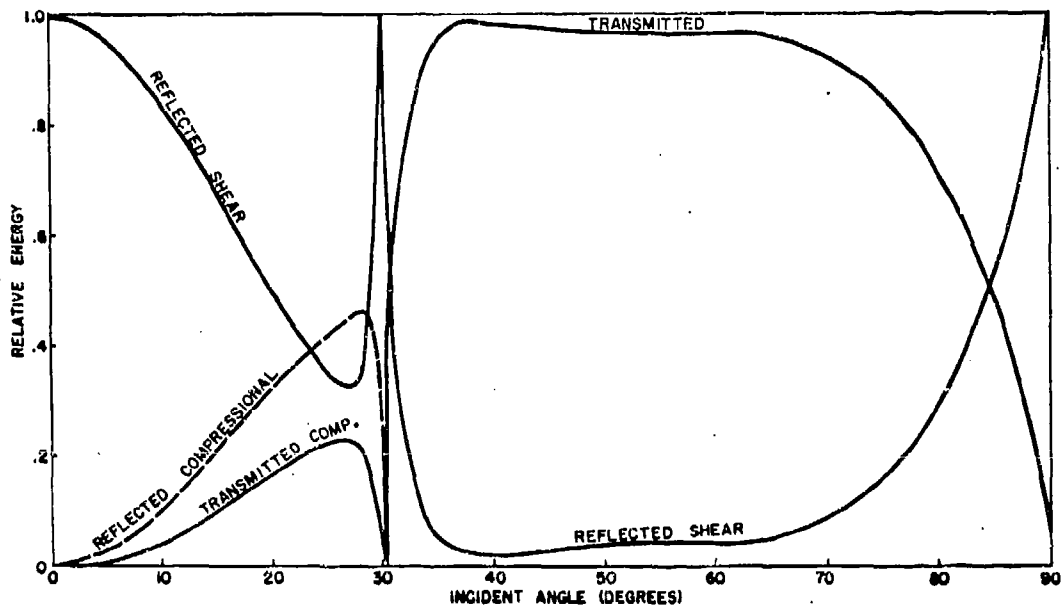


Figure 19. Relative energy distribution, transverse wave incident on ice-water boundary ($C_L = 3840$ m/sec; $C_T = 1870$ m/sec; $\rho = 0.94$ g/cc).

path has been interrupted, the first arrival at the sensor is the compressional wave echo from the interface and is indicated by arrow 1 in the figures. The initial signal is followed by reverberation until the arrival of the shear wave reflection denoted by arrow 2.*

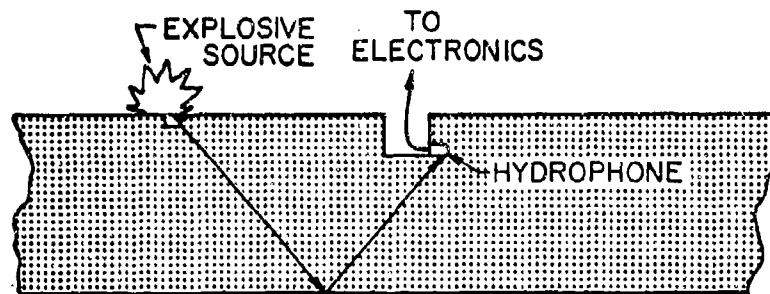


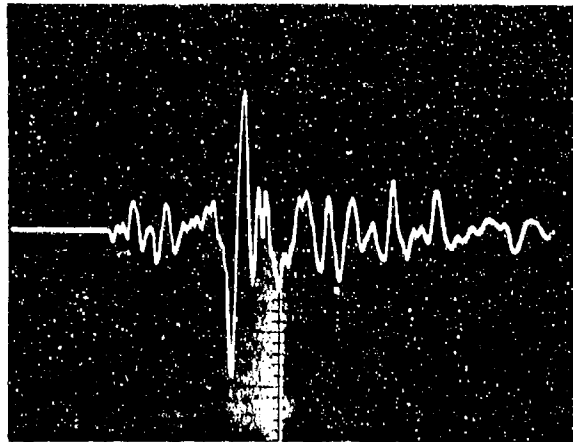
Figure 20. Diagram of reflectivity experiment.

Correcting for delays in the oscilloscope triggering circuit and averaging over all measurements, the shear wave velocity was 1746 m/sec. This value is 125 m/sec lower than that predicted by the velocity calculations. However, there are two shear modes that can be excited, vertical and horizontal, each of which can propagate at different speeds because of the anisotropic nature of the medium. It is impossible to determine which mode has been observed in the experiment, but it is believed that, because of the nature of the sound source, the horizontally polarized mode is the principal contributor. The results of the *in situ* tests are therefore not necessarily inconsistent with the predicted values.

Figure 23 shows the result of a similar experiment performed on summer sea ice. Even though this medium is quite different from annual sea ice, the form of the acoustic echo from the interface is very similar. The compressional and shear wave contributions are designated by arrows 1 and 2, respectively.

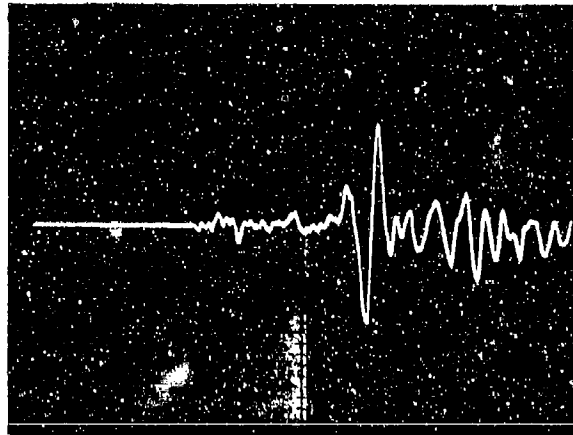
There are two obvious differences in the structure of the return echoes for summer and annual sea ice that can be correlated to differences in the medium. First, the acoustic returns in summer ice do not exhibit the reverberation observed for the annual ice. This indicates that the medium is more homogeneous during the summer months, which, in fact, it is because of the free flooded conditions. Second, the well-defined return echoes, particularly for the shear wave, are indicative of an abrupt transition at the interface; i.e., the skeleton layer is not well formed during the summer months.

*Because of triggering difficulties, T=0 in Figures 21-23 does not represent the initiation of the sound source.



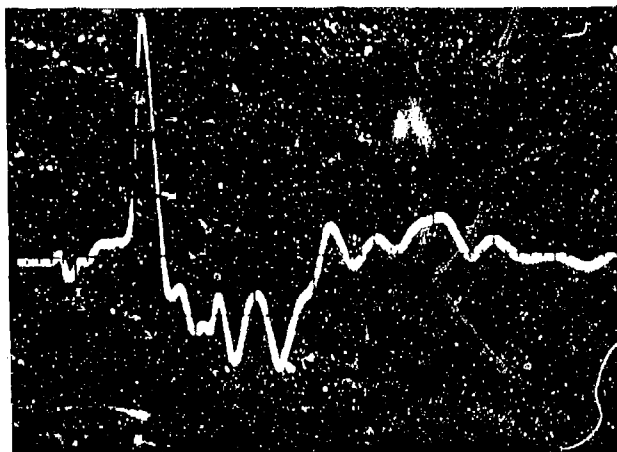
Sweep = 0.5 msec/div, Amp = 0.01 V/div
 Ice depth = 1.5 m
 Source to receiver distance = 3.6 m

Figure 21. Typical return from pulse echo experiment in annual sea ice.



Sweep = 0.5 msec/div, Amp = 0.005 V/div
 Ice depth = 1.5 m
 Source to receiver distance = 5 m

Figure 22. Typical return from pulse echo experiment in annual sea ice.



Sweep = 1 msec/div, Amp = 1 V/div
 Ice depth = 2,286 m
 Source to receiver distance = 2 m

Figure 23. Typical return from pulse echo experiment in summer sea ice.

Unfortunately, certain difficulties during the summer ice experiments did not allow a calculation of the trigger delay so that the average velocities cannot be directly determined. However, assuming the compressional velocity is 3840 m/sec, the transverse wave velocity is calculated to be 1765 m/sec. Therefore, although it has been shown⁴ that the acoustic parameters exhibit some seasonal dependence, this effect has not necessarily been observed during the experiments reported here.

Although the experiments performed have not directly measured the acoustic impedance mismatch, they have demonstrated that sufficient energy is reflected from the interface to monitor the thickness using acoustic pulse techniques, at least for annual and summer sea ice.

SEISMIC MEASUREMENTS

As discussed in the introduction, many seismic studies have been performed to measure acoustic velocities in sea ice. Great significance has been placed on the speed of the plate wave to determine the compressional wave velocity, and the frequency of the air-coupled wave^{4,6,33} to determine ice thickness. However, other acoustic modes such as the Lamb waves⁸ and the Rayleigh wave³⁴ could be as important for the determination of these parameters as the plate or air-coupled wave. Some preliminary experimentation was performed to better understand the mechanism of long-range acoustic transmission parallel to the ice cover.

High frequency propagation, i.e., wavelengths much smaller than the ice thickness, will not contribute to the energy observed at significant

distances from the sound source. There are two reasons for this: (1) The attenuation of the sound wave increases at least as the fourth power of the inverse wavelength so that the energy is dissipated very quickly for the frequencies being discussed, and (2) the radical velocity profile through the medium causes extensive refraction of the wave front. Using the horizontal velocity profile discussed in a previous section of this report and the computer program RAY005 given in Appendix B, the refraction was calculated for a sound source located on the surface, near mid-depth and at the interface. The result of this calculation is shown in Figures 24-26. It is obvious from this representation that the only condition under which appreciable energy will be transferred is for the source to be located at mid-depth because of the sound channel at that location. Even this condition may be unique because of the formation history of the 1973 ice cover.

To examine the longer wavelength contributions to the transmitted acoustic energy, the experiment illustrated in Figure 27 was performed. A line array of geophones composed of eight elements (four sensing vertical displacements and four sensing horizontal displacements) was located on the ice such that each sensing station was a known distance from the source of the acoustic disturbance (a small explosive charge). The received signal at each of the geophones was recorded on an analytic recorder for later laboratory analysis. Typical results of the horizontally oriented array are displayed in Figure 28. Results for the vertically oriented array are shown in Figure 29.

Although the ice surface was fairly rough, the geophones were located as equidistantly as possible. Thus, in the representation used in Figures 28 and 29 the velocity of the wavefronts is given by the slope of the line connecting the arrival times of initial impulse on the individual traces. For the horizontal geophone array, there were two obvious wavefront arrivals, one travelling at 3050 m/sec and one at 1538 m/sec. Except for the air wave at the 17-meter geophone there is no clear separation in the arrival times of other acoustic modes. This could be caused by the long oscillation times and the close proximity of the geophones, because on several shots there were signal interferences that indicated the possible arrival of another acoustic mode. An example is shown by the broken line on Figure 28. A best guess for this data indicates that this mode has a velocity of 1445 m/sec, which is very close to the velocity of sound in water. Future experimentation with the sensors located further from the sound source should separate this wave front.

The intermediate velocity wave has been previously reported by Oliver,³ who was unable to explain its origin. Given that C_R is the velocity of the Rayleigh wave and C_T and C_L are the velocities of the transverse and longitudinal wave, respectively, Viktorov³⁵ shows that the Rayleigh wave velocity can be determined from the equation

$$\eta^3 - 8\eta^2 + 8(3 - 2\xi^2)\eta - 16(1 - \xi^2) = 0, \quad (27)$$

where

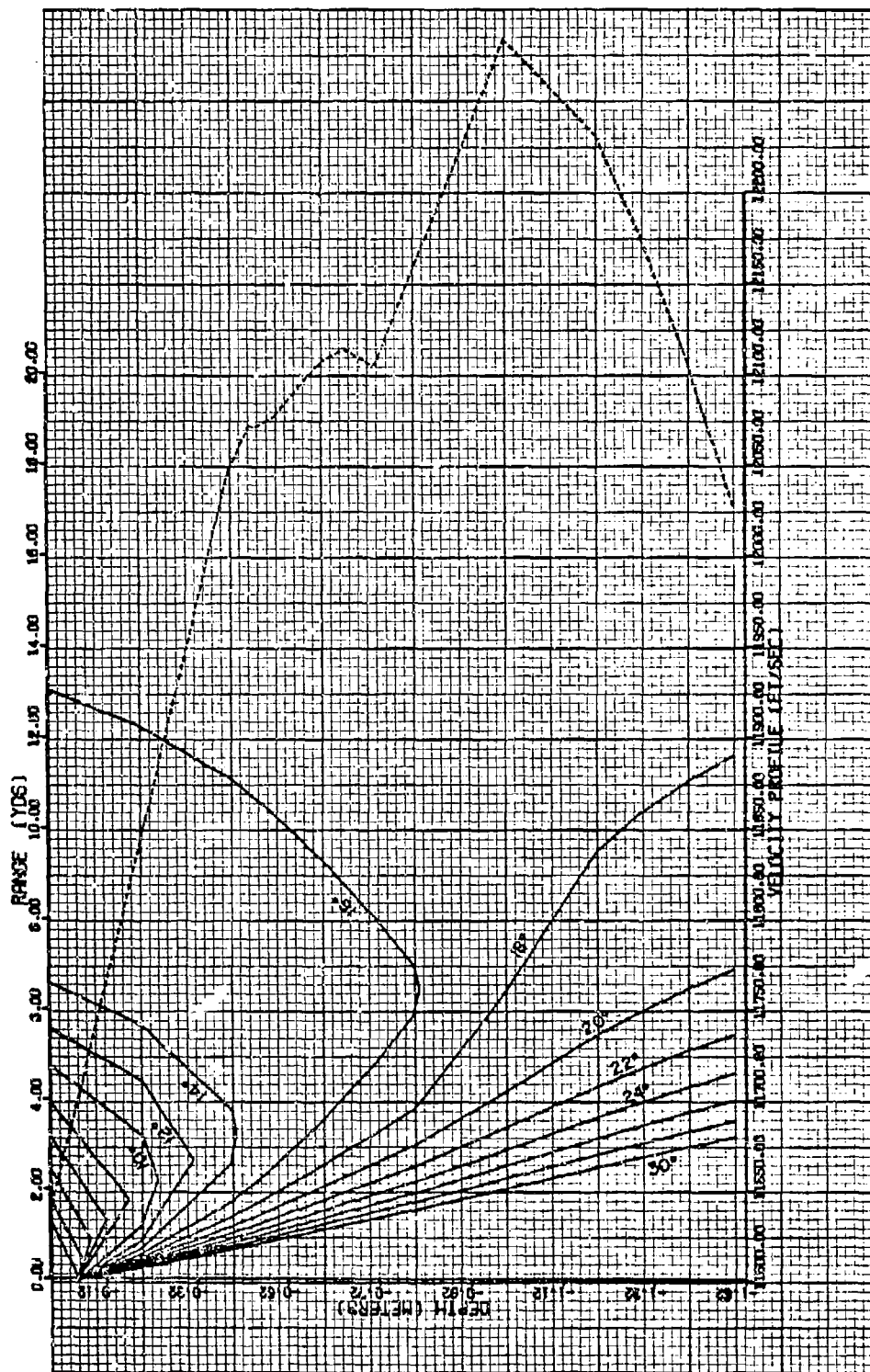


Figure 24. Sound ray plot for annual sea ice; source at surface.

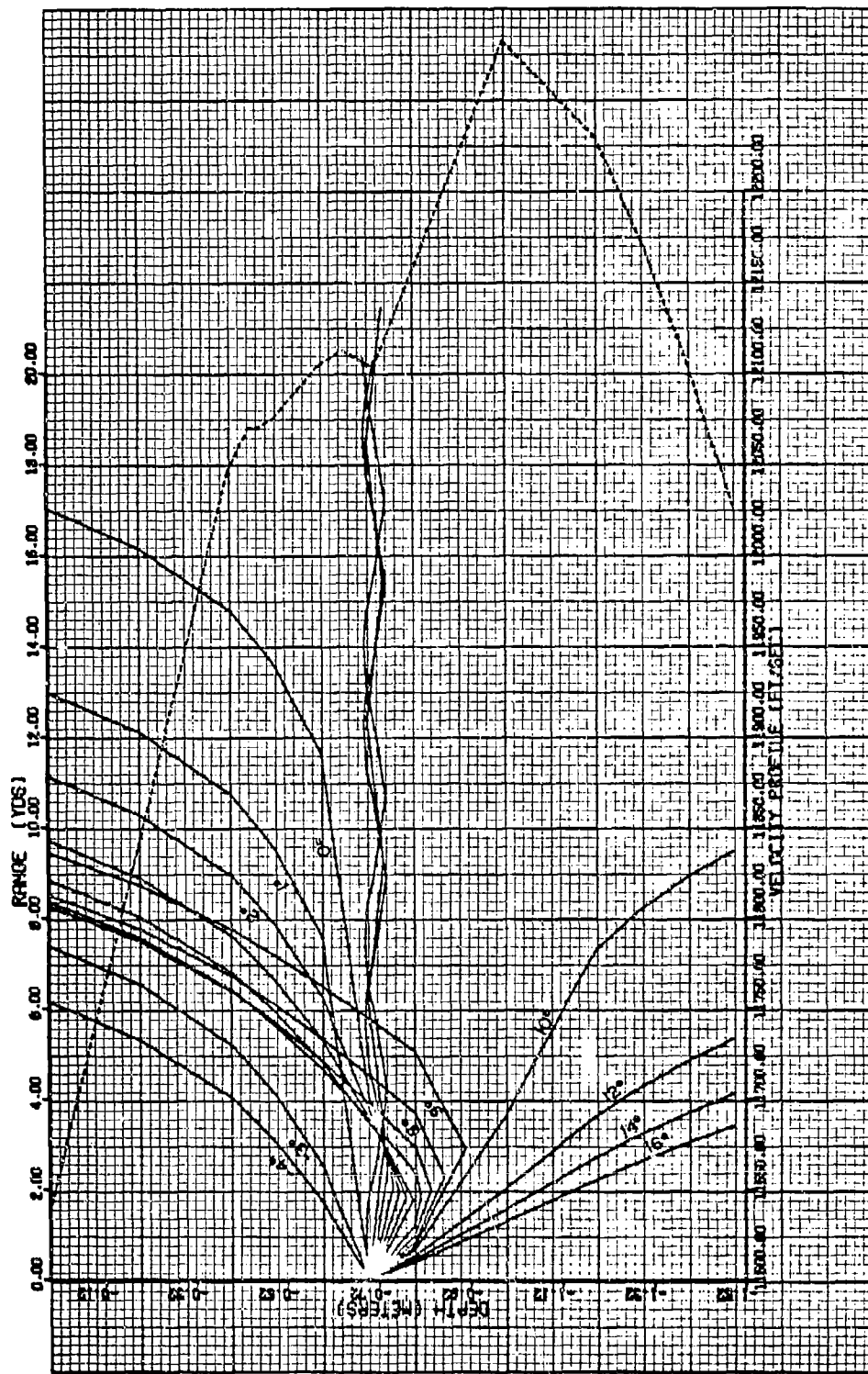


Figure 25. Sound ray plot for annual sea ice; source at mid-depth.

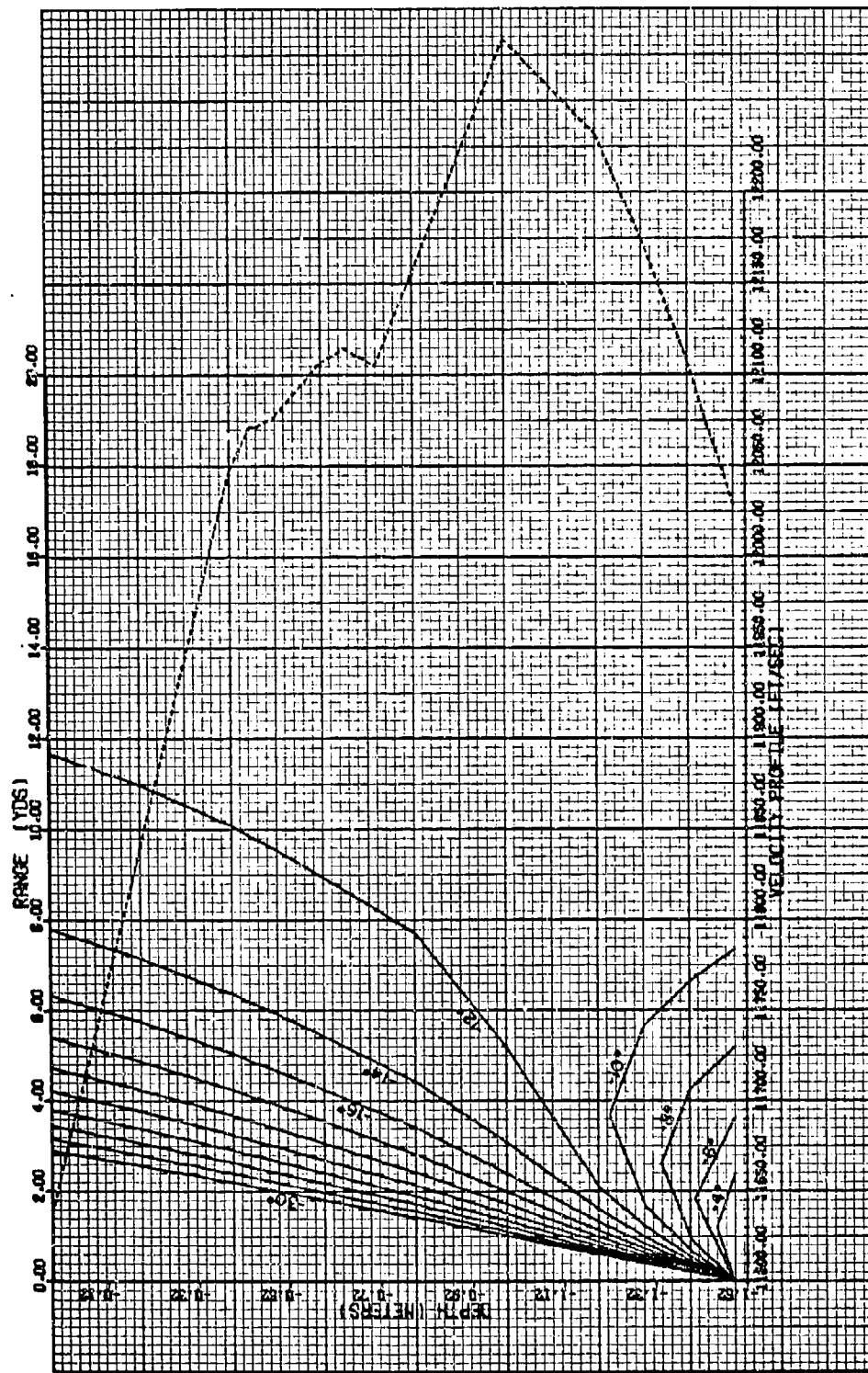


Figure 26. Sound ray plot for annual sea ice; source at ice-water interface.

$$\eta = \left(\frac{C_R}{C_T} \right)^2$$

$$\xi = \left(\frac{C_T}{C_L} \right)^2$$

Using the known values of the longitudinal velocity, density, and plate velocity for ice, and the identities

$$C_P^2 = \frac{1}{\rho(1-\sigma^2)}$$

$$C_L^2 = \frac{E}{\rho} \frac{(1-\sigma)}{(1+\sigma)(1-2\sigma)} \quad (28)$$

$$C_T^2 = \frac{E}{2\rho(1+\sigma)}$$

where ρ is the density, E is Young's modulus and σ is Poisson's ratio, a value of $C_T = 1763$ m/sec was derived. This is in excellent agreement with the reflectivity measurements discussed earlier. Equation 27 was then solved for the Rayleigh velocity for this medium and found to be 1677 m/sec, a value very near that observed for the intermediate speed wave.

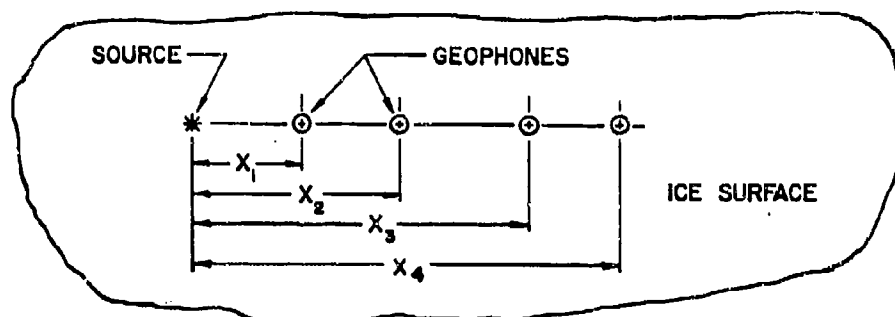


Figure 27. Diagram of seismic experiment.

Other evidence indicates that the observed disturbance is due to the Rayleigh surface wave. It is known that this wave is propagated with an elliptical particle motion that is unique to this particular mode. Thus, the orientation of displacement sensors, such as geophones, is unimportant in the detection of this wave. Examination of Figures 28 and 29 shows that this disturbance is detected by both the vertically and horizontally oriented geophone arrays, while the plate wave excites only the horizontally sensitive geophones. This indicates that the particle motion for this mode is indeed elliptical. Finally, Bunney and Goodman³⁶ have shown that the Rayleigh wave, once excited, is the predominant mode of energy

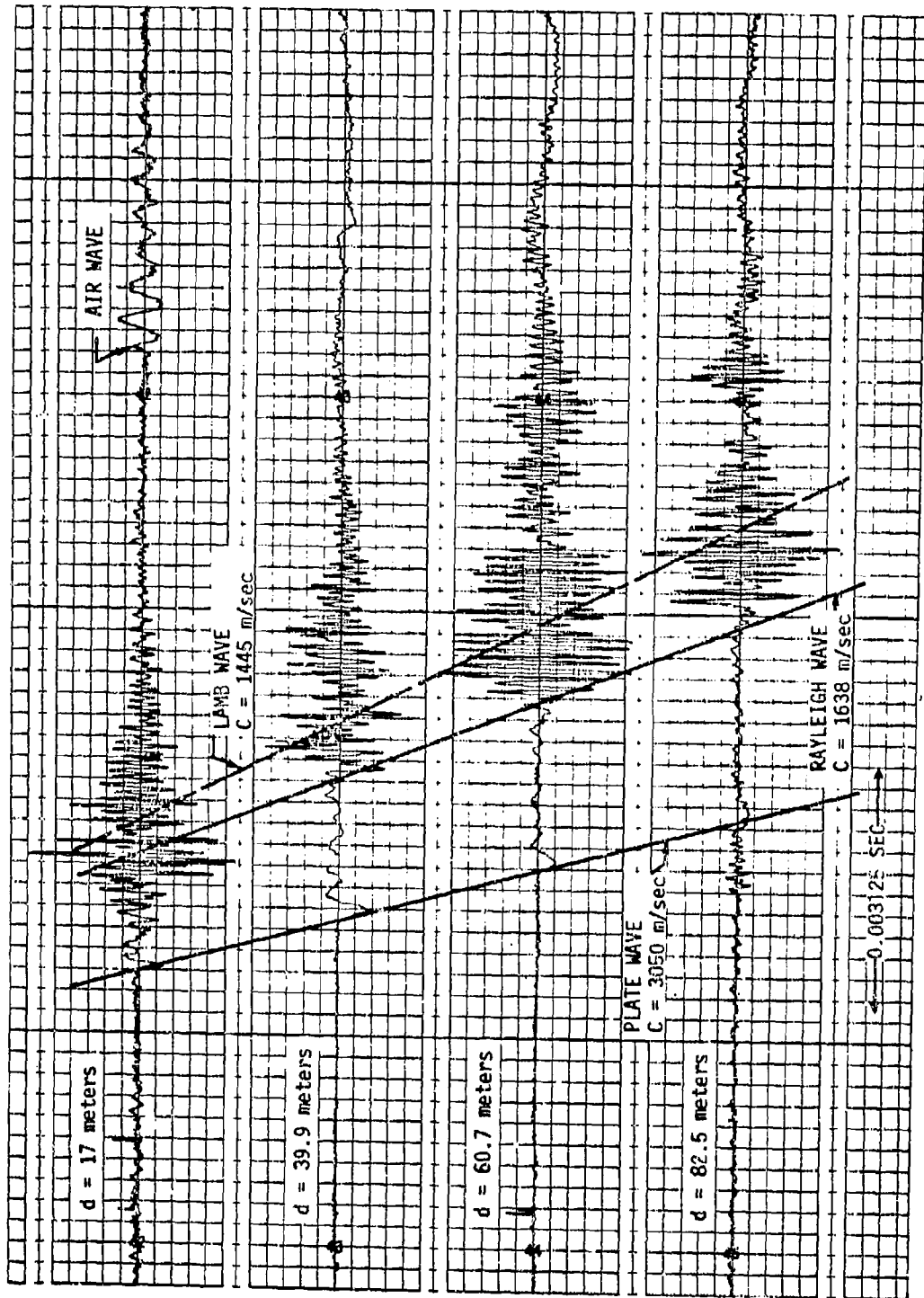


Figure 28. Result of pilot study to measure Lamb waves in annual sea ice; horizontally polarized geophones.

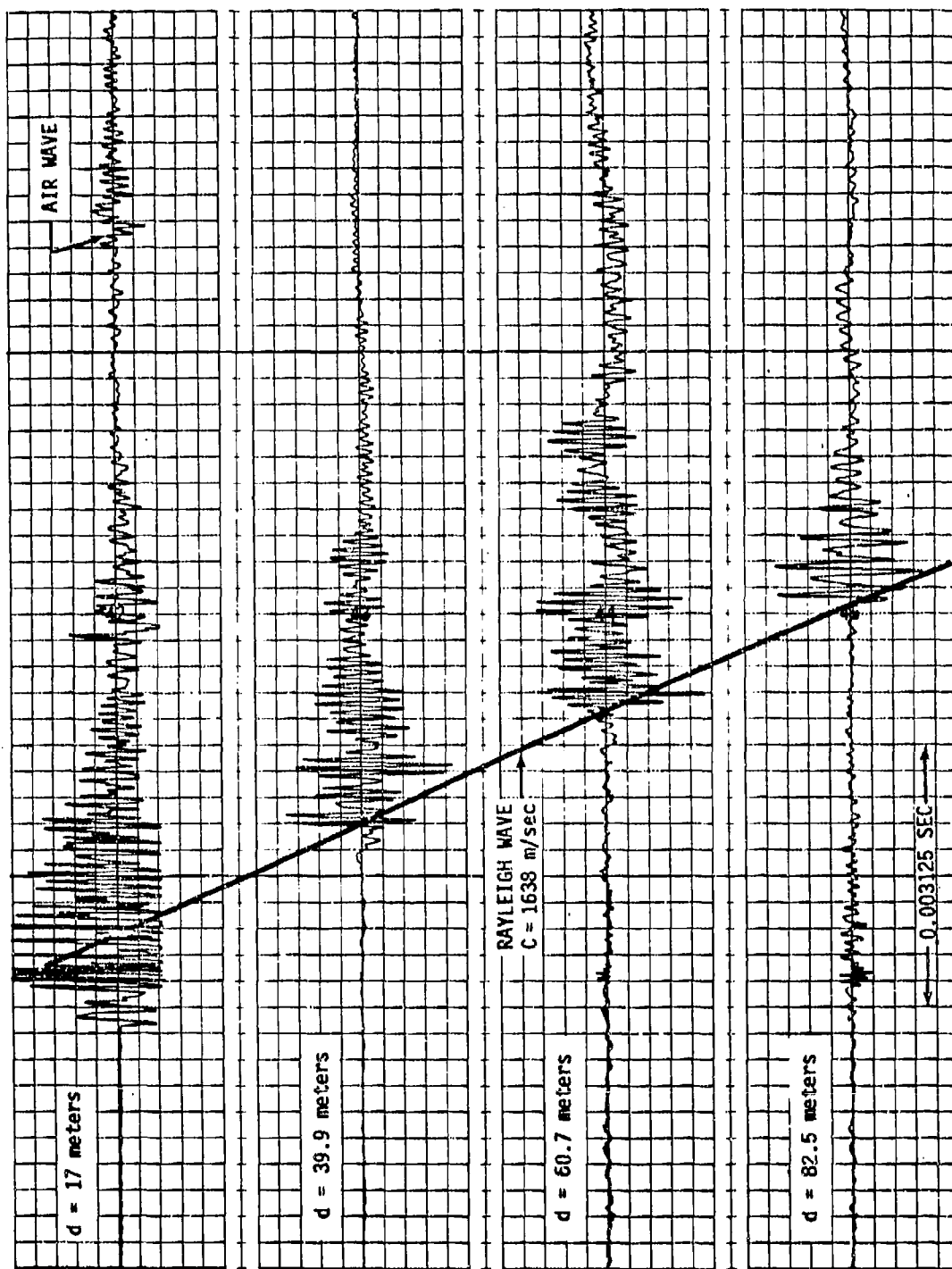


Figure 29. Result of pilot study to measure Lamb waves in annual sea ice; vertically polarized geophones.

transfer and propagates with very little attenuation, which is consistent with the behavior of the observed wave.

To fully interpret the results of the seismic experiment, the theory of Bunney and Goodman¹⁰ has been extended to allow excitations in a plate bounded by air on one side and water on the other (see Appendix A). The predicted velocity dispersion for the case of sea ice, using the acoustic parameters previously discussed in this report, is shown in Figure 30. There are two surface wave modes predicted: (1) the symmetric Lamb wave, which for small thickness-to-wavelength ratios ($kh \leq 1$) is indistinguishable from the plate wave (C_p) and appears to asymptotically approach the shear wave velocity (C_T) as the layer thickness increases, and (2) the Rayleigh wave, or the antisymmetric Lamb wave, which appears to propagate near the Rayleigh wave velocity. These two waves were the principal excitations observed during the experiment.

CONCLUSIONS AND RECOMMENDATIONS

The ability to efficiently and accurately determine the thickness of sea ice using acoustic pulse echo techniques is dependent on several factors. The more critical problems, those associated with the velocity and attenuation of the acoustic wave in the medium and with the acoustic impedance mismatch at the ice-water interface, have been investigated in the laboratory and in situ for both summer and annual sea ice. The results of these measurements indicate that, if sufficient coupling between the sound source and the medium can be obtained, and if the acoustic frequency is maintained such that the wavelength is long compared to the scattering centers in the medium, the determination of ice thickness using pulse echo methods is entirely feasible. This technique was demonstrated in situ.

For thicknesses up to 2.5 meters (the maximum depth available during the field tests) reflections of both the compressional and transverse waves were observed. Although the compressional wave velocity measurements exhibited radical fine structure with depth into the medium, the average values varied by less than 1.5%. This is indicative of the accuracy with which the ice thickness can be measured. Either the compressional or the transverse wave can be used for the measurements. Because of the large acoustic impedance mismatch for the shear wave at the ice-water boundary, the energy returned is several decibels greater than that for the compressional wave. This advantage may be negated, however, by the relative difficulty in generating this acoustic mode.

The small explosive charges used as sound sources during these experiments worked very well for generating all of the acoustic modes, including the shear wave. Because of the time required to set up the apparatus, this technique would be very inefficient for surveying large areas; thus other methods of coupling energy into sea ice should be studied.

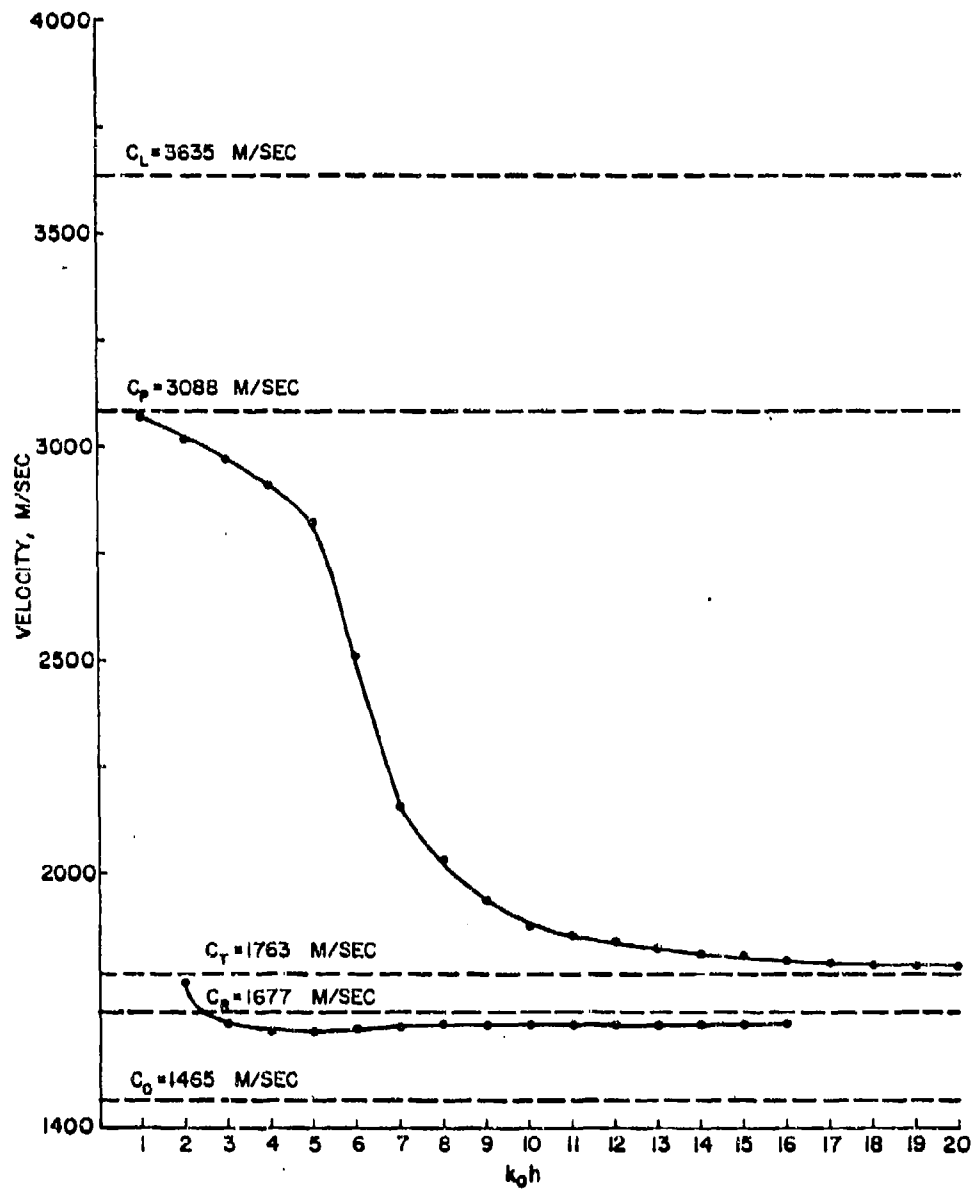


Figure 30. Dispersion of Lamb waves on sea ice for horizontally polarized case.

Hunkins⁴ has reported seasonal variations in both the compressional and shear wave velocities approaching 20%. We did not obtain sufficient reliable data during these tests to verify this result. Further, the theory shows that, for high frequencies, scattering processes are the largest contributor to the attenuation of the sound wave in the medium. For the annual ice observed, the attenuation becomes significant for frequencies above approximately 50 kHz and is dependent on the size of the scattering centers, in this case the brine cells. Because the size of these cells can have a large seasonal variation, a dramatic effect may be observed in the attenuation of sound in the medium. It is recommended that tests be conducted to measure the seasonal dependence of the acoustic parameters in the medium.

The empirical relationships developed from the experimental data for predicting the depth dependence of the acoustic parameters (such as the transverse wave velocity) appear to become invalid near the transition layer between the ice and seawater. Because a reliable prediction of the relative amount of energy each mode reflects from this interface is dependent on a thorough understanding of the acoustic properties of this transition layer, it is recommended that a program be initiated to study the physics of this "skeleton layer."

Preliminary experiments have shown that energy can be propagated parallel to the surface of the ice canopy in both the Rayleigh and Lamb modes. Theoretical results have shown that the Lamb waves are highly dispersive with the thickness of the layer. The introduction of pure tone acoustic waves into the media may well provide first order approximations to the average ice thickness over significant ranges. It is recommended that this technique receive further attention.

APPENDIX A - THEORIES

I. THEORY OF SOUND WAVE PROPAGATION VELOCITY AND ATTENUATION IN VISCO-ELASTIC MEDIA

A. Long Wavelength Solution

1. *Derivation of the General Equations for Wavenumber and Attenuation in an Isotropic Medium*

For wavelengths that are long compared to the size of the scattering centers, scattering theory can be ignored in deriving the formulation of acoustic velocity and attenuation. The introduction of viscoelasticity is accomplished by the replacement of the Lamé constants Λ and M in the elastic stress-strain relations by the first order differential operators

$$M = \mu + \mu' \frac{\partial}{\partial t} \tag{A1}$$

$$\Lambda = \lambda + \lambda' \frac{\partial}{\partial t} ,$$

where the unprimed terms are the elastic and the primed terms the viscous contributions.

Consider an acoustic shear wave* moving in the positive (downward) x-direction. The displacement potential is given by

$$\psi = Ae^{i(\omega t - \alpha x)} , \tag{A2}$$

where ω is the circular frequency, t is the time, and α is the complex wavenumber. The potential obeys the wave equation

$$\rho \frac{\partial^2 \psi}{\partial t^2} = M \nabla^2 \psi , \tag{A3}$$

where ρ is the density of the medium. Substitution of Eqs. A1 and A2 yields

$$\rho \frac{\partial^2 \psi}{\partial t^2} = \mu \nabla^2 \psi + \mu' \nabla^2 \frac{\partial \psi}{\partial t} \tag{A4}$$

*The derivation for compressional wave propagation is similar to that presented here for shear waves, the difference being the introduction of $\Lambda+2M$ in the wave equation rather than the shear modulus M . The displacement potential must, of course, be associated with the compressional rather than the shear wave.

or

$$\rho\omega^2 = \alpha^2(\mu + i\omega\mu'). \quad (\text{A5})$$

For a dissipative medium,

$$\alpha = k - i\tau, \quad (\text{A6})$$

where k is the running vector (ω/c) and τ is the attenuation. Making this substitution and separating real and imaginary components yield the simultaneous equations

$$\begin{aligned} \rho\omega^2 &= \mu(k^2 - \tau^2) + 2\mu'\omega k\tau \\ 0 &= \omega\mu'(k^2 - \tau^2) - 2\mu k\tau \end{aligned} \quad (\text{A7})$$

Setting

$$R = \frac{\mu'}{\mu},$$

these equations have the solution

$$\tau = \frac{k}{R\omega} \left\{ \sqrt{1 + R^2\omega^2} - 1 \right\} \quad (\text{A8})$$

$$k^2 = \frac{1}{2} \frac{\rho\omega^2}{\mu} \left\{ \frac{\sqrt{1 + R^2\omega^2} + 1}{1 + R^2\omega^2} \right\},$$

where both μ and R may be frequency dependent.

2. *Mathematical Models of Sea Ice*

Historically, there have been four different rheological models used to represent sea ice. These models relate the stress tensor as a function of density, strain and time rate of strain. Only two models will be discussed here, that of Maxwell and that of Voigt. The linear standard model and the four-element model are combinations of these two, and their introduction would only lead to undue complexity.

a. *The Maxwell Model²⁶*

Consider the mechanical representation shown in Figure A1, where the ice is represented by a spring denoting the elastic element (E_m) in series with a dashpot denoting the viscous element (η_m). Both E_m and η_m are frequency independent. Maxwell defined the stress-strain relationship for this viscoelastic solid as

$$\frac{d}{dt} \sigma_{ij} = 2\mu \frac{d}{dt} S_{ij} - \frac{\sigma_{ij}}{\delta} \quad (i \neq j), \quad (A9)$$

where σ is the stress, S is the strain and δ is the relaxation time of the material. If the wave equation (Eq. A3) is to be applicable, Hooke's law states that the relationship between stress and strain must be of the form

$$\sigma = 2MS, \quad (A10)$$

which may be accomplished by writing M as an operator,

$$M = \frac{\mu}{1 + \frac{1}{\delta \left(\frac{d}{dt}\right)^{-1}}} \quad (A11)$$

or, in terms of the elastic and viscous constants of Figure A1,

$$M = \frac{E_m}{1 + \frac{E_m}{\eta_m} \left(\frac{d}{dt}\right)^{-1}}$$

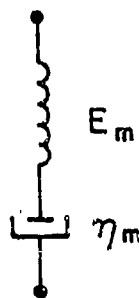


Figure A1. Maxwell's mechanical representation of viscoelastic solids.

Thus, substituting into Eq. A10 and simplifying give

$$\frac{d}{dt} \sigma + \frac{E_m}{\eta_m} \sigma = E_m \frac{d}{dt} S \quad (A12)$$

Now, for periodic stresses, both σ and S have time dependence of the form $e^{i\omega t}$. Equation A12 can then be reduced to

$$\sigma = \frac{E_m \omega^2 + i\omega \frac{E_m^2}{\eta_m}}{\left(\frac{E_m}{\eta_m}\right)^2 + \omega^2} S . \quad (A13)$$

It was assumed earlier that

$$M = \mu + i\omega\mu' .$$

Therefore, separating real and imaginary parts of Eq. A13,

$$\mu = \frac{E_m \omega^2}{\left(\frac{E_m}{\eta_m}\right)^2 + \omega^2}$$

and

(A14)

$$\mu' = \frac{E_m^2 / \eta_m}{\left(\frac{E_m}{\eta_m}\right)^2 + \omega^2} .$$

so that

$$R\omega = \frac{\mu'}{\mu} \omega = \frac{E_m}{\eta_m \omega} . \quad (A15)$$

The solution given by Eq. A8 can then be immediately written as

$$\tau = \frac{k\eta_m \omega}{E_m} \left\{ \sqrt{1 + \left(\frac{E_m}{\eta_m \omega}\right)^2} - 1 \right\} \quad (A16)$$

$$k^2 = \frac{\rho \omega^2}{2\mu} \left\{ \frac{\sqrt{1 + \left(\frac{E_m}{\eta_m \omega}\right)^2} + 1}{1 + \left(\frac{E_m}{\eta_m \omega}\right)^2} \right\}$$

b. The Voigt Model²⁹

Figure A2 shows the mechanical representation of the Voigt Model. In this configuration, a spring representing the elasticity (E_v) is in parallel with a dashpot representing the viscous term (η_v). As in the previous model, both E_v and η_v are assumed to be frequency independent. The stress-strain relationship is given by

$$\sigma_v = (E_v + \eta_v \frac{d}{dt} S_v) \quad (A17)$$

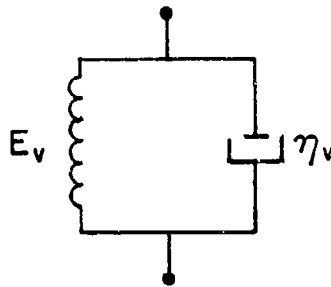


Figure A2. Voigt's mechanical representation of viscoelastic solids.

Using techniques and arguments similar to those for the Maxwell model above, it can be shown that the solutions for the Voigt model are given by the equations

$$\tau = \frac{kE_v}{\eta_v \omega} \left\{ \sqrt{1 + \left(\frac{\eta_v}{E_v} \omega\right)^2} - 1 \right\} \quad (A18)$$

$$k^2 = \frac{1}{2} \frac{\rho \omega^2}{E_v} \left\{ \frac{\sqrt{1 + \left(\frac{\eta_v}{E_v} \omega\right)^2} \omega^2 + 1}{1 + \left(\frac{\eta_v}{E_v} \omega\right)^2} \right\}$$

B. Extension of the Theory to Include Anisotropy

Thus far in the theory, only the solutions for an isotropic medium have been discussed. It is known, however, that for many materials, including naturally occurring ice, the acoustic properties exhibit a dependence on the direction of the propagation of the wave relative to the growth axis, i.e., the media are anisotropic. A method of including anisotropy in the theory follows.

Stresses and strains in the medium can be specified in terms of the resolved displacements in a unit cube of the material.³⁸ There are six components of stress and six of strain, which can be written in terms of tensor notation as

$$\sigma_{ij} \text{ and } S_{ij} ,$$

where i, j denotes the x -, y -, z - or 1-, 2-, 3-component of the stress or strain. The force on a unit cube in the i^{th} direction is given by

$$F_i = \frac{\partial \sigma_{ij}}{\partial x_j} dx dy dz \quad (i, j = 1, 2, 3) , \quad (\text{A19})$$

where repeated indices indicate a summation. The tensor strains are defined by

$$S_{ij} = \frac{1}{2} \left(\frac{\partial u_i}{\partial x_j} + \frac{\partial u_j}{\partial x_i} \right) , \quad (\text{A20})$$

where the u 's are the displacements of the body along the coordinate direction x_j .

Utilizing the reduced tensor convention for the stresses

$$\sigma_1 = \sigma_{11}; \sigma_2 = \sigma_{22}; \sigma_3 = \sigma_{33}$$

$$\sigma_4 = \sigma_{23} = \sigma_{32}; \sigma_5 = \sigma_{13} = \sigma_{31}; \sigma_6 = \sigma_{12} = \sigma_{21} ,$$

and, similarly, for the strains

$$S_1 = S_{11}; S_2 = S_{22}; S_3 = S_{33}$$

$$\frac{1}{2} S_4 = S_{23} = S_{32}; \frac{1}{2} S_5 = S_{13} = S_{31}; \frac{1}{2} S_6 = S_{12} = S_{21} ,$$

the generalized Hooke's law can then be written

$$t_i = c_{ij} S_j \quad (i, j = 1, 2, \dots, 6) \quad (A21)$$

and it can be shown that for the elastic constants

$$c_{ij} = c_{ji}. \quad (A22)$$

There are a maximum of 21 elastic constants for the most unsymmetrical crystal. As the degree of symmetry increases, the number of elastic constants decreases until there are only two for an isotropic medium. These are the Lamé constants λ and μ , where

$$\begin{aligned} \lambda + 2\mu &= C_{11} = C_{22} = C_{33}, \\ \lambda &= C_{12} = C_{13} = C_{23} = C_{21} = C_{31} = C_{32}, \\ \mu &= C_{44} = C_{55} = C_{66}, \end{aligned} \quad (A23)$$

and all other constants are zero.

To include viscosity in this theory, each of the elastic constants is replaced by a differential operator of the proper form for the model being considered. Therefore, a complete solution will require the determination of two or more elastic and viscous constants for each operator used.

C. Short Wavelength Solution

For wavelengths on the order of or shorter than the size of the scattering centers in the medium, the energy loss due to scattering must be considered.

Assume a plane wave propagating through an isotropic solid to be scattered by a sphere of radius "a." Both the wave and the scatterer are characterized by their longitudinal (k_1 and k_2) and shear (κ_1 and κ_2) wavenumbers. The energy scattered out of the sound beam by the sphere is equal to the time rate at which energy is being carried away across a spherical surface concentric with the scatterer and of radius "b" > "a." The scattered energy is then written mathematically as

$$E_{\text{scattered}} = \iint_A \left\{ \sigma_{xr} \frac{\partial u_x}{\partial t} + \sigma_{yr} \frac{\partial u_y}{\partial t} + \sigma_{zr} \frac{\partial u_z}{\partial t} \right\}_{\text{scattered}} dA, \quad (A24)$$

where σ_{xr} , σ_{yr} , and σ_{zr} are the complex stress components acting in the three rectangular axes on a surface normal to the radius vector \vec{r} and where u_x , u_y , and u_z are the complex displacements in the same three axes. Since the final expression for the scattered energy must be real, and both the σ 's and u 's are generally complex, only

the real part of Eq. A24 will be taken. Rewriting Eq. A24 in spherical coordinates and determining the real part gives

$$E_{\text{scattered}} = \frac{i\omega}{2} \int_0^\pi \left\{ \left[\sigma_{rr} u_r^* + \sigma_{\theta r} u_\theta^* + \sigma_{zr} u_z^* \right] - \left[\sigma_{rr}^* u_r + \sigma_{\theta r}^* u_\theta + \sigma_{zr}^* u_z \right] \right\} 2r^2 \sin\theta d\theta \quad \text{scattered wave} \quad (A25)$$

The displacements of the sound waves can, in general, be written as

$$\vec{u} = \text{grad } \phi + \text{curl } \vec{\psi}, \quad (A26)$$

where ϕ is the scalar potential and ψ is the vector potential (0, 0, ψ). The displacements for the incident, scattered and internal* waves can be written in terms of Eq. A26 with the incident wave potentials

$$\phi_{\text{in}} = \sum_{m=0}^{\infty} I_m j_m(k_1 r) P_m(\cos\theta) \quad (A27)$$

$$\psi_{\text{in}} = \sum_{m=0}^{\infty} J_m j_m(k_1 r) P_m(\cos\theta) ,$$

the scattered wave potentials

$$\phi_s = \sum_{m=0}^{\infty} A_m h_m(k_1 r) P_m(\cos\theta) \quad (A28)$$

$$\psi_s = \sum_{m=0}^{\infty} B_m h_m(k_1 r) P_m(\cos\theta) ,$$

and the internal wave potentials

$$\phi_q = \sum_{m=0}^{\infty} C_m j_m(k_2 r) P_m(\cos\theta) \quad (A29)$$

$$\psi_q = \sum_{m=0}^{\infty} D_m j_m(k_2 r) P_m(\cos\theta) ,$$

*the waves inside the scattering sphere

where j_m , h_m and p_m are the spherical Bessel function, the spherical Hankel function and the Legendre polynomials,³⁷ respectively. The stress and displacement components in terms of the potentials are³⁹

$$\begin{aligned} \sigma_{rr} &= \rho\omega^3 \left\{ \phi + \frac{2}{\kappa^2} \left[\frac{2}{r} \frac{\partial\phi}{\partial r} - \frac{1}{r^2} \Omega\phi - \frac{\partial}{\partial r} \left(\frac{1}{r} \Omega\psi \right) \right] \right\} \\ \sigma_{\theta r} &= \frac{2\rho\omega^2}{\kappa^2} \frac{\partial}{\partial\theta} \left\{ \frac{1}{r} \frac{\partial\phi}{\partial r} - \frac{1}{r^2} \phi + \frac{1}{r} \frac{\partial\psi}{\partial r} + \frac{1}{r^2} (1 + \frac{1}{2} \kappa^2 r^2) \psi + \frac{1}{r^2} \Omega\psi \right\} \quad (A30) \\ \sigma_{\phi r} &= 0 \end{aligned}$$

and

$$\begin{aligned} u_r &= - \left[\frac{\partial\phi}{\partial r} + \frac{1}{r} \Omega\psi \right] \\ u_\theta &= - \frac{1}{r} \frac{\partial\phi}{\partial\theta} + \frac{1}{r} \frac{\partial^2}{\partial r \partial\theta} (r\psi) \quad (A31) \\ u_\phi &= 0 \end{aligned}$$

with

$$\Omega = \frac{1}{\sin\theta} \frac{\partial}{\partial\theta} \left(\sin\theta \frac{\partial}{\partial\theta} \right) . \quad (A32)$$

Applying Eqs. A28, A30, and A31 to Eq. A25 yields the scattered energy:

$$E_{\text{scattered}} = 4\pi\rho_1\omega^3 \sum_{m=0}^{\infty} \frac{1}{2m+1} \left[\frac{1}{\kappa_1} |A_m|^2 + \frac{m(m+1)}{\kappa_1} |B_m|^2 \right] , \quad (A33)$$

The scattering cross section is defined as the ratio of the scattered energy to the total energy, or

$$\gamma = \frac{E_{\text{scattered}}}{E_{\text{total}}} . \quad (A34)$$

For an incident plane compressional wave with amplitude coefficients

$$I_m = \frac{1}{\kappa_1} (-i)^{m+1} (2m+1)$$

and

$$J_m = 0$$

the total energy in the absence of a scatterer is

$$E_{\text{total}} = \frac{\rho_1 \omega^3}{k_1} \quad (\text{A35})$$

and the scattering cross section is

$$\gamma_{\text{shear}} = 4\pi \sum_{m=0}^{\infty} \frac{1}{2m+1} \left[|A_m|^2 + m(m+1) \frac{k_1}{k_1} |B_m|^2 \right]. \quad (\text{A36})$$

The final solution depends on the amplitudes A_m and B_m which must be evaluated in terms of the boundary conditions defining the stress and displacement at the scattering sphere surface.

The scattering cross section for a shear wave incident on a spherical scatterer is

$$\gamma_{\text{comp}} = 4\pi \sum_{m=0}^{\infty} \frac{1}{2m+1} \left[\frac{k_1}{k_1} |A_m|^2 + m(m+1) |B_m|^2 \right], \quad (\text{A37})$$

where again the boundary conditions are solved for the A_m 's and B_m 's. The solution of this equation using the best known values for the parameters shows that, except in the region where the ratio of the circumference to the wavelength is approximately 1:1, the scattering cross section obeys the relationship

$$\begin{aligned} \gamma_{\text{shear}} &= \frac{\nu^4 a^6}{4.151 \times 10^{-9} + 2.35 \times 10^{-5} \nu^{2.2} a^{2.2}} \text{ dB/cm}^2 \\ \gamma_{\text{comp}} &= \frac{\nu^4 a^6}{2.163 \times 10^{-7} + 0.017 \nu^2 a^4} \end{aligned} \quad (\text{A38})$$

where γ is the scattering cross section, a is the scattering radius, and ν is the frequency in megahertz.

To determine the effect of scattering on the acoustic attenuation of sea ice, the distribution of the scatterers in size and space must be considered.

II. THEORY OF ACOUSTIC REFLECTION AND TRANSMISSION AT THE ICE-WATER INTERFACE

The equations to be developed here are for isotropic, homogeneous media whose extent is very much larger than the acoustic wavelength. Complexities such as the anisotropic nature and the viscoelastic properties of sea ice are not considered, since much of this theory is already complete.⁴⁰⁻⁴⁴

Elementary tests on acoustics, such as Lindsay,⁴⁵ show that for an acoustic wave striking normal to an interface such as that shown in Figure A3 (where the ρ 's are the densities, the A's are amplitudes, and the C's are the velocities of the acoustic wave in the media) the relative amplitude of the reflected wave is given by

$$\frac{A_R}{A_i} = \frac{1 - Z}{1 + Z}, \quad (\text{A39})$$

where $Z = (\rho_2 C_2) / (\rho_1 C_1) =$ the acoustic impedance of the boundary. The above model shows, in a very simplified way, that the acoustic energy reflected is wholly dependent upon the impedance mismatch of the interface.

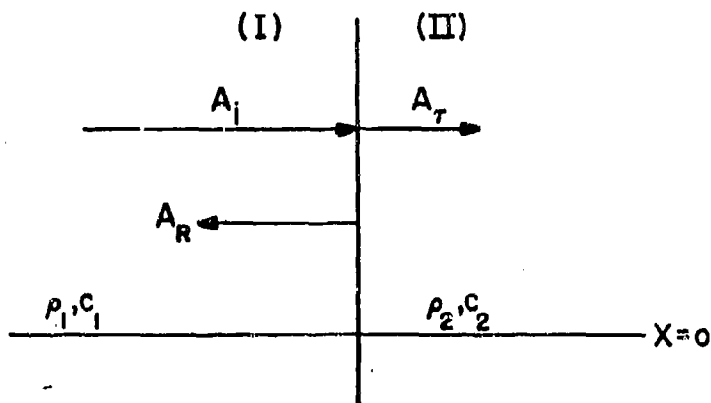


Figure A3. Acoustic wave reflection and transmission at an interface for a normal incident wave.

For the case of an incident wave not normal to the boundary, consider the diagram of Figure A4, where medium I (the ice) is assumed to be isotropic and homogeneous and medium II (the water) is assumed to be an ideal fluid. Then the potential functions are given by

$$\begin{aligned}
 \phi &= e^{i(\omega t - \beta y)} \left[\delta_L e^{-i\alpha_L x} + B e^{i\alpha_L x} \right] \\
 \psi &= e^{i(\omega t - \beta y)} \left[(1 - \delta_L) e^{-i\alpha_T x} + D e^{i\alpha_T x} \right] \\
 \phi_0 &= e^{i(\omega t - \beta y)} E e^{-i\alpha_0 x}
 \end{aligned}
 \tag{A40}$$

where

$$\delta_L = \begin{cases} 1 & \text{incident compressional wave} \\ 0 & \text{incident transverse wave} \end{cases}$$

$$\beta = k_0 \sin \theta_0 = k_L \sin \theta_L = k_T \sin \theta_T$$

$$\alpha_0 = k_0 \cos \theta_0$$

$$\alpha_T = k_T \cos \theta_T$$

$$\alpha_L = k_L \cos \theta_L$$

$$\theta_L = \sin^{-1} \left[\frac{k_0}{k_L} \sin \theta_0 \right]$$

$$\theta_T = \sin^{-1} \left[\frac{k_0}{k_T} \sin \theta_0 \right]$$

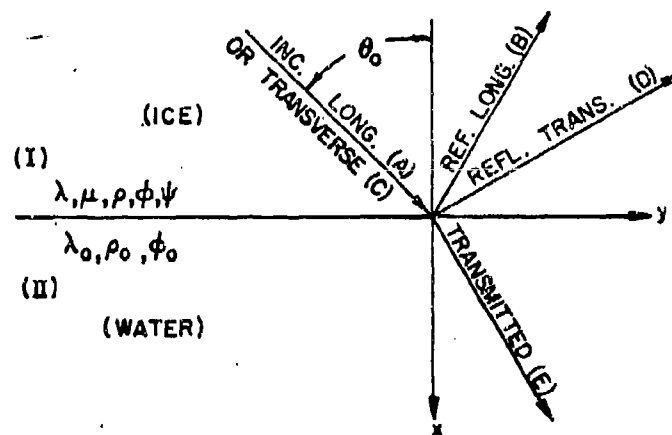


Figure A4. Acoustic wave reflection and transmission at an interface for non-normal incidence.

At the boundary, $x = 0$, the normal displacement and pressure are continuous and the shear stress vanishes. That is,

$$\begin{aligned} u_x^I &= u_x^{II} \\ \sigma_{xy}^{II} &= 0 \\ \sigma_{xx}^I &= \sigma_{xx}^{II} \end{aligned} \quad (A41)$$

where

$$\begin{aligned} \vec{u} &= \text{grad } \phi + \text{curl } \vec{\psi} \\ \vec{\psi} &= (0, 0, \psi) \\ \sigma_{ij} &= \lambda \delta_{ij} \nabla^2 \phi + 2\mu S_{ij} \\ S_{ij} &= \frac{1}{2} \left(\frac{\partial u_i}{\partial x_j} + \frac{\partial u_j}{\partial x_i} \right) \end{aligned}$$

and i and j denote direction. Solving the boundary conditions, the amplitude of the reflected compressional wave is given by the expression:

$$B = \frac{\left\{ \frac{\alpha_L}{\alpha_0} \left(\frac{k_T^2}{\alpha_T^2 - \beta^2} \right) - \frac{\rho}{\rho_0} \left[1 - \frac{2\beta^2}{k_T^2} \left(\frac{2\alpha_T \alpha_L}{\alpha_T^2 - \beta^2} + 1 \right) \right] \right\} \delta_L - \frac{\rho}{\rho_0} \frac{4\beta \alpha_T}{k_T^2} (1 - \delta_L)}{\frac{\alpha_L}{\alpha_0} \left(\frac{k_T^2}{\alpha_T^2 - \beta^2} \right) + \frac{\rho}{\rho_0} \left[1 + \frac{2\beta^2}{k_T^2} \left(\frac{2\alpha_T \alpha_L}{\alpha_T^2 - \beta^2} - 1 \right) \right]} \quad (A42)$$

The amplitude of the reflected transverse wave is given by

$$D = \frac{4 \frac{\rho}{\rho_0} \frac{\beta}{\alpha_0} \frac{k_L^2}{k_T^2} \delta_L - \left\{ \frac{\alpha_L}{\alpha_0} \left(\frac{k_T^2}{\alpha_T^2 - \beta^2} \right) + \frac{\rho}{\rho_0} \left[1 - \frac{2\beta^2}{k_T^2} \left(\frac{2\alpha_T \alpha_L}{\alpha_T^2 - \beta^2} + 1 \right) \right] \right\} (1 - \delta_L)}{\frac{\alpha_L}{\alpha_0} \left(\frac{k_T^2}{\alpha_T^2 - \beta^2} \right) + \frac{\rho}{\rho_0} \left[1 + \frac{2\beta^2}{k_T^2} \left(\frac{2\alpha_T \alpha_L}{\alpha_T^2 - \beta^2} - 1 \right) \right]} \quad (A43)$$

Finally, the amplitude of the transmitted compressional wave is

$$E = \frac{2 \frac{\rho}{\rho_0} \frac{\alpha_L}{\alpha_0} \delta_L + 4 \frac{\rho}{\rho_0} \frac{\beta}{\alpha_0} \frac{\alpha_L \alpha_T}{(\alpha_T^2 - \beta^2)} (1 - \delta_L)}{\frac{\alpha_L}{\alpha_0} \left(\frac{k_T^2}{\alpha_T^2 - \beta^2} \right) + \frac{\rho}{\rho_0} \left[1 + \frac{2\beta^2}{k_T^2} \left(\frac{2\alpha_L \alpha_T}{\alpha_T^2 - \beta^2} - 1 \right) \right]} \quad (A44)$$

From these equations, the energy distribution relative to that of the impinging wave can then be calculated as a function of incident angle. The results of these calculations, using the best known values of the necessary parameters, are shown in Figures 18 and 19 of the text.

III. ENERGY OF THE ACOUSTICALLY EXCITED SURFACE WAVES ON A PLATE

Consider a plane wave travelling in an ideal fluid striking a plate of thickness (h) at an angle θ_0 . The following mathematical development calculates the energy per unit length per second flowing in the y-direction (see Figure A5), where it is assumed that the plate is bounded on each side by a (but not necessarily the same) fluid. The problem is to determine if enhancement occurs near the Rayleigh and Lamb wave excitation angles.

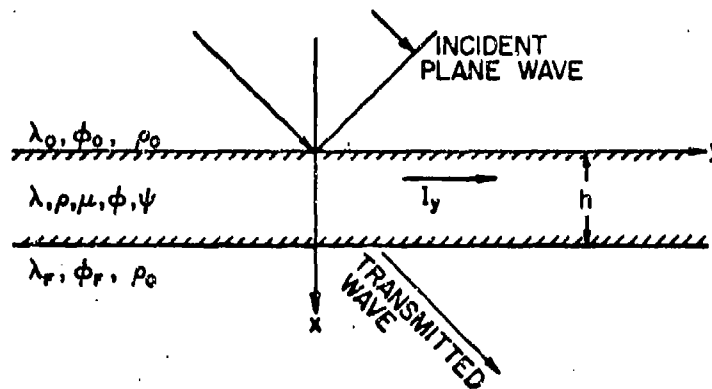


Figure A5. Schematic representation of the problem.

If the displacement potentials are ϕ and ψ , then the displacement \vec{u} is

$$\vec{u} = \text{grad } \phi + \text{curl } \psi, \quad (\text{A45})$$

where the potential of an incoming wave with angular frequency ω , wave number k_0 and unit amplitude is

$$\phi_i = e^{i(\omega t - k_0 \sin \theta_0 y - k_0 \cos \theta_0 x)}, \quad (\text{A46})$$

the potential of the reflected wave is

$$\phi_r = e^{i(\omega t - k_0 \sin \theta_0 y + k_0 \cos \theta_0 x)}, \quad (\text{A47})$$

the potential of the transmitted wave is

$$\phi_t = e^{i(\omega t - k_F \sin \theta_F y - k_F \cos \theta_F x)}, \quad (\text{A48})$$

and the potentials ϕ and ψ in the elastic medium are

$$\phi = e^{i(\omega t - k_L \sin \theta_L y)} \left[B e^{-i k_L \cos \theta_L x} + C e^{i k_L \cos \theta_L x} \right] = \phi_{\downarrow} + \phi_{\uparrow} \quad (\text{A49})$$

$$\psi = (0, 0, \psi) \quad (\text{A50})$$

$$\psi = e^{i(\omega t - k_T \sin \theta_T y)} \left[D e^{-i k_T \cos \theta_T x} + E e^{i k_T \cos \theta_T x} \right] = \psi_{\downarrow} + \psi_{\uparrow}. \quad (\text{A51})$$

The intensity of the wave in the i^{th} direction is given by³⁷

$$I_i = \frac{1}{4} \left\{ \lambda (\dot{u}_i^* S_{\alpha\alpha} + \dot{u}_i S_{\alpha\alpha}^*) + 2\mu (\dot{u}_\alpha^* S_{i\alpha} + \dot{u}_\alpha S_{i\alpha}^*) \right\}, \quad (\text{A52})$$

where

$$S_{ij} = \frac{1}{2} \left(\frac{\partial u_i}{\partial x_j} + \frac{\partial u_j}{\partial x_i} \right),$$

the Lamé constants are λ and μ , and repeated indices denote summation.

According to Snell's law

$$k_o \sin \theta_o = k_L \sin \theta_L = k_T \sin \theta_T = k_F \sin \theta_F \equiv \beta, \quad (\text{A53})$$

and letting

$$\begin{aligned} \alpha_L &= k_L \cos \theta_L = k_L \sqrt{1 - \left(\frac{c_L}{c_o}\right)^2 \sin^2 \theta_o} \\ \alpha_T &= k_T \cos \theta_T = k_T \sqrt{1 - \left(\frac{c_T}{c_o}\right)^2 \sin^2 \theta_o} \\ \alpha_F &= k_F \cos \theta_F = k_F \sqrt{1 - \left(\frac{c_F}{c_o}\right)^2 \sin^2 \theta_o} \\ \alpha_o &= k_o \cos \theta_o, \end{aligned} \quad (\text{A54})$$

the intensities in the x- and y-direction can be given by

$$\begin{aligned} \frac{4I_x}{\rho\omega^3} &= \left\{ (\alpha_L + \alpha_L^*) (\phi_{\downarrow}\phi_{\downarrow}^* - \phi_{\uparrow}\phi_{\uparrow}^*) + (\alpha_L - \alpha_L^*) (\phi_{\downarrow}\phi_{\uparrow}^* - \phi_{\uparrow}\phi_{\downarrow}^*) \right. \\ &\quad \left. + (\alpha_T + \alpha_T^*) (\psi_{\downarrow}\psi_{\downarrow}^* - \psi_{\uparrow}\psi_{\uparrow}^*) + (\alpha_T - \alpha_T^*) (\psi_{\downarrow}\psi_{\uparrow}^* - \psi_{\uparrow}\psi_{\downarrow}^*) \right\} \end{aligned} \quad (\text{A55})$$

and

$$\begin{aligned} \frac{2I_y}{\rho\omega^3} &= \left\{ \beta \left[1 + \frac{2}{k_T^2} (\beta^2 - k_L^2 + \alpha_L \alpha_L^*) \right] \phi\phi^* + \beta \frac{2}{k_T^2} \left(\alpha_T \alpha_T^* - \frac{\alpha_T^2 - \beta^2}{2} \right) \psi\psi^* \right\} \\ &\quad + \frac{1}{k_T^2} \left\{ -4\beta \left[\alpha_L \alpha_L^* (\phi_{\uparrow}\phi_{\downarrow}^* + \phi_{\downarrow}\phi_{\uparrow}^*) + \alpha_T \alpha_T^* (\psi_{\uparrow}\psi_{\downarrow}^* + \psi_{\downarrow}\psi_{\uparrow}^*) \right] \right. \\ &\quad + \left(2\beta^2 - k_L^2 + \frac{k_T^2}{2} \right) \left[\alpha_T \phi^* (\psi_{\uparrow} - \psi_{\downarrow}) + \alpha_T^* \phi (\psi_{\uparrow}^* - \psi_{\downarrow}^*) \right] \\ &\quad \left. - \left(2\beta^2 - \frac{k_T^2}{2} \right) \left[\alpha_L^* (\phi_{\uparrow}^* - \phi_{\downarrow}^*) \psi + \alpha_L (\phi_{\uparrow} - \phi_{\downarrow}) \psi^* \right] \right\}, \end{aligned} \quad (\text{A56})$$

where the asterisk denotes the complex conjugate, and both α_L and α_T are either purely real or purely imaginary depending upon whether the incident angle is less than or greater than the compressional or transverse Snell's law critical angle. To evaluate the wave amplitude coefficients A...F, we have applied the well-known boundary conditions of continuity of displacement and pressure across the interfaces at $x=0$ and $x=h$, and the shear stress must vanish because a fluid medium on each side of the layer has been assumed. Mathematically the boundary conditions can be represented as

$$\begin{aligned} u_x^o &= u_x \\ \sigma_{xx}^o &= \sigma_{xx} & (X=0) \\ \sigma_{xy} &= 0 \end{aligned}$$

and

$$\begin{aligned} u_x &= u_x^F \\ \sigma_{xx} &= \sigma_{xx}^F & (X=h) \\ \sigma_{xy} &= 0 \end{aligned} \tag{A57}$$

where

$$\begin{aligned} \sigma_{ij} &= \lambda \nabla^2 \phi \delta_{ij} + 2\mu S_{ij} \\ S_{ij} &= \frac{1}{2} \left(\frac{\partial u_i}{\partial x_j} + \frac{\partial u_j}{\partial x_i} \right) \end{aligned} \tag{A58}$$

and δ_{ij} is the Kronecker delta.

Solution of these boundary conditions results in six simultaneous equations, in which the unknowns are the desired amplitudes. Letting A...F = A₁...A₆, the solution can be put in the form

$$\begin{aligned} A_i &= \frac{2a_i}{D} (-1)^{i-1} & i \leq 5 \\ &= \frac{2a_i}{D} (-1)^{i-1} e^{i\alpha_T h} & i = 6 \end{aligned} \tag{A59}$$

where

$$\begin{aligned} \frac{1}{4} a_1 = & 2 \frac{\rho_o}{\rho_F} s_{12} s_{32} s_{34} (1 - \cos \alpha_L h \cos \alpha_T h) - \left[\frac{\rho_o}{\rho_F} (s_{12}^2 s_{34}^2 + s_{32}^2) \right. \\ & \left. - \frac{\alpha_o}{\alpha_F} (s_{12} s_{24} - s_{22})^2 \right] \sin \alpha_L h \sin \alpha_T h \\ & + i (s_{12} s_{24} - s_{22}) \left(\frac{\alpha_o}{\alpha_F} - \frac{\rho_o}{\rho_F} \right) \left[-s_{12} s_{34} \sin \alpha_L h \cos \alpha_T h \right. \\ & \left. + s_{32} \sin \alpha_T h \cos \alpha_L h \right] , \end{aligned}$$

$$\begin{aligned} \frac{1}{2} a_2 = & \frac{\rho_o}{\rho_F} s_{12} s_{34} (1 - \cos \alpha_L h \cos \alpha_T h) - \left[\frac{\rho_o}{\rho_F} s_{32} \right. \\ & \left. + \frac{\alpha_o}{\alpha_F} (s_{12} s_{24} - s_{22}) \right] \sin \alpha_L h \sin \alpha_T h \\ & + i \left[\frac{\rho_o}{\rho_F} s_{32} + \frac{\alpha_o}{\alpha_F} (s_{12} s_{24} - s_{22}) \right] \sin \alpha_T h \cos \alpha_L h \\ & - i \frac{\rho_o}{\rho_F} s_{12} s_{34} \cos \alpha_T h \sin \alpha_L h , \end{aligned}$$

$$\begin{aligned} \frac{1}{2} a_3 = & - \frac{\rho_o}{\rho_F} s_{12} s_{34} (1 - \cos \alpha_L h \cos \alpha_T h) + \left[\frac{\rho_o}{\rho_F} s_{32} \right. \\ & \left. - \frac{\alpha_o}{\alpha_F} (s_{12} s_{24} - s_{22}) \right] \sin \alpha_L h \sin \alpha_T h \\ & + i \left[\frac{\rho_o}{\rho_F} s_{32} - \frac{\alpha_o}{\alpha_F} (s_{12} s_{24} - s_{22}) \right] \sin \alpha_T h \cos \alpha_L h \\ & - i \frac{\rho_o}{\rho_F} s_{12} s_{34} \cos \alpha_T h \sin \alpha_L h , \end{aligned}$$

$$\begin{aligned} \frac{1}{2} a_4 = & s_{12} \left\{ \frac{\rho_o}{\rho_F} s_{32} (1 - \cos \alpha_L h \cos \alpha_T h) - \left[\frac{\rho_o}{\rho_F} s_{12} s_{34} \right. \right. \\ & \left. \left. - \frac{\alpha_o}{\alpha_F} (s_{12} s_{24} - s_{22}) \right] \sin \alpha_L h \sin \alpha_T h \right. \\ & + i \left[\frac{\rho_o}{\rho_F} s_{12} s_{34} - \frac{\alpha_o}{\alpha_F} (s_{12} s_{24} - s_{22}) \right] \sin \alpha_L h \cos \alpha_T h \\ & \left. - i \frac{\rho_o}{\rho_F} s_{32} \cos \alpha_L h \sin \alpha_T h \right\} , \end{aligned}$$

$$\begin{aligned} \frac{1}{2} a_5 = & s_{12} \left\{ \frac{\rho_o}{\rho_F} s_{32} (1 - \cos \alpha_L h \cos \alpha_T h) - \left[\frac{\rho_o}{\rho_F} s_{12} s_{34} \right. \right. \\ & \left. \left. + \frac{\alpha_o}{\alpha_F} (s_{12} s_{24} - s_{22}) \right] \sin \alpha_L h \sin \alpha_T h \right. \\ & - i \left[\frac{\rho_o}{\rho_F} s_{12} s_{34} + \frac{\alpha_o}{\alpha_F} (s_{12} s_{24} - s_{22}) \right] \sin \alpha_L h \cos \alpha_T h \\ & \left. + i \frac{\rho_o}{\rho_F} s_{32} \cos \alpha_L h \sin \alpha_T h \right\} , \end{aligned}$$

$$-\frac{1}{8} a_6 = i \frac{\rho_o}{\rho_F} \frac{\alpha_o}{\alpha_F} (s_{12} s_{24} - s_{22}) \left[s_{34} \sin \alpha_L h - s_{32} \sin \alpha_T h \right] ,$$

$$\begin{aligned} \frac{1}{4} D = & 2 \frac{\rho_o}{\rho_F} s_{12} s_{34} s_{32} (1 - \cos \alpha_T h \cos \alpha_L h) - \left[\frac{\rho_o}{\rho_F} (s_{12}^2 s_{34}^2 + s_{32}^2) \right. \\ & \left. - \frac{\alpha_o}{\alpha_F} (s_{12} s_{24} - s_{22})^2 \right] \sin \alpha_L h \sin \alpha_T h \\ & + i (s_{12} s_{24} - s_{22}) \left(\frac{\alpha_o}{\alpha_F} + \frac{\rho_o}{\rho_F} \right) \left[-s_{12} s_{34} \sin \alpha_L h \cos \alpha_T h \right. \\ & \left. + s_{32} \sin \alpha_T h \cos \alpha_L h \right] , \end{aligned}$$

and

$$s_{12} = \frac{2\alpha_L \beta}{\alpha_T^2 - \beta^2} ; s_{22} = \alpha_L / \alpha_0 ; s_{24} = \beta / \alpha_0$$

$$s_{32} = \frac{\rho}{\rho_0} \left(\frac{2\beta^2}{k_T^2} - 1 \right) ; s_{34} = - \frac{\rho}{\rho_0} \frac{2\beta\alpha_T}{k_T^2}$$

These equations have been solved using Program LAYER in Appendix B for the case of sea ice bounded on one side by water and on the opposite side by air. Although the results of this calculation predict anomalies that remain to be interpreted, the dispersion of the Lamb waves can be extracted from the calculation and are shown in Figure 30 of the text.

APPENDIX B - COMPUTER PROGRAMS

```

PROGRAM RAY005(INPUT,OUTPUT,TAPE5=INPUT,TAPE6=OUTPUT,TAPE99)
C   RAY TRACING PROGRAM,APPLIED PHYSICS LABORATORY
C   READ IN TABLE OF VELOCITIES FOR DECREASING DEPTHS
DIMENSION VELOC(500),ID(500),DEPTH(500),SHIP(3),DATE(3)
DATA TEST1,PI/1.E-6,3.14159265358/
CALL PLOTS
READ(5,201) NOFLT
201 FORMAT(I5)
702 READ(5,896) SHIP,DATE
896 FORMAT(3A10,3A10)
DO 3 M=1,500
READ(5,1) DEPTH(M),VELOC(M),ID(M)
1 FORMAT(2F20.1,I1)
IF(ID(M)-9)3,4,3
4 II=M-1
GO TO 5
3 CONTINUE
5 READ(5,6) DSOURC,SVEL,RMAX ,DELTA,ANGMAX,ANGMIN
6 FORMAT(3F10.1,3F10.5)
WRITE(6,60) SHIP,DATE
60 FORMAT(1H1/1H 34X,20H RAY TRACING PROGRAM/14 31X,27H APPLIED PHYSICS
LABORATORY/1H 30X,3A10/1H 30X3A10//)
WRITE(6,162) (DEPTH(M),VELOC(M),M=1,II)
162 FORMAT(7H DEPTH=F10.1,10X,10H VELOCITY=F13.4)
WRITE(6,109) SVEL,RMAX ,DELTA,ANGMAX,ANGMIN
109 FORMAT(1H ,2F10.1,3F10.3/ )
C
C READ IN THE SCALE
C
READ(5,701)YMIN,YMAX,DY,SY,XMIN,XMAX,DX,SX,DIM,TD,VMIN,VMAX,DV,SV
701 FORMAT(4F10.2/6F10.2/4F10.2)
C
IF(TD.EQ.0.) TD = DEPTH(II)
SUM = 0.0
DO 130 L=1,II
IF(DEPTH(L).LT.DSOURC) GO TO 130
IF(DEPTH(L).GE.TD)GO TO 110
SUM=(VELOC(L)+VELOC(L+1))/2.*(DEPTH(L+1)-DEPTH(L)) + SUM
GO TO 130
110 CONTINUE
IF(DEPTH(L).EQ.TD) GO TO 125
DEL = DEPTH(L)-TD
VIN = (VELOC(L-1)-VELOC(L))/(DEPTH(L-1)-DEPTH(L)) * DEL
SUM = SUM - (VELOC(L)-VIN/2.) * DEL
125 CONTINUE
VAV = SUM / (TD-DSOURC)
IF(DIM.GT.0.5) GO TO 127
WRITE(6,126) DSOURC,TD,VAV
126 FORMAT(1H0,25H AVERAGE VELOCITY BETWEEN ,F8.2,4H AND,F8.2,
X 8H FEET IS,F8.2,10H FEET/SEC //28H ALL DISTANCES ARE IN FEET
X /1H1)
GO TO 135
127 CONTINUE
WRITE(6,128) DSOURC,TD,VAV
128 FORMAT(1H0,25H AVERAGE VELOCITY BETWEEN ,F8.2,4H AND,F8.2,10H MET
XERS IS ,F8.2,12H METERS/SEC //28H ALL DISTANCES ARE IN METERS
X /1H1)
GO TO 135
130 CONTINUE
135 CONTINUE
C

```

C PLOT AXIS

```

C
PLOTY= (YMAX-YMIN)/OY
IF(DIM.LT.0.5) GO TO 400
CALL AXIS(0.0,0.0 ,24H , 25,SV,
10.0,VMIN,OV,10.)
CALL AXIS(0.0,PLOTY,13HDEPTH (METER),13,SY,90.0,YMAX,OY,10.)
CALL AXIS(0.0,PLOTY,24HVELOCITY PROFILE (M/SEC),-25,SV,
10.0,VMIN,OV,10.)
CALL AXIS(SV+1.,PLOTY,13HRANGE (METER),-13, SX,0.0,XMIN,OX,10.)
CALL AXIS(SV+1.,PLOTY,13HDEPTH (METER),13,SY,90.0,YMAX,OY,10.)
CALL AXIS(SV+1.,0.0,13H , 12, SX,0.0,XMIN,OX,10.)
GO TO 410
400 CONTINUE
CALL AXIS(0.0,0.0 ,25H , 25,SV,
10.0,VMIN,OV,10.)
CALL AXIS(0.0,PLOTY,13HDEPTH (FEET) ,13,SY,90.0,YMAX,OY,10.)
CALL AXIS(0.0,PLOTY,25HVELOCITY PROFILE (FT/SEC),-25,SV,
10.0,VMIN,OV,10.)
CALL AXIS(SV+1.,0.0,13H , 12, SX,0.0,XMIN,OX,10.)
CALL AXIS(SV+1.,PLOTY,13HDEPTH (FEET) ,13,SY,90.0,YMAX,OY,10.)
CALL AXIS(SV+1.,PLOTY,13HRANGE (FEET) ,-13, SX,0.0,XMIN,OX,10.)
410 CONTINUE
C
C WRITE HEADING
C
PLOTX=(VELOC(1)-VMIN)/DV
PLOTY=(-DEPTH(1)-YMIN)/OY
CALL PLOT(PLOTX,PLOTY,3)
DO 700 IN1=2,II
PLOTX=(VELOC(IN1)-VMIN)/DV
PLOTY=(-DEPTH(IN1)-YMIN)/OY
700 CALL PLOT(PLOTX,PLOTY,2)
NOPLT=NOPLT-1
CALL PLOT(SV+1.,0.0,-3)
PLOTY= (YMAX-YMIN)/OY
PLOTY=PLOTY-.6
PLOTX=PLOTY-.4
CALL SYMBOL(6.25,PLOTY,0.14,SHIP ,0.0,30)
CALL SYMBOL(6.25,PLOTX,0.14,DATE ,0.0,30)
PLOTSY=(-DSOURC-YMIN)/OY
DO 170 I=1,II
IF (DEPTH(I)-DSOURC) 170,171,170
171 ISOURC=I
GO TO 172
170 CONTINUE
WRITE (6,202)
202 FORMAT (5X,52HDEPTH OF SOURCE HAS NOT BEEN INCLUDED IN YOUR TABLE )
STOP
172 K=ISOURC
ATHETA=ANGMAX
24 THETAJ=ATHETA*PI/180.
ANGLEB=ABS (SIN (THETAJ))
IF (ANGMIN-ATHETA-TEST1)9,9,200
9 WRITE (6,7) DEPTH(ISOURC),ATHETA
7 FORMAT (14H0SOURCE DEPTH=F8.2, 3X,13HSOURCE ANGLE=F8.2,8H DEG
1REES//4X5HPOINT5X 7HRANGE 3X10HTIME (SEC)6X10HDEPTH ///)
CALL PLOT(0.0,PLOTSY,3)
10 R=0.
IP=1
161 T=0.
IPOINT=1
11 RL=COS (THETAJ)/VELOC(ISOURC)
12 IF (IP-1)13,14,13

```

```

14  HOLD=ABS (THETAJ)
    IF (HOLD-(1.0E-6)) 330,821,821
821  IF (THETAJ)16,330,500
500  I=ISOURC -1
    GO TO 13
330  J=ISOURC-1
    N=ISOURC
    AHIGH=(VELOC(J)-VELOC(N))/ABS (DEPTH(J)-DEPTH(N))
    J=ISOURC+1
    ALOW =(VELOC(J)-VELOC(N))/ABS (DEPTH(J)-DEPTH(N))
    PLOTX=RMAX/DX
332  IF (AHIGH)333,331,150
333  I=ISOURC-1
    IZERO=1
    GO TO 13
150  IF (ALOW)151,152,153
151  IZERO=3
    I=ISOURC+1
    GO TO 13
153  IZERO=3
    GO TO 22
152  WRITE (6,334)
334  FORMAT (55H0          RAY TRAVELS HORIZONTALLY TO NEXT PROFILE
1///)
    IZERO=3
    CALL PLOT (PLOTX,PLOTSY,2)
    GO TO 22
331  WRITE (6,334)
    CALL PLOT (PLOTX,PLOTSY,2)
    IF (ALOW)335,153,153
335  WRITE (6,336)
336  FORMAT (64H0ZERO GRADIENT ABOVE,NEGATIVE GRADIENT BELOW.RAY ALSO 3
1ENDS DOWN///)
    CALL PLOT (0.0,PLOTSY,3)
    GO TO 151
16   I=ISOURC+1
13   IF (I)17,18,17
17   IF ((I-I)19,20,20
18   WRITE (6,21)
21   FORMAT (29H RAY GOES ABOVE MINIMUM DEPTH//)
    GO TO 22
19   WRITE (6,23)
23   FORMAT (29H RAY GOES BELOW MAXIMUM DEPTH//)
22   IP=1
    ATHETA=ATHETA-DELTA A
    ANGLEB=ABS (SIN (THETAJ))
    K=ISOURC
    IZERO=3
    GO TO 24
20   VL=VELOC(I)*RL
25   IF (VL.LE.1.) ANGLEA=SQRT(1.-VL**2)
26   A=(VELOC(I)-VELOC(K))/ABS (DEPTH(I)-DEPTH(K))
27   IF (A)28,29,28
28   IF (VL-1.)30,30,31
31   ANGLEA=0.
    IN=1
    GO TO 32
30   IN=3
32   DELTA R=(ANGLEB-ANGLEA)/A/RL
33   DELTA T=ALOG((1.+ANGLEB)/(1.-ANGLEB)*(1.-ANGLEA)/(1.+ANGLEA))/2./A
    IF (IN-1)37,34,37
34   D=(1./RL-VELOC(K))/(VELOC(I)-VELOC(K))
    D=D*ABS (DEPTH(I)-DEPTH(K))
    ISAVE=K

```

```

36 IF (I-K)38,200,39
39 DD=DEPTH(K)+D
   INEXT=K-1
   GO TO 41
38 DD=DEPTH(K)-D
   INEXT=K+1
41 R=R+ABS (DELTAR)
   T=T+ABS (DELTAT)
   PLOTX=R/OX
   PLOTY=(-DD-YMIN)/OY
   CALL PLOT(PLOTX,PLOTY,2)
   IF (ATHETA.EQ.-6..AND.PLOTY.LT.-2.) CALL SYMBOL(PLOTX,PLOTY,.015,
114,0.,-2)
   WRITE(6,42)          IPOINT,R,T,DD
42 FORMAT(5X13,5XF7.1,5XF8.5,5XF8.2)
43 IF (IN-1)44,45,44
45 R=K+ABS (DELTAR)
   T=T+ABS (DELTAT)
   IPOINT=IPOINT+1
   I=ISAVE
   IN=2
   GO TO 46
37 R=R+ABS (DELTAR)
   T=T+ABS (DELTAT)
46 WRITE(6,42)          IPOINT,R,T,DEPTH(I)
   PLOTX=R/OX
   PLOTY=(-DEPTH(I)-YMIN)/OY
   CALL PLOT(PLOTX,PLOTY,2)
   IF (ATHETA.EQ.-6..AND.PLOTY.LT.-2.) CALL SYMBOL(PLOTX,PLOTY,.015,
114,0.,-2)
   GO TO 43
29 DELTAR=ABS (DEPTH(I)-DEPTH(K))*VL/ANGLEA
48 DELTAT=ABS (DEPTH(I)-DEPTH(K))/VELOC(I)/ANGLEA
   IN=3
   GO TO 37
44 IF (IN-2)49,50,49
49 IF (I-K)53,200,52
53 K=I
   I=I-1
   GO TO 54
52 K=I
   I=I+1
54 IPOINT=IPOINT+1
   ANGLEB=ANGLEA
   GO TO 55
50 K=ISAVE
   IPOINT=IPOINT+1
   ANGLEB=ABS (ANGLEB)
   I=INEXT
55 IF (RMAX-R)56,57,57
56 IF (IZERO-1)137,138,137
137 WRITE(6,611)
611 FORMAT (28H RANGE EXCEEDS MAXIMUM RANGE///)
   GO TO 22
57 IP=2
   GO TO 12
138 IF (ALOW)139,152,153
139 WRITE(6,140)
140 FORMAT (54H NEGATIVE GRADIENT BELOW AND ABOVE.RAY ALSO BENDS DOWN/
1//)
   I=ISOURC+1
   IZERO=3
   IP=2

```

```

ANGLE=THETAJ*57.29578
ANGLEB=ABS (SIN (THETAJ))
K=ISOURC
WRITE (6,7)          DEPTH(ISOURC),ANGLE
R=0.
GO TO 161
200 FINAL=SX+10.0
CALL PLOT(FINAL,0.0,-3)
NOPLT = NOPLT-1
IF(NOPLT.NE.0) GO TO 702
CALL PLOT(0.,0.,999)
STOP
END

```

```

PROGRAM SSCTR(INPUT,OUTPUT,TAPE5=INPUT,TAPE6=OUTPUT)
C THIS PROGRAM CALCULATES THE SCATTERING CROSS SECTION TIMES THE
C FREQUENCY SQUARED. THE VALUE IS CALCULATED FOR A SHEAR PLANE
C WAVE IN A SOLID STRIKING A FLUID FILLED SPHERE. THE CASE OF A
C COMPRESSIONAL WAVE STRIKING THE SPHERE IS ALSO CALCULATED. THE
C VALUE IS CALCULATED AS A FUNCTION OF THE DIMENSIONLESS PARAMETER
C KA WHERE  $K=2*PI*FREQ/VELOCITY$  AND A IS THE SPHERE RADIUS.
C THE CALCULATION IS MADE IN THE C.G.S.SYSTEM. THE SCATTERING
C CROSS SECTION HAS UNITS OF  $DB-CM**2$ . CS1 IS THE SHEAR VELOCITY
C AND CL1 IS THE COMPRESSIONAL VELOCITY IN THE SOLID. CL2 IS THE
C COMPRESSIONAL VELOCITY IN THE SCATTERER. RHO IS THE RATIO OF THE
C DENSITY OF THE SPHERE TO THE DENSITY OF THE SOLID.
READ(5,49) CS1,CL1,CL2,RHO
49 FORMAT(3F8.0,F6.3)
WRITE(6,51)
51 FORMAT(42H KA GAMMA,SHEAR GAMMA,COMP)
1 READ(5,50) AKA
50 FORMAT(F7.2)
IF(EOF,5) 7,8
8 CONTINUE
PI=3.141592654
C FIRST THE SHEAR SCATTERING IS CALCULATED.
BKS1=AKA
BKL1=BKS1*CS1/CL1
BKL2=BKS1*CS1/CL2
SIM=CS1/(2.*PI)
C IF CIM=0. THEN A SHEAR WAVE IS INCIDENT.
CIM=0.
CALL COEF(BKS1,BKL1,BKL2,SIM,CIM,RHO,GAMAS)
GAMAS=GAMAS*BKS1
C GAMAS IS THE SHEAR SCATTERING CROSS SECTION*FREQ**2.
C NOW THE COMPRESSIONAL SCATTERING IS CALCULATED.
BKL1=AKA
BKS1=BKL1*CL1/CS1
BKL2=BKL1*CL1/CL2
C IF SIM=0. THEN A COMPRESSIONAL WAVE IS INCIDENT.
SIM=0.
CIM=CL1/(2.*PI)
CALL COEF(BKS1,BKL1,BKL2,SIM,CIM,RHO,GAMAC)
GAMAC=GAMAC*BKL1
C GAMAC IS THE COMPRESSIONAL SCATTERING CROSS SECTION*FREQ**2.
WRITE(6,55) AKA,GAMAS,GAMAC
55 FORMAT(2XF7.2,2(5XE13.4))
GO TO 1
7 CONTINUE
END

```

```

SUBROUTINE COEF(AKS1,AKL1,AKL2,SI,CI,RHA,GAMMA)
DIMENSION AJ1(400), AJ2(400), AJ3(400), Y1(400), Y2(400)
C THIS SOLVES THE BOUNDARY CONDITIONS FOR THE AMPLITUDES OF THE
C SCATTERED WAVES. THE AMPLITUDES ARE USED TO CALCULATE THE
C SCATTERING CROSS SECTION.
CALL SPBES(AKS1,N1,AJ1)
CALL SPBES(AKL1,N2,AJ2)
CALL SPBES(AKL2,N3,AJ3)
PI=3.141592654
IF(N1-N2) 10,11,11
10 N=N2
GO TO 12
11 N=N1
12 IF(N-N3) 13,14,14
13 NM=N3
GO TO 15
14 NM=N
C NM IS THE UPPER LIMIT OF THE SUM IN THE SCATTERING CROSS SECTION.
15 CALL SNMN(AKS1,NM,Y1)
CALL SNMN(AKL1,NM,Y2)
GAMMA=0.
DO 100 M=1,NM
F=FLOAT(M)-1.
ZERO=0.
O11=F*AJ2(M)-AKL1*AJ2(M+1)
O12=ZERO-F*(F+1.)*AJ1(M)
RAT=F*(1.-F)+AKS1**2/2.
O21=RAT*AJ2(M)-2.*AKL1*AJ2(M+1)
O22=F*(F+1.)*(F-1.)*AJ1(M)-AKS1*AJ1(M+1)
O31=(F-1.)*AJ2(M)-AKL1*AJ2(M+1)
ROT=1.-F**2+AKS1**2/2.
O32=ROT*AJ1(M)-AKS1*AJ1(M+1)
CI11=F*Y2(M)-AKL1*Y2(M+1)
CI12=F*(F+1.)*Y1(M)
CI13=F*AJ3(M)-AKL2*AJ3(M+1)
CI21=RAT*Y2(M)-2.*AKL1*Y2(M+1)
CI22=F*(F+1.)*((F-1.)*Y1(M)-AKS1*Y1(M+1))
C23=RHA*AKS1**2*AJ3(M)/2.
CI31=(F-1.)*Y2(M)-AKL1*Y2(M+1)
CI32= ROT*Y1(M)-AKS1*Y1(M+1)
Z1=(O11*CI+O12*SI)
Z2=(O21*CI+O22*SI)
Z3=(O31*CI+O32*SI)
ARM=O22*C13*Z3+C23*O32*Z1-C23*Z3*O12-O32*Z2*C13
AIM=C13*CI22*Z3+C23*CI32*Z1+C23*Z3*CI12-CI32*Z2*C13
BRM=O31*Z2*C13+C23*Z3*O11-C13*Z3*O21-C23*Z1*O31
BIM=C13*Z2*CI31+C23*Z3*CI11-C13*Z3*CI21-C23*Z1*CI31
DRM=C23*(O12*O31+CI12*CI31-O11*O32+CI11*CI32)+C13*(O21*O32-CI21*
1CI32-O22*O31+CI22*CI31)
DIM=C23*(CI31*O12-CI12*O31-CI11*O32-CI32*O11)+C13*(O32*CI21+O21*
1CI32-CI22*O31-O22*CI31)
P=ARM/DRM
Q=BRM/DRM
R=DIM/DRM
S=AIM/DRM
T=BIM/DRM
DEN=1.+R**2
C AM AND BM ARE THE SQUARES OF THE MAGNITUDE OF THE SCATTERED WAVES.
AM=(P**2+S**2)/DEN
BM=(Q**2+T**2)/DEN
GP=(2.*F+1.)*4.*PI*(AM/AKL1+F*(F+1.)*BM/AKS1)

```

```

100 GAMMA=GAMMA+GP
CONTINUE
GAMMA=8.686*GAMMA
RETURN
END

```

```

SUBROUTINE SMNM(ZT,NN,Y)
DIMENSION Y(400)
C THIS CALCULATES THE SPHERICAL NEUMANN FUNCTION(Y(I)) OF ARG ZT AND
C UP TO ORDER NN. THE VALUES ARE CALCULATED BY UPWARD RECURSION
C RELATIONS.
ZERO=0.
DO 1 I=1,400
1 Y(I)=0.
Y(1)=ZERO-COS(ZT)/ZT
Y(2)=ZERO-COS(ZT)/ZT**2-SIN(ZT)/ZT
NT=NN+2
DO 2 I=3,NT
AJ=FLOAT(I)-2.
Y(I)=((2.*AJ+1.)/ZT)*Y(I-1)-Y(I-2)
2 CONTINUE
RETURN
END

```

```

SUBROUTINE SPBES(ZT,NT,AJ)
DIMENSION R(400),RJ(400),AJ(400)
C THIS CALCULATES THE SPHERICAL BESSELS FUNCTIONS(AJ(I)) OF ARG
C ZT UP TO ORDER NT.
C THIS ROUTINE IS VALID FOR ARGUMENTS AS LOW AS 0.05.
BT=ZT
NDIM=400
NNT=IFIX(ZT)
DO 100 I=1,NDIM
100 AJ(I)=0.
C THIS SECTION SETS THE UPPER LIMIT OF NT FOR THE GIVEN ARG SUCH
C THAT ALL AJ'S OF HIGHER ORDER CAN BE SET TO ZERO.
N=NNT+10
DO 1 I=N,1850,5
J=I
FI=FLOAT(I)
SECA=ZT/(FI+.5)
TACA=SQRT(1.-SECA**2)
COSA=1./SECA
SINA=SQRT(1.+COSA**2)
ALP=ALOG(COSA+SQRT(COSA**2-1.))
DELT=EXP((FI+.5)*(TACA-ALP))/(2.*(FI+.5)*SQRT(SINA))
IF (DELT-1.E-27) 5,5,1
1 CONTINUE
GO TO 12
5 N=J
FN=FLOAT(N)
NP=N+1
NT=N+2

```

```

NU=N+10
EXPR=EXP(1.)
DO 7 I=NU,1890,5
K=I
FI=FLOAT(I)
D=0.434294
A1=2.*(FI-FN+1.)*D*ALOG(ZT)
A2=(2.*FI-2.*FN+1.)*D*ALOG(EXPR)
A3=(FN+2.5)*D*ALOG(FN+2.)+(FN-1.5)*D*ALOG(FN-2.)
A4=(FI+3.5)*D*ALOG(FI+3.)
A5=(FI-.5)*D*ALOG(FI-1.)
E=A1+A2+A3-A4-A5
IF(E+10.) 9,9,7
7 CONTINUE
C THIS SECTION CALCULATES THE BESSEL FUNCTIONS.
GO TO 12
9 NU=K
J=NU
R(NU+1)=0.
DO 2 I=1,NU
K=I
SJ=FLOAT(J)
R(J)=ZT/(1.+2.*SJ-ZT*R(J+1))
IF(R(J)-1.) 2,2,8
2 J=J-1
GO TO 200
8 IF(J-2) 200,200,14
200 RJ(NU+1)=R(NU)
RJ(NU)=1.
J=NU
NUP=NU-1
DO 210 I=1,NUP
J=J-1
SJ=FLOAT(J)
RJ(J)=(1.+2.*SJ)/ZT*RJ(J+1)-RJ(J+2)
210 CONTINUE
ALPH=(RJ(1)-ZT*RJ(2))*COS(3T)+ZT*SIN(BT)*RJ(1)
DO 220 I=1,NT
220 AJ(I)=RJ(I)/ALPH
333 CONTINUE
RETURN
14 RJ(J+1)=R(J)
LAN2=J+2
IF(LAN2-NP) 15,44,44
15 RJ(J)=1.
J=J-1
K=K+1
DO 3 I=K,NU
SJ=FLOAT(J)
RJ(J)=(1.+2.*SJ)/ZT*RJ(J+1)-RJ(J+2)
3 J=J-1
DO 4 I=LAN2,NT
4 RJ(I)=RJ(I-1)*R(I-1)
ALPH=(RJ(1)-ZT*RJ(2))*COS(BT)+ZT*SIN(BT)*RJ(1)
NDM=NDIM-1
IF(NT-NOM) 16,16,17
17 NT=NOM
16 DO 6 I=1,NT
6 AJ(I)=RJ(I)/ALPH
105 CONTINUE
RETURN
44 WRITE(6,45)
45 FORMAT(25H LAMBDA+2.GE.N+1 END XEQ)
GO TO 105

```

```

12 WRITE(6,13) ZT
13 FORMAT(26H ARG 3ES FTN TOO LARGE ZT=,E20.8,5X14H END EXECUTION)
STOP
END

```

```

PROGRAM LAYER(INPUT,OUTPUT,TAPE5=INPUT,TAPE6=OUTPUT)
C THIS PROGRAM SOLVES THE PROBLEM OF AN ELASTIC LAYER
C BOUNDED ON EACH SIDE BY DIFFERENT IDEAL FLUIDS.
C IMPLICIT COMPLEX(A,B,F,G,P,S),REAL(K)
C IMPLICIT COMPLEX NOTATION MAY BE VALID FOR THE U/W CDC 6400 ONLY.
C DIFFERENT COMPUTERS MAY REQUIRE ANOTHER NOTATION.
C COMPLEX CC,DD,EE,CAB,CSINE,O,J
C DIMENSION F(6),KK(6)
C NECESSARY FUNCTION STATEMENTS FOLLOW.
CAB(A,B)=A*CONJG(B)
ARG(A,B)=0.5*(A+CONJG(B))
CSINE(A,B)=CSIN(ARG(A,B))/ARG(A,B)
J=CMPLX(0.,1.)
C DATA INPUT REQUIREMENTS TO THE PROGRAM FOLLOW-
C NNN IS THE NUMBER OF INDIVIDUAL SETS TO BE CONSIDERED,CO,CL,CT,AN)
C CF ARE THE ACOUSTIC WAVE VELOCITIES OF THE INCIDENT WAVE, THE
C LONGITUDINAL AND TRANSVERSE WAVE IN THE PLATE AND THE VELOCITY OF
C THE TRANSMITTED WAVE RESPECTIVELY. RHO,RHOO AND RHOF ARE THE
C DENSITIES OF THE PLATE, INCIDENT MEDIUM AND FINAL MEDIUM
C RESPECTIVELY IN GRAMS PER CUBIC CENTIMETER.
READ(5,99)NNN
99 FORMAT(I2)
NNX=1
100 READ(5,101)CO,CL,CT,CF,RHO,RHOO,RHOF
101 FORMAT(4F5.0,3F7.4)
C KH IS 2*PI*(THICKNESS/WAVELENGTH IN THE INCIDENT MEDIUM),CHIO IS
C THE INITIAL INPUT ANGLE,DCHI IS THE INCREMENTAL ANGLE OF CHANGE,
C CHIF IS THE FINAL ANGLE TO BE CONSIDERED AND X IS THE DEPTH/WAVE-
C LENGTH IN THE INCIDENT MEDIUM.
102 READ(5,401)KH,CHIO,DCHI,CHIF,X
401 FORMAT(5F8.4)
PI=CMPLX(3.141592654,0.)
R=RHO/RHOO
R1=RHOO/RHOF
C DETERMINATION OF THE ACOUSTIC RUNNING VECTORS FOLLOW-
KLH=(CO/CL)*KH
KTH=(CO/CT)*KH
KFH=(CO/CF)*KH
C LL DETERMINES THE NUMBER OF ANGULAR INCREMENTS TO BE CONSIDERED
LL=IFIX((CHIF-CHIO)/DCHI)
C ALTHOUGH PI IS SPECIFIED COMPLEX, ONLY THE REAL COMPONENT
C CONTRIBUTES--STATEMENTS CHANGE DEGREES TO RADJANS
CHID=CHIO*PI/180.
DCHI=DCHI*PI/180.
C FOLLOWING STATEMENT SETS INITIAL ANGULAR PARAMETER.
CHI=CHIO
DO 121 IL=1,LL
IF(CHI)200,201,200
200 IF(IL-1)202,202,201
201 CHI=CHI+DCHI
C FROM SNELL'S LAW
C COMPLEXITY OF THE FOLLOWING STATEMENT ORIGINATES FROM LACK OF
C INSTANTIAL FORTITUDE TO USE BETA=KH*CSIN(CHI).
202 BETA=KH*CSIN(CMPLX(CHI,0.))

```

```

C   DIRECTION COSINE DETERMINATION FOLLOWS-
    AOH=CMPLX(KH*COS(CHI),0.)
C   CONJUGATE CONSIDERATIONS NECESSARY TO ASSURE A DECAYING WAVE IN
C   THE MEDIUM FOR ANGLES OF INCIDENCE BEYOND THE CRITICAL ANGLE.
    ALH=CONJG(CSQRT(KLH**2-BETA**2))
    ATH=CONJG(CSQRT(KTH**2-BETA**2))
    AFH=CONJG(CSQRT(KFH**2-BETA**2))
    IF(CF-C0)108,107,108
107 AH=(1.,0.)
    GO TO 109
108 AH=AOH/AFH
C   THE SPECIFICATION OF AFH AND R1 ASSUMES DIFFERENT MEDIA ON EACH
C   SIDE OF THE PLATE IF DESIRED.
109 S12=-2.*ALH*BETA/(ATH**2-BETA**2)
    S22=ALH/AOH
    S24=BETA/AOH
    S32=R*(2.*BETA**2/KTH**2-1.)
    S34=-R*2.*BETA*ATH/KTH**2
    S1=(S12*S24-S22)*AH
    G1=1.-CCOS(ATH)*CCOS(ALH)
    G2=CSIN(ATH)*CSIN(ALH)
    G3=CCOS(ATH)*CSIN(ALH)
    G4=CCOS(ALH)*CSIN(ATH)
    A1=4.*(2.*R1*S12*S32*S34*G1-(R1*((S12*S34)**2+S32**2)
1-S1**2)*G2+J*(S12*S24-S22)*(AH-R1)*(-S12*S34*G3+S32*G4))
    A2=2.*(R1*S12*S34*G1-(R1*S32+S1)*G2+J*(R1*S32+S1)*G4
1-J*R1*S12*S34*G3)
    A3=2.*(-R1*S12*S34*G1+(R1*S32-S1)*G2+J*(R1*S32-S1)*G4
1-J*R1*S12*S34*G3)
    A4=2.*S12*(R1*S32*G1-(R1*S12*S34-S1)*G2+J*(R1*S12*S34-S1)*G3
1-J*R1*S32*G4)
    A5=2.*S12*(R1*S32*G1-(R1*S12*S34+S1)*G2-J*(R1*S12*S34+S1)*G3
1+J*R1*S32*G4)
    A6=-8.*J*R1*AH*S1*(S12*S34*CSIN(ALH)-S32*CSIN(ATH))
    D=4.*(2.*R1*S12*S32*S34*G1-(R1*((S12*S34)**2+S32**2)+S1**2)*G2
1+J*(S12*S24-S22)*(AH+R1)*(-S12*S34*G3+S32*G4))
    F(1)=A1/D
    F(2)=-2.*A2/D
    F(3)=2.*A3/D
    F(4)=-2.*A4/D
    F(5)=2.*A5/D
    F(6)=-A6*CEXP(J*AFH)/D
    DO 203 IJ=1,6
203 KK(IJ)=CABS(F(IJ))**2
C   THE FOLLOWING DETERMINES THE SNELL'S LAW CRITICAL ANGLE FOR THE
C   COMPRESSIONAL AND TRANSVERSE ACOUSTIC WAVES RELATIVE TO ANGLES OF
C   INCIDENCE IN DEGREES.
    CRITL=ASIN(C0/CL)*180./PI
    CRITT=ASIN(C0/CT)*180./PI
    THETA=CHI*180./PI
C   THE FOLLOWING CHECKS TO DETERMINE IF ENERGY IS CONSERVED.
    CHEK=REAL(KK(1)+(AFH/AOH)*KK(6)/R1)
C   IT IS NOT OBVIOUS THAT UNITS ARE CONSERVED IN THE FOLLOWING
C   STATEMENTS--HOWEVER, RECALL THAT X IS THE (DEPTH INTO THE PLATE)
C   DIVIDED BY (WAVELENGTH IN THE INCIDENT MEDIUM).
    ARG1=-J*2.*PI*ALH*X/KH
    ARG2=ARG1*ATH/ALH
C   THE FOLLOWING DETERMINES THE COMPRESSIONAL AND TRANSVERSE
C   DISPLACEMENT POTENTIAL REQUIREMENTS OF THE PROBLEM.
    PHIN=F(2)*CEXP(ARG1)
    PNIP=F(3)*CEXP(-ARG1)
    PSIN=F(4)*CEXP(ARG2)
    PSIP=F(5)*CEXP(-ARG2)

```

```

PHI=PHIN+PHIP
PSI=PSIN+PSIP
PHN=PHIP-PHIN
PSN=PSIP-PSIN
C THE FOLLOWING DETERMINES THE ENERGY PER UNIT AREA PER UNIT TIME
C (INTENSITY) FLOWING IN A DIRECTION PERPENDICULAR TO THE PLATE
C SURFACE (MULTIPLIED BY THE SOUND VELOCITY IN THE INCIDENT MEDIUM)
C DIVIDED BY THE (DENSITY OF THE PLATE MULTIPLIED BY THE FOURTH
C POWER OF THE CIRCULAR FREQUENCY).
GX=(1./KH)*(ARG(ALH,ALH)*(CAB(PHIN,PHIN)-CAB(PHIP,PHIP))
1*ARG(ALH,-ALH)*(CAB(PHIN,PHIP)-CAB(PHIP,PHIN))
2*ARG(ATH,ATH)*(CAB(PSIN,PSIN)-CAB(PSIP,PSIP))
3*ARG(ATH,-ATH)*(CAB(PSIN,PSIP)-CAB(PSIP,PSIN)))
B1=1.+2.*(BETA**2 +CAB(ALH,ALH)-KLH**2)/(KTH**2)
B2=2.*(CAB(ATH,ATH)-0.5*(ATH**2 -BETA**2))/(KTH**2)
B3=(2.*BETA**2 -KLH**2 +0.5*KTH**2)/(KTH**2)
B4=(2.*BETA**2 -0.5*KTH**2)/(KTH**2)
C THE FOLLOWING DETERMINES THE ENERGY PER UNIT AREA PER UNIT TIME
C (INTENSITY) FLOWING IN A DIRECTION PARALLEL TO THE PLATE SURFACE
C MULTIPLIED BY THE SOUND VELOCITY IN THE INCIDENT MEDIUM DIVIDED
C BY THE FOURTH POWER OF THE CIRCULAR FREQUENCY.
GY=(1./KH)*(BETA*B1+CAB(PHI,PHI)+BETA*B2*CAB(PSI,PSI)
1-(4.*BETA/KTH**2.)*(CAB(ALH,ALH)*(CAB(PHIP,PHIN)+CAB(PHIN,PHIP))
2+CAB(ATH,ATH)*(CAB(PSIP,PSIN)+CAB(PSIN,PSIP)))
3+B3*(CAB(PSN,PHI)*ATH+CAB(PHI,PSN)*CONJG(ATH))
4-B4*(CAB(PHN,PSI)*ALH+CAB(PSI,PHN)*CONJG(ALH)))
IF(CHI-REAL(ASIN(CO/CL)))300,300,301
300 BN=1
BP=CSINE(ALH,ALH)
PN=1
PP=CSINE(ATH,ATH)
GO TO 304
301 BN=CSINE(ALH,-ALH)
BP=1
IF(CHI-REAL(ASIN(CO/CL)))302,302,303
302 PN=1
PP=CSINE(ATH,ATH)
GO TO 304
303 PN=CSINE(ATH,-ATH)
PP=1
304 CONTINUE
C THE FOLLOWING SPECIFIES AMPLITUDES AND ALGEBRAIC TERMS NECESSARY
C FOR THE DETERMINATION OF THE TOTAL ENERGY BEING PROPAGATED
C PARALLEL TO THE PLATE BOUNDARIES AS A FUNCTION OF THE INCIDENT
C ANGLE, I.E., SIGMA IS THE INTEGRATED INTENSITY ACROSS THE PLATE.
AA=F(1)
BB=F(2)
CC=F(3)
DD=F(4)
EE=F(5)
FF=F(6)
P1=(CAB(BB,BB)*CEXP(-J*ARG(ALH,-ALH))+CAB(CC,CC)*CEXP(J*ARG(ALH,
1-ALH)))*BN+(CAB(BB,CC)*CEXP(-J*ARG(ALH,ALH))+CAB(CC,BB)*CEXP(J*
2ARG(ALH,ALH)))*BP
P2=(CAB(DD,DD)*CEXP(-J*ARG(ATH,-ATH))+CAB(EE,EE)*CEXP(J*ARG(ATH,
1-ATH)))*PN+(CAB(DD,EE)*CEXP(-J*ARG(ATH,ATH))+CAB(EE,DD)*CEXP(J*
2ARG(ATH,ATH)))*PP
P3=(CAB(BB,CC)*CEXP(-J*ARG(ALH,ALH))+CAB(CC,BB)*CEXP(J*ARG(ALH,
1ALH)))*BP
P4=(CAB(DD,EE)*CEXP(-J*ARG(ATH,ATH))+CAB(EE,DD)*CEXP(J*ARG(ATH,
1ATH)))*PP
P5=(CAB(EE,BB)*CEXP(J*ARG(ATH,ALH))-CAB(DD,CC)*CEXP(-J*ARG(ATH
1,ALH)))*ATH*CSINE(ATH,ALH)
P6=(CAB(DD,BB)*CEXP(J*ARG(-ATH,ALH))-CAB(EE,CC)*CEXP(-J*ARG(-ATH

```

```

1,ALH)))*ATH*CSINE(-ATH,ALH)
P7=(CAB(CC,DD)*CEXP(J*ARG(ALH,ATH))-CAB(BB,EE)*CEXP(-J*ARG(ALH
1,ATH)))*ATH*CSINE(-ATH,ALH)
P8=(CAB(CC,EE)*CEXP(J*ARG(ALH,-ATH))-CAB(BB,DD)*CEXP(-J*ARG(ALH
1,-ATH)))*ALH*CSINE(ALH,ATH)
SIGMA=BETA*(B1*P1+B2*P2-4.*(CAB(ALH,ALH)*P3+CAB(ATH,ATH)*P4)
1+2.*B3*(ARG(P5,P5)-ARG(P6,P6))-2.*B4*(ARG(P6,P6)+ARG(P7,P7))
C SPECIFYING REAL IN THE FOLLOWING ONLY SERVES TO ACCOMMODATE MINIMUM
C OUTPUT FIELDS AS THE IMAGINARY COMPONENT OF GX,GY, AND SIGMA MUST
C BE ZERO SINCE THESE PARAMETERS ARE REAL.
305 KX=REAL(X)
KY=REAL(GY)
TENGY=REAL(SIGMA)
VR=CG*KH/REAL(BETA)
IF(IIL-1)116,116,116
116 WRITE(6,204)
204 FORMAT(1H1)
WRITE(6,205)CG,CI,CT,RHO,KH,CRITL,CRITT
205 FORMAT(3X,5HCG = ,F5.0,3X,5HCL = ,F5.0,3X,5HCT = ,F5.0,
14X,6HRHO = ,F4.2,3X,6HKOH = ,F4.1,3X,13HPHIL(CRIT) = ,F6.3,
23X,13HPHIY(CRIT) = ,F6.3,/)
WRITE(6,117)
117 FORMAT(5X,5HTHETA,5X,2HAA,6X,2HBB,6X,2HCC,6X,2HDD,6X,2HEE,
16X,2HFF,3X,5HCHECK,9X,2HIX,11X,2HIY,6X,2HCR,12X,5HSIGMA)
118 WRITE(6,119)THETA,(KK(NM),NM=1,6),CHK,KX,KY,VR,TENGY
119 FORMAT(5X,F5.2,6(2X,F6.3)2X,F5.3,2(2X,F11.4),2X,F8.2,2X,F11.4)
121 CONTINUE
NNX=NNX+1
C FOLLOWING DETERMINES REPEAT OF PRECEEDING PROCESSES UNTIL MAXIMUM
C INCIDENT ANGLE SPECIFIED IS ACHIEVED.
IF(NNX-NNN)100,100,122
122 CONTINUE
STOP
END

```

REFERENCES

1. W. Weeks and A. Assur, "The Mechanical Properties of Sea Ice," Cold Regions Research and Engineering Laboratory, Hanover, New Hampshire (1967).
2. M. Ewing and A.P. Crary, "Propagation of Elastic Waves in Ice. Part II," *Physics* 5, 181-184 (1934).
3. J. Oliver, et al., "Elastic Waves in Pack Ice," *Trans. Amer. Geophys. Union* 35, 282-292 (1954).
4. K. Hunkins, "Seismic Studies of Sea Ice," *J. Geophys. Res.* 65, 3459-3472 (1960).
5. G.K.C. Clarke, "Seismic Survey - Northwest Greenland," Cold Regions Research and Engineering Laboratory, Hanover, New Hampshire, Rpt. 191 (1966).
6. A.P. Crary, "Seismic Studies on Fletcher's Ice Island, T-3," *Trans. Amer. Geophys. Union* 35, 293-300 (1954).
7. R.E. Bunney and J.G. Hanse, "Elastic Waves in Sea Ice," (manuscript in preparation).
8. H. Lamb, "On Elastic Waves in a Plate," *Proc. R. Soc. London* A93, 114-128 (1917).
9. M.F.M. Osborn and S.D. Hart, "Reflection and Guiding of an Exponential Pulse by a Steel Plate in Water, I," *J. Acoust. Soc. Am.* 17, 1-18 (1945).
10. R.R. Goodman and R.E. Bunney, "Surface Waves on Elastic Plates in a Fluid Medium," (to be submitted to *J. Acoust. Soc. Am.* for publication).
11. R.E. Bunney, et al., "Rayleigh and Lamb Waves on Cylinders," *J. Acoust. Soc. Am.* 42, 1223-1233 (1969).
12. M. Ewing, et al., "Propagation of Elastic Waves in Ice. Part I," *Physics* 5, 165-168 (1934).
13. N. Smith, "Determining the Dynamic Properties of Snow and Ice by Forced Vibration," Cold Regions Research and Engineering Laboratory, Hanover, New Hampshire, Rpt. 216 (1969).
14. R.E. Green and L. MacKinnon, "Determination of the Elastic Constants of Ice Single Crystals by an Ultrasonic Pulse Method," *J. Acoust. Soc. Am.* 6, 1292L (1956).
15. V.V. Bogorodskii, "Elastic Moduli of Ice Crystals," *Soviet Physics - Acoust.* 10, 124-126 (1964).

16. H. Roethlisberger, "Ultrasonic Pulse Measurements in Anisotropic Lake Ice," Cold Regions Research and Engineering Laboratory, Hanover, New Hampshire, Rpt. 126 (1966).
17. E.R. Pounder and P. Stalinski, "Elastic Properties of Arctic Sea Ice," Intern. Assoc. Sci. Hydrol. Pub. 54, 35 (1960).
18. M.P. Langleben, "Young's Modulus for Sea Ice," Can. Journ. Phy. 40, 1-8 (1962).
19. E.R. Pounder, The Physics of Ice (Pergammon Press, London, 1965).
20. A. Assur, "Composition of Sea Ice and Its Tensile Strength," National Academy of Sciences-National Research Council Pub. 598, 106-138 (1958).
21. R.E. Bunney and J.G. Hanse, "Acoustic Velocity Profiles in Annual Sea Ice," (submitted to J. Acoust. Soc. Am. for publication).
22. M.P. Langleben and E.R. Pounder, "Acoustic Attenuation in Sea Ice," Macdonald Physics Laboratory, McGill University Rpt. S-14 (1968).
23. J.G. Hanse and R.E. Bunney, "Attenuation of Acoustic Waves in Annual Sea Ice - A First Approximation," (submitted to J. Acoust. Soc. Am. for publication).
24. J.G. Hanse and R.E. Bunney, "A Calculation of the Acoustic Shear Wave Attenuation in Sea Ice," Applied Physics Laboratory, University of Washington Rpt. 7310 (1973).
25. G. Frankenstein and R. Garner, "Equations for Determining the Brine Volume of Sea Ice from -0.5° to -22.9°C ," J. Glaciology 6, 943-44 (1967).
26. N. Untersteiner, "On the Mass and Heat Budget of Arctic Sea Ice," Arch. Meteorol. Bioklimatol 12, 151-182 (1961).
27. W.M. Ewing, W.S. Jardetzky, and F. Press, Elastic Waves in Layered Media (McGraw-Hill, New York, 1957).
28. C. Maxwell, Scientific Papers (Cambridge University Press, Cambridge, England, 1890).
29. W. Voigt, Ann. d. Phys. 47, 671 (1892).
30. W.P. Mason, Physical Acoustics and the Properties of Solids (Van Nostrand, Princeton, New Jersey, 1958).
31. D.R. Bland, The Theory of Linear Viscoelasticity (Pergammon Press, New York, 1960).
32. H. Kolsky, Stress Waves in Solids (Dover, New York, 1963).

33. F. Press and M. Ewing, "Theory of Air Coupled Flexural Waves," J. Appl. Phys. 22, 892-899 (July 1951).
34. Lord Rayleigh, "On Waves Propagated Along the Plane Surface of an Elastic Solid," Proc. London Math. Soc. 17, 4-11 (1885).
35. I.A. Viktorov, Rayleigh and Lamb Waves (Plenum Press, New York, 1967).
36. R.E. Bunney and R.R. Goodman, "Energy of the Acoustically Excited Surface Wave on a Flat Semi-Infinite Elastic Medium," J. Acoust. Soc. Am. 53, 1658-1673 (1973).
37. P.M. Morse and H. Feshbach, Methods of Theoretical Physics, (McGraw-Hill, New York, 1953).
38. H. Love, The Mathematical Theory of Elasticity (Cambridge University Press, New York, 1927).
39. C.F. Ying and R. Truell, "Scattering of a Plane Longitudinal Wave by a Spherical Obstacle in an Isotropically Elastic Solid," J. Appl. Phys. 27, 1086-1096 (1956).
40. T.M. Lee, "Method of Determining Dynamic Properties of Viscoelastic Solids Employing Forced Vibrations," J. Appl. Phys. 34, 1524-1529 (1963).
41. M.A. Boit, "Theory of Elasticity and Consolidation for a Porous Anisotropic Solid," J. Appl. Phys. 26, 182-185 (1955).
42. M.A. Boit, "Theory of Propagation of Elastic Waves in a Fluid-Saturated Porous Solid, Part I, Low Frequency Range," J. Acoust. Soc. Am. 28, 1968 (1956).
43. M.A. Boit, "Theory of Propagation of Elastic Waves in a Fluid-Saturated Porous Solid, Part II, High Frequency Range," J. Acoust. Soc. Am. 28 179 (1956).
44. T.M. Lee, "Spherical Waves in Viscoelastic Media," Cold Regions Research and Engineering Laboratory Rpt. 158 (1965).
45. B. Linsay, Mechanical Radiation (McGraw-Hill, New York, 1960).

UNCLASSIFIED
Security Classification

DOCUMENT CONTROL DATA - R&D		
<i>(Security classification of title, body of abstract and indexing annotation must be entered when the overall report is classified)</i>		
1. ORIGINATING ACTIVITY (Corporate author)		2a. REPORT SECURITY CLASSIFICATION
University of Washington Seattle, Washington 98195		Unclassified
		2b. GROUP
3. REPORT TITLE		
FEASIBILITY OF ACOUSTICALLY DETERMINING THE THICKNESS OF SEA ICE (U)		
4. DESCRIPTIVE NOTES (Type of report and inclusive dates)		
Final Report		
5. AUTHOR(S) (Last name, first name, initial)		
Bunney, Robert E.		
6. REPORT DATE	7a. TOTAL NO. OF PAGES	7b. NO. OF REFS
April 1974	82	45
8a. CONTRACT OR GRANT NO.	9a. ORIGINATOR'S REPORT NUMBER(S)	
DAAG 17-73-C-0028		
b. PROJECT NO.		
c.	9b. OTHER REPORT NO(S) (Any other numbers that may be assigned this report)	
d.	APL-UW 7317	
10. AVAILABILITY/LIMITATION NOTICES		
Distribution of this document is unlimited.		
11. SUPPLEMENTARY NOTES	12. SPONSORING MILITARY ACTIVITY	
	U.S. Army Natick Laboratories, Natick, Massachusetts 01760	
13. ABSTRACT		
<p>The results of laboratory and field tests on the acoustic properties of sea ice are reported. Velocity, density and salinity profiles were taken and the results used to predict depth dependence of the elastic constants of the medium. Shear and compressional wave attenuation calculations were made and empirically "fit" to the data to determine frequency dependence. The relative energy reflected from the ice-water interface from an incident wave of unit amplitude is calculated and the ability to detect this energy at the ice surface is shown. As a result of these tests, the feasibility of measuring sea ice thickness using pulse echo techniques is demonstrated, and recommendations for further study are made. Preliminary tests to measure Lamb wave propagation were successfully made and the results are reported. (U)</p>		

DD FORM 1473
1 JAN 64

Unclassified
Security Classification

14. KEY WORDS Acoustic Measurements of Sea Ice Sea Ice Thickness, Acoustic Measurements of	LINK A		LINK B		LINK C	
	ROLE	WT	ROLE	WT	ROLE	WT

INSTRUCTIONS

1. **ORIGINATING ACTIVITY:** Enter the name and address of the contractor, subcontractor, grantee, Department of Defense activity or other organization (*corporate author*) issuing the report.
- 2a. **REPORT SECURITY CLASSIFICATION:** Enter the overall security classification of the report. Indicate whether "Restricted Data" is included. Marking is to be in accordance with appropriate security regulations.
- 2b. **GROUP:** Automatic downgrading is specified in DoD Directive 5200.10 and Armed Forces Industrial Manual. Enter the group number. Also, when applicable, show that optional markings have been used for Group 3 and Group 4 as authorized.
3. **REPORT TITLE:** Enter the complete report title in all capital letters. Titles in all cases should be unclassified. If a meaningful title cannot be selected without classification, show title classification in all capitals in parenthesis immediately following the title.
4. **DESCRIPTIVE NOTES:** If appropriate, enter the type of report, e.g., interim, progress, summary, annual, or final. Give the inclusive dates when a specific reporting period is covered.
5. **AUTHOR(S):** Enter the name(s) of author(s) as shown on or in the report. Enter last name, first name, middle initial. If military, show rank and branch of service. The name of the principal author is an absolute minimum requirement.
6. **REPORT DATE:** Enter the date of the report as day, month, year; or month, year. If more than one date appears on the report, use date of publication.
- 7a. **TOTAL NUMBER OF PAGES:** The total page count should follow normal pagination procedures, i.e., enter the number of pages containing information.
- 7b. **NUMBER OF REFERENCES:** Enter the total number of references cited in the report.
- 8a. **CONTRACT OR GRANT NUMBER:** If appropriate, enter the applicable number of the contract or grant under which the report was written.
- 8b, 8c, & 8d. **PROJECT NUMBER:** Enter the appropriate military department identification, such as project number, subproject number, system numbers, task number, etc.
- 9a. **ORIGINATOR'S REPORT NUMBER(S):** Enter the official report number by which the document will be identified and controlled by the originating activity. This number must be unique to this report.
- 9b. **OTHER REPORT NUMBER(S):** If the report has been assigned any other report numbers (*either by the originator or by the sponsor*), also enter this number(s).
10. **AVAILABILITY/LIMITATION NOTICES:** Enter any limitations on further dissemination of the report, other than those

imposed by security classification, using standard statements such as:

- (1) "Qualified requesters may obtain copies of this report from DDC."
- (2) "Foreign announcement and dissemination of this report by DDC is not authorized."
- (3) "U. S. Government agencies may obtain copies of this report directly from DDC. Other qualified DDC users shall request through _____."
- (4) "U. S. military agencies may obtain copies of this report directly from DDC. Other qualified users shall request through _____."
- (5) "All distribution of this report is controlled. Qualified DDC users shall request through _____."

If the report has been furnished to the Office of Technical Services, Department of Commerce, for sale to the public, indicate this fact and enter the price, if known.

11. **SUPPLEMENTARY NOTES:** Use for additional explanatory notes.
12. **SPONSORING MILITARY ACTIVITY:** Enter the name of the departmental project office or laboratory sponsoring (*paying for*) the research and development. Include address.
13. **ABSTRACT:** Enter an abstract giving a brief and factual summary of the document indicative of the report, even though it may also appear elsewhere in the body of the technical report. If additional space is required, a continuation sheet shall be attached.

It is highly desirable that the abstract of classified reports be unclassified. Each paragraph of the abstract shall end with an indication of the military security classification of the information in the paragraph, represented as (TS), (S), (C), or (U).

There is no limitation on the length of the abstract. However, the suggested length is from 150 to 225 words.

14. **KEY WORDS:** Key words are technically meaningful terms or short phrases that characterize a report and may be used as index entries for cataloging the report. Key words must be selected so that no security classification is required. Identifiers, such as equipment model designation, trade name, military project code name, geographic location, may be used as key words but will be followed by an indication of technical content. The assignment of links, roles, and weights is optional.